



TAMPEREEN TEKNILLINEN YLIOPISTO  
TAMPERE UNIVERSITY OF TECHNOLOGY

**EEMELI HÄSÄNEN**  
**COMPOSITION ANALYSIS AND COMPATIBILIZATION OF**  
**POST-CONSUMER RECYCLED MULTILAYER PLASTIC FILMS**  
Master's thesis

Examiner: professor Jyrki Vuorinen  
The examiner and the topic approved in the council meeting of the Automation, Mechanical and Materials Engineering Faculty on 4<sup>th</sup> May 2016

## ABSTRACT

**EEMELI HÄSÄNEN:** Composition analysis and compatibilization of post-consumer recycled multilayer plastic films  
Tampere University of Technology  
Master of Science Thesis, 58 pages, 36 Appendix pages  
May 2016  
Master's Degree Programme in Materials Science  
Major: Technical Polymer Materials  
Examiner: Professor Jyrki Vuorinen

Keywords: plastics, plastic, multilayer, film, recycling, compatibilization, polymer blend, blending, recyclate, DSC, FTIR, composition, composition analysis, optical microscopy, cross-section

The goal of this thesis was to deduct the composition for recycled multilayer film plastic waste and how it could be compatibilized in theory. The composition analysis was carried out using three different methods: differential scanning calorimetry (DSC), Fourier transform infrared spectroscopy (FTIR) and polarized light optical microscopy. Recycled multilayer plastic film samples were provided by Arcada University of applied sciences after initial screening.

FTIR and optical microscopy were used on all samples. Some samples had their materials written on the packages. DSC was used only on samples with unknown material composition. Optical microscopy was used to produce cross-section images of the multilayer films. Layer thicknesses and the number of layers were differentiated from these images. Different plastics exhibit various interference colors with polarized light, thus individual layers could be identified. Top and bottom layers were analyzed by FTIR and then cross-referenced with the data from the layer analysis.

Analysis was carried out for 121 samples and 738 layers. This led to the total thickness of each material used in the sample pool, which was used to further calculate the proportions of each material in relation to volume for different package types and the whole sample pool. The sample pool consisted of 56.7 % polyethylene (PE), 13.5 % of polypropylene (PP), 9.5 % of polyamide-6 (PA-6), 7.8 % of polyethylene terephthalate (PET), 4.5 % of copolymers of PE and PP, 4.1 % of print, 2.0 % of ethylene vinyl acetate (EVA) or tie layers and of 1.9 % ethylene vinyl alcohol (EVOH). This data could be possibly used for future research into the compatibilization of commingled post-consumer multilayer plastic film waste and possible applications.

## TIIVISTELMÄ

**HÄSÄNEN, EEMELI:** Kierrätettyjen kuluttajamonikerrosmuovikalvojen koostumuksen analysointi ja kompatibilisointi  
Tampereen teknillinen yliopisto  
Diplomityö, 58 sivua, 36 liitesivua  
Toukokuu 2016  
Materiaalitekniikan diplomi-insinöörin tutkinto-ohjelma  
Pääaine: Tekniset polymeerimateriaalit  
Tarkastaja: professori Jyrki Vuorinen

Avainsanat: muovi, monikerros, kalvo, muovikalvo, monikerrosmuovikalvo, kierrätys, koostumus, koostumuksen analysointi, kompatibilisointi, DSC, FTIR, mikroskopia, yhteensovittaminen, poikkileike

Tämän diplomityön tavoitteena oli selvittää kierrätettyjen kuluttajamonikerrosmuovikalvojen koostumus ja miten kyseisiä kalvoja voisi teoriassa kompatibilisoida. Koostumuksen selvitykseen käytettiin kolmea eri tapaa: differentiaalista pyyhkäisykalorimetriä (DSC), Fourier-muunnos infrapuna spektroskopiaa (FTIR) sekä polarisoidun valon optista mikroskopiaa. Diplomityössä tutkitut kierrätetyt monikerrosmuovikalvonäytteet toimitti Arcada ammattikorkeakoulu.

Osassa pakkauksista oli kirjoitettuna niissä käytetyt materiaalit. FTIR:iä ja optista mikroskopiaa hyödynnettiin kaikissa näytteissä. DSC:tä käytettiin ainoastaan näytteisiin, joiden koostumus ei ollut selvä pakkausten merkintöjen perusteella. Optisella mikroskopiolla saatiin aikaan poikkileikekuvia monikerrosmuovikalvoista. Poikkileikekuvista voitiin havaita muovikerrosten kerrospaksuudet sekä kerrosten määrä. Eri muovityypeillä on havaittavissa polarisoidun valon käytön yhteydessä ns. interferenssivärejä, joiden perusteella yksittäiset muovikalvokerrokset pystyttiin tunnistamaan. Päälimmäinen ja alimmainen monikerrosmuovikalvon kerros analysoitiin lisäksi FTIR:llä ja saatuja tuloksia vertailtiin kerrosanalyysin tuloksiin.

Yhteensä analysoitiin 121 näytettä ja 738 eri kerrosta. Tästä saatiin kokonaispaksuus jokaiselle materiaalille, jota näytteissä esiintyi. Yksittäisten materiaalien kokonaistilavuutta verrattiin kaikkien materiaalien kokonaistilavuuteen, jolloin saatiin selville jokaisen materiaalin suhteellinen osuus tässä näyte-erässä. Näyte-erästä 56,7 % oli polyeteeniä (PE), 13,5 % polypropeenia (PP), 9,5 % polyamidi-6:tta (PA-6), 7,8 % polyeteenitereftalaattia (PET), 4,5 % PE:n ja PP:n kopolymeerejä, 4,1 % painatusta, 2,0 % etyylivinyliasetaattia (EVA) tai sidoskerroksia sekä 1,9 % etyylivinyylialkoholia (EVOH). Tätä tietoa voidaan mahdollisesti hyödyntää tulevaisuudessa esimerkiksi kierrätettyjen monikerrosmuovikalvojen kompatibilisoinnin edistämiseksi ja mahdollisissa sovelluskohteissa.

## PREFACE

This thesis was made due to the increasing need to better recycle commingled plastic waste. Originally the idea was to make this thesis only about compatibilization of the recycled post-consumer multilayer films, but in the end the composition analysis was quite large in scope by itself and the compatibilization was left in theory only. It is my hope that the information gathered in this thesis warrants further research into how recycled commingled plastic waste can be further reprocessed.

I'd like to take this opportunity to thank everyone who was involved in the making of this thesis. Special thanks go to my thesis director M.Sc. Ville Mylläri who offered me this position to begin with. I'd also like to thank M.Sc. Ilari Jönkkäri from TUT, B. Eng. Valeria Poliakova and the rest of the team from Arcada University of applied sciences, M. Sc. Reetta Anderson of Ekokem Ltd, Auli Nummila-Pakarinen of Borealis AG, research assistant Pasi Seppälä and lastly professor Jyrki Vuorinen for taking the time to be the official examiner of this thesis. I also have gratitude for the laboratory personnel of the paper and packaging department for having the chance to work in the department laboratory.

In Tampere, 13.5.2016

Eemeli Häsänen

## CONTENTS

1.	INTRODUCTION .....	1
2.	THEORY .....	2
2.1	Multilayer films.....	2
2.1.1	Structure .....	2
2.2	Materials.....	4
2.2.1	Polyethylene.....	4
2.2.2	Polypropylene .....	7
2.2.3	Polyethylene terephthalate .....	8
2.2.4	Polyamide.....	9
2.2.5	Ethylene vinyl alcohol .....	12
2.2.6	Ethylene vinyl acetate .....	13
2.2.7	Additives .....	14
2.3	Methods of composition analysis.....	15
2.3.1	Polarized light optical microscopy.....	15
2.3.2	Differential scanning calorimetry .....	16
2.3.3	Fourier transform infrared spectroscopy.....	18
2.4	Compatibilization .....	22
2.4.1	Blending and miscibility .....	23
2.4.2	Incorporation of specific interacting groups .....	24
2.4.3	Ternary polymer addition.....	25
2.4.4	Polymer-polymer reactions .....	26
2.4.5	Reactive compatibilization.....	26
2.4.6	Compatibilization of recycled & commingled polymers.....	28
3.	THE SAMPLE POOL.....	30
4.	RESULTS FROM THE COMPOSITION ANALYSIS METHODS.....	33
4.1	Cross-section images from polarized light optical microscopy .....	33
4.2	DSC sample preparation & measurements.....	37
4.3	FTIR measurements .....	39
5.	COMPOSITION ANALYSIS.....	43
5.1	Polymer identification from DSC data.....	43
5.2	Identification of different polymer layers .....	46
5.3	Calculation of material proportions.....	48
5.4	Sources of error .....	54
6.	CONCLUSION .....	55
	REFERENCES.....	56
	APPENDIX A: CROSS-SECTION FIGURES .....	59
	APPENDIX B: DSC FIGURES.....	80
	APPENDIX C: FTIR SPECTRA.....	87

## LIST OF FIGURES

<i>Figure 1. A typical five-layer multilayer film structure (Breil 2010).</i>	3
<i>Figure 2. Chemical structure of PE (Ashter 2014).</i>	5
<i>Figure 3. Chemical structure of PP (Ashter 2014).</i>	7
<i>Figure 4. Chemical structure of PET (Ravve 2012).</i>	9
<i>Figure 5. Chemical structure of PA-6,6 (upper) and PA-6,10 (lower) (Ashter 2014).</i>	11
<i>Figure 6. Chemical structure of EVOH (Mokwena &amp; Tang 2012).</i>	12
<i>Figure 7. Chemical structure of EVA (Andersen 2004).</i>	13
<i>Figure 8. Principle of a polarized light optical microscope (Ockenga 2011).</i>	16
<i>Figure 9. The measuring cell of a heat-flux DSC system (Netzsch 2016).</i>	17
<i>Figure 10. Fingerprinting of an unknown polymer, DSC curve for PET (Wunderlich 2005).</i>	18
<i>Figure 11. Infrared bands of polymers (Stuart 2004).</i>	20
<i>Figure 12. Basic design of a "Michelson" interferometer (Gaffney et al. 2012).</i>	21
<i>Figure 13. Ethylene-propylene copolymer with varying amounts of ethylene: (a) 0 %, (b) below 10 % and (c) 68 % (Lobo &amp; Bonilla 2003).</i>	22
<i>Figure 14. Cross-section of sample 1.</i>	34
<i>Figure 15. Cross-section of sample 15.</i>	35
<i>Figure 16. Cross-section of sample 23.</i>	35
<i>Figure 17. Cross-section of sample 12.</i>	36
<i>Figure 18. Cross-section of sample 55.</i>	37
<i>Figure 19. The temperature program for DSC samples.</i>	38
<i>Figure 20. DSC curve for sample 43-1.</i>	38
<i>Figure 21. DSC curve for sample 46-2.</i>	39
<i>Figure 22. FTIR spectrum of a PE reference sample.</i>	40
<i>Figure 23. FTIR spectrum of the PP reference sample.</i>	41
<i>Figure 24. FTIR spectrum of the PA reference sample.</i>	41
<i>Figure 25. FTIR spectrum of the PET reference sample.</i>	42
<i>Figure 26. FTIR spectrum of the top layer of sample 38.</i>	42
<i>Figure 27. Amount of layers versus the type of material.</i>	47
<i>Figure 28. Volume percentages of materials in the sample pool.</i>	49
<i>Figure 29. Volume percentages of materials for frozen product packages.</i>	50
<i>Figure 30. Volume percentages of materials for chilled product packages.</i>	50
<i>Figure 31. Volume percentages of materials for processed meat packages.</i>	51
<i>Figure 32. Volume percentages of materials for fresh meat and fish packages.</i>	51
<i>Figure 33. Volume percentages of materials for dry product packages.</i>	52
<i>Figure 34. Volume percentages of materials for cheese packages.</i>	53
<i>Figure 35. Volume percentages of materials for miscellaneous packages.</i>	53

## LIST OF SYMBOLS AND ABBREVIATIONS

ABS	acrylonitrile butadiene styrene
aPP	atactic polypropylene
BOPP	biaxially oriented polypropylene
DSC	differential scanning calorimetry
EMA	ethylene methacrylate
EVA	ethylene vinyl acetate
EVOH	ethylene vinyl alcohol
FIR	far-infrared region
FTIR	Fourier transform infrared spectroscopy
HDPE	high density polyethylene
iPP	isotactic polypropylene
LDPE	low density polyethylene
LLDPE	linear low density polyethylene
MDPE	medium density polyethylene
MIR	mid-infrared region
NIR	near-infrared region
OM	optical microscopy
OPA	oriented polyamide
OPP	oriented polypropylene
PA	polyamide
PC	polycarbonate
PCL	polycaprolactone
PCW	post-consumer waste
PE	polyethylene
PET	polyethylene terephthalate
PLLA	poly-L-lactide
PMMA	polymethyl methacrylate
PP	polypropylene
PPE	polyphenyl ether
PS	polystyrene
PVC	polyvinyl chloride
PVDC	polyvinylidene chloride
PVOH	polyvinyl alcohol
SEBS	styrene ethylene butylene styrene
SBR	styrene butadiene rubber
sPP	syndiotactic polypropylene
$T_g$	glass transition temperature
$T_m$	melting temperature
UHMWPE	ultra-high molecular weight polyethylene
ULDPE	ultra-low density polyethylene
UV	ultraviolet
VLDPE	very low density polyethylene

# 1. INTRODUCTION

Multilayer films are used in the packaging industry for various reasons, such as enhancing the oxygen barrier properties or improving resistance against moisture. Recycling of multilayer films poses a problem due to lack of methods to separate the individual plastic layers effectively in large quantity. Therefore it's necessary to blend together several dissimilar plastics, which is difficult due to the very different chemical natures of various polymers. This is the reason that compatibilization is needed.

Previous research on flexible packaging multilayer films in Europe has been performed by Pardos Marketing in 2005. This study takes into account all types of multilayer films whereas this thesis focuses on post-consumer multilayer plastic films used in food packaging. The study found that the multilayer film materials consisted of 34 % polyethylene (PE), 26 % of oriented polypropylene (OPP), 23 % of non-polymeric substrates, 4 % of co-polymer polypropylene (PP), 3 % each of polyvinyl chloride (PVC), ethylene vinyl alcohol (EVOH), polyamide (PA) and polyethylene terephthalate (PET) and lastly 1 % of oriented polyamide (OPA). (Pardos Marketing 2005)

The aim of this thesis is to gain knowledge of the composition of post-consumer multilayer plastic film waste in Finland. With the results it would be possible to further research how to compatibilize the waste and find new applications for the recycled waste material. The composition analysis is carried out by differential scanning calorimetry (DSC), Fourier transform infrared spectroscopy (FTIR) and polarized light optical microscopy. FTIR and optical microscopy are used on every sample in this thesis. DSC is used on multilayer films with unknown composition. The samples were provided by Arcada University of applied sciences in cooperation with Ekokem Ltd. as part of the ARVI research program.

The theory in this thesis includes general information about multilayer films, detailed information on different polymeric materials in multilayer films, methods of composition analysis and the compatibilization of polymeric materials. Cross-section images of multilayer structures produced by optical microscopy are compared against the data from FTIR and DSC, which results in proportions in relation to volume for different materials in the sample pool. Proportions of each material type for different package types are also calculated.



## 2. THEORY

This section covers the theory behind the materials that are used in multilayer films in addition to the methods of composition analysis in this thesis. Different compatibilization methods are also described.

### 2.1 Multilayer films

Multilayer structures are used to provide protective, functional and decorative properties. They consist of at least two layers, aiming to meet the required performance for a particular application. Multilayer structures may lower the total cost of production by incorporating inexpensive materials such as recycled material in addition to the expensive polymers or by film thickness reduction. (Butler & Morris 2010) Flexible packaging structures for medical applications have from three up to eleven layers. Multilayer structures with barrier films such as EVOH often require a tie layer, thus producing a five or seven layer structure. (Breil 2010; Butler & Morris 2013)

Multilayer structures can be produced by coextrusion, blown film extrusion, cast film extrusion, lamination and extrusion coating methods. Two or more films that cannot be coextruded can be combined into a single structure using lamination. Double bubble or tenter frame process can be used to produce oriented films. Oriented films often exhibit better optical properties, higher stiffness and higher shrinkage during packaging. (Butler & Morris 2010)

Individual layers contribute to specific functional properties, such as enhancing permeation resistance or tensile strength. Other common properties that need to be taken into account include optics, formability, machinability, economics, sealability and adhesion. An individual layer may contain polymer blends, neat polymer, recycled material or additives. Important key properties for multilayer structures in flexible packaging include good barrier properties, selective permeability, machinability, sealability, esthetics and damage preventing properties, such as impact strength. (Butler & Morris 2010)

#### 2.1.1 Structure

Coextruded structures have varied amounts of bulk/core layers, sealant layers, barrier layers and tie layers. Common materials for forming the bulk layer include PE, PP, acrylates, ethylene vinyl acetate (EVA) and polystyrene (PS) (Wagner Jr. & Marks 2010). A typical five-layer multilayer film structure consisting of a core layer, two intermediate layers and two skin layers is illustrated in Figure 1.

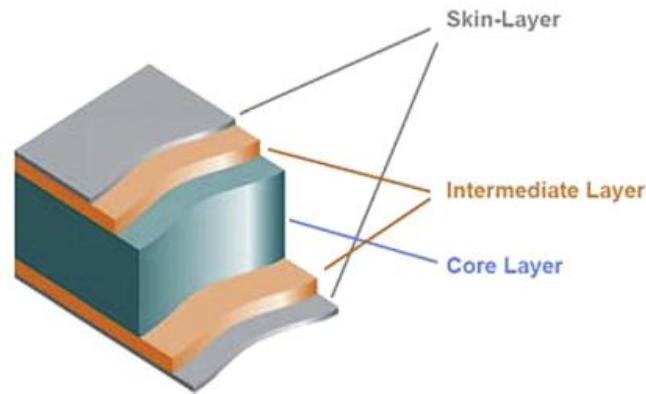


**Figure 1.** A typical five-layer multilayer film structure (Breil 2010).

Packaging industry generally requires that films are sealable and this is often done thermally. Various sealing methods include constant temperature sealing or variable temperature sealer in addition to high frequency, radiofrequency, ultrasonic and pressure sensitive sealing. Common polymer resins for a sealant layer include LDPE (low density polyethylene), PP, ionomers of acid copolymers, EMA (ethylene methacrylate) or EVA blends with LLDPE (linear low density polyethylene) and metallocene VLDPE (very low density polyethylene). Important factors when choosing the sealant layer include heat seal strength and hot tack strength, sealing speed, economics, seal initiation temperature and coefficient of friction. (Wagner Jr. & Marks 2010)

Tie layer's main task is to provide adhesion in order to join incompatible layers together. The bonding between layers happens in molten state and the bonds are mechanical and/or chemical in nature. Modifiers or grafted functional groups are often used together with a base polymer to reach a sufficient adhesion level. Common tie layer resins include EVA, PP, LDPE, LLDPE, HDPE (high density polyethylene), acid copolymers and acrylate copolymers. They are often modified with rubbers, tackifiers, maleic anhydride or olefinic tougheners. (Wagner Jr. & Marks 2010) Anhydride-modified polyolefins are common tie resins for the bonding of EVOH and PA in barrier film structures. Other common functional groups in tie resins are listed in Table 1. (Butler & Morris 2013)

**Table 1.** Common functional groups in tie resins (Butler & Morris 2013).

Functional group	Adheres to
Acid	Aluminum foil, PA
Anhydride	EVOH, PA
Acrylate	PP, PET, some inks
Epoxy	PET
Silane	Glass
Vinyl alcohol	PP, PET, PVDC

Barrier layer is used to provide resistance against certain elements, such as oxygen, aroma, moisture, chemicals, flavor, oil and grease. PET, PP and HDPE are used for moisture barrier, whereas EVOH, PA and PVDC (polyvinylidene chloride) provide oxygen, aroma and flavor barrier properties. Crystallinity and polarity influence a polymer's oil resistance, thus ionomers and PA are also used as oil barriers. PP and HDPE generally have the greatest oil resistance among polyolefins due to their crystallinity. PET and PVDC both provide for some chemical barrier needs. (Wagner Jr. & Marks 2010; Butler & Morris 2013)

## 2.2 Materials

This section covers some of the most common polymer resins used in the manufacturing of multilayer films. Their properties and roles of each material in building a multilayer film structure are explained.

### 2.2.1 Polyethylene

PE is a semi-crystalline thermoplastic polyolefin that possesses a chemical structure consisting of hydrocarbons (see Figure 2.). PE is chemically extremely inert and its physical strength decreases at a lower temperature when compared to high-performance engineering thermoplastics. (Ashter 2014)

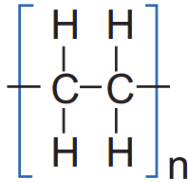


**Figure 2.** Chemical structure of PE (Ashter 2014).

General properties of PE include excellent chemical resistance, good abrasion and impact resistance, very low moisture absorption, good processability and toughness but medium tensile strength. It's also an excellent electrical insulator due to the non-polar nature of the macromolecule. (Vasile & Pascu 2005) The melting temperature ( $T_m$ ) of PE is dependent on the molecular structure and the method of polymerization. For commercial polymer grades the  $T_m$  is around 108–130 °C (Ravve 2012). Glass transition temperature ( $T_g$ ) of PE varies between -130 °C and -20 °C where values near -20 °C are more likely (Ashter 2014).

PE is a solid and has no solvents at room temperature, but dissolves in a variety of hydrocarbons with similar solubility parameters at elevated temperatures. PE types with higher density require even more elevated temperatures. PE is resistant against alkalis, non-oxidizing acids and a variety of aqueous solutions. Nitric acid causes oxidation which deteriorates the mechanical properties and causes structural changes. (Brydson 1999)

Types of PE are differentiated mainly in accord to their density, molecular weight and the type of branching of the polymer chains (see Table 2.) Generally, increasing the density leads to decreased low-temperature impact strength and stress crack resistance but increased chemical resistance, stiffness, melting point and tensile strength (Berins 1991). Higher degree of crystallinity increases the modulus and density of PE.  $T_m$  of PE increases linearly with density as seen in Table 2. (Utracki 2003) Increased branching lowers crystallinity and consequently it affects many of the properties of PE (Vasile & Pascu 2005). Higher crystallinity causes more shrinkage during processing (Brydson 1999).

**Table 2.** Different types of PEs (Utracki 2003; Wypych 2012).

Abbreviation	Name	Density [kg/m <sup>3</sup> ]	T <sub>m</sub> [°C]	Crystallization temperature [°C]	Characteristics
<b>UHMWPE</b>	Ultra-High Molecular Weight PE	~969	133–140	-	Molecular weight > 3000 kg/mol
<b>HDPE</b>	High Density PE	941–969	125–135	114–120	High crystallinity and molecular weight
<b>MDPE</b>	Medium Density PE	926–940	-	-	-
<b>LDPE</b>	Low Density PE	910–925	105–115	96–100	Long chain branching
<b>LLDPE</b>	Linear Low Density PE	910–925	120–136	107–123	Short chain branching
<b>VLDPE</b>	Very Low Density PE	900–910	-	-	-
<b>ULDPE</b>	Ultra-Low Density PE	855–900	123–124	-	-

LDPE is flexible, tough, easily processable; resistant to corrosion, chemicals and weathering and it has low water absorption. Negative properties include low tensile strength, stiffness and gas permeability, environmental stress cracking susceptibility, poor UV resistance and limited use in high temperatures. LDPE has a higher clarity and lower T<sub>m</sub> compared to LLDPE. Blending LDPE with LLDPE increases melt strength and processability. (Vasile & Pascu 2005) ULDPE and VLDPE are used to modify impact properties of other polyolefins. LLDPE has a much higher elongation compared to LDPE, which can be utilized to reduce the material costs and still retain good strength. LLDPE's properties include good toughness, puncture and tear resistance. (Massey 2004)

MDPE exhibits a good impact resistance and its general properties lie somewhere between LDPE and HDPE. Compared to HDPE it's less rigid and hard, in addition it also has a better resistance to cracks. MDPE is most commonly used as a component in blends with LDPE, HDPE or LLDPE. It can also be used in multilayer structures such as LDPE/MDPE/LDPE three-layer laminate combining good optical, mechanical and sealing properties. (Vasile & Pascu 2005)

HDPE polymers are rigid and tough due to their high crystallinity. Properties of HDPE include good impact strength, nonexistent moisture absorption, translucency, flexibility, processability, weather resistance and chemical resistance. HDPE is tough in temperatures as low as -60 °C. Disadvantages of HDPE include poor UV resistance, high mold shrinkage and stress cracking susceptibility when compared to PEs with lower stiffness. (Vasile & Pascu 2005)

HD-, LLD-, LD-, and VLDPE are used as bulk layers in multilayer structures. LD-, LLD- and HDPE are also used as tie layers (Wagner Jr. & Marks 2010). Low density PEs are also used as sealants in multilayer structures, while high density PEs can be used to provide moisture resistance. LDPE, LLDPE and HDPE are used for moisture barrier properties in bakery applications. LDPE also provides good optics and printability. (Butler & Morris 2010) In many cases compatibilization is required for blending PEs since they are highly immiscible with many other polymers. PEs can also be used to modify impact behavior of other common thermoplastics such as PP. (Utracki 2003).

### 2.2.2 Polypropylene

PP is a crystalline thermoplastic polyolefin which consists of a linear hydrocarbon chain and an alternating methyl group as shown in Figure 3 (Ashter 2014). PP can be divided into three types based on its tacticity (position of the methyl groups): amorphous/atactic (aPP), isotactic (PP) and syndiotactic (sPP). Syndiotactic PP has a significantly higher tensile modulus and impact strength compared to isotactic PP. PP suffers from brittleness in low temperature environments. Aforementioned properties among others can be improved via blending. Elastomers are often used to improve processability and mechanical properties. (Utracki 2003)

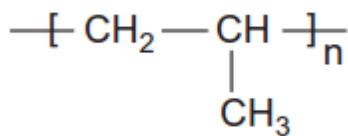


**Figure 3.** Chemical structure of PP (Ashter 2014).

Isotactic PP's crystallinity is typically between 40–70 %, which results in a higher density, strength and  $T_m$  when compared to sPP and aPP. Due to the crystallinity of iPP it has a high resistance to chemicals in addition to low vapor and solvent permeability. Isotactic PP is typically opaque in color. (Calhoun 2010) Atactic PP is amorphous and sticky due to its irregular structure and its main applications are roofing tars and adhesives but it can also be used together with other PP types to modify properties such as impact strength and stretchability (Maier & Calafut 1998).

Commercial iPP has a  $T_m$  range of 151–166 °C,  $T_g$  of -10 °C and crystallization temperature range of 138–144 °C whereas sPP has a  $T_m$  range of 117–156 °C and  $T_g$  range from -15 to 3 °C. Decomposition temperatures for iPP and sPP are 240 and 260 °C respectively. (Wypych 2012)

Broad molecular weight distribution leads to higher impact strength and melt viscosity, but it decreases hardness, yield strength, stiffness and softening point of PP (Ashter 2014). PP has an excellent chemical resistance but it is susceptible to very strong oxidizing agents. Apart from those, it has excellent resistance against most organic solvents. PP is effective as an electrical insulator due to its high dielectric strength, low dissipation factor and low dielectric constant. It has higher rigidity when compared to other polyolefins and it can withstand heat better than other low-cost thermoplastics. PP also exhibits good fatigue resistance, processability, clarity and often insusceptibility to environmental stress cracking. (Maier & Calafut 1998)

Processed PP is generally more transparent than PE and the transparency of the polymer can be affected by use of nucleation agents (Ashter 2014). Orientation can be used to modify PP properties, resulting either in biaxially oriented PP (BOPP) or OPP. BOPP films can be manufactured by double-bubble or flat tenter stretching processes. These processes can also be used in coextrusion of multilayer structures. (Massey 2004) Orienting PP increases crystallinity which makes oriented films stiffer. Strength is also increased in the orientation direction and likewise decreased in the direction perpendicular to the orientation. Increased crystallinity also lowers permeability to gases and moisture and increases grease and oil resistance and dielectric strength. Biaxial orientation also increases the clarity of the film. Oriented films exhibit higher shrinkage than unoriented films. (Maier & Calafut 1998)

PP is used as a bulk layer in many applications to provide structural strength. Functional applications include a moisture barrier layer in bakery applications and using PP copolymer with ethylene or butylene as skin layer in packaging applications. PP is also a common material for a sealant layer or a tie layer. (Wagner Jr. & Marks 2010; Butler & Morris 2010; Calhoun 2010)

### **2.2.3 Polyethylene terephthalate**

PET is water white thermoplastic polyester produced by using a polycondensation reaction between a diol and a dicarboxylic acid. The chemical structure of PET is illustrated in Figure 4. PET exists both in crystalline and amorphous forms and the properties of the polymer depend largely on the crystallinity and morphology of the polymer. PET is widely used in the production of fibers, films and other high-strength products because of high crystallinity and orientation. (Ashter 2014; Massey 2004)

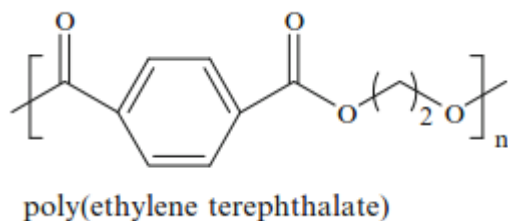


**Figure 4.** Chemical structure of PET (Ravve 2012).

Attributing to the stiff polymer chain, PET has very good mechanical and chemical properties: abrasion resistance, hardness, toughness, fatigue resistance, stress crack resistance and very low moisture absorption. It also exhibits good melt flow properties such as high melt strength, high temperature resistance and low coefficient of friction. PET generally possesses a good surface quality. Amorphous PET exhibits brittleness in room temperature and has a  $T_g$  of 67 °C. (Ashter 2014; Massey 2004) PET has a  $T_m$  range of 245–265 °C,  $T_g$  range of 60–85 °C and a decomposition temperature range of 285–329 °C (Wypych 2012).

Despite being a polar polymer PET exhibits good electrical insulating properties at room temperature. PET has a hygroscopic nature and due to that it is recommended to thoroughly dry it before melt processing. (Brydson 1999) Additives used to prevent hydrolysis during processing include epoxide, phosphorus acid ester and carbodiimide. They are typically added during compounding. (Keck-Antoine et al. 2010)

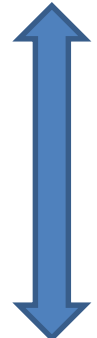
In multilayer structures, PET can be utilized as a printing surface that also provides damage resistance during end-use and distribution and thermal resistance during sealing (Butler & Morris 2010). PET also provides some benefits as a flavor/aroma and chemical barrier material (Wagner Jr. & Marks 2010).

## 2.2.4 Polyamide

PAs are thermoplastics that are prepared using polycondensation between diamines and dicarboxylic acids. Polycondensation process can be done via melt, solution or interfacial approach. (Ashter 2014) They are often abbreviated PA-X,Y; where X denominates the number of carbons in a diamine and Y the number of carbons in the di-carboxylic acid (Utracki 2003). Different types of PAs include PA-6, PA-66, PA-6,6; PA-6,66; PA-6,10; PA-6,12; PA-11 and PA-12 to mention a few (Massey 2004). Differences in the properties of some commercial PAs are listed in Table 3. Chemical structures of PA-6,6 and PA-6,10 are illustrated in Figure 5.



**Table 3.** Differences in commercial PAs (Massey 2004; Wypych 2012).

	T <sub>m</sub> [°C]	T <sub>g</sub> [°C]	Decomposition temperature [°C]	Crystallization temperature [°C]	Maximum water absorption [%]	Gas and aroma barrier	Relative cost
<b>PA-6</b>	220–260	50–75	>300	173–180	9.5	Highest	100
<b>PA-6,66</b>	189–199	42	340	-	9.0		120
<b>PA-66</b>	257–270	60–70	340	230	8.5		130
<b>PA-6,10</b>	215–230	65–70	350	179	3.3		140
<b>PA-6,12</b>	215–218	54–62	291	181	3.3		150
<b>PA-11</b>	178–195	42–46	240–270	-	1.8		180
<b>PA-12</b>	174–185	55	-	-	1.6	Lowest	170

PAs exhibit good tensile, impact and flexural strength in a wide temperature range from subzero up to 300 °C. They are fairly good in electrical insulation under low humidity and temperature conditions. They also have excellent low-friction properties. Viscosity behavior of PA is non-Newtonian with sufficient shear stress. The melt viscosity increases with higher values of molecular weight distribution. The cyclic groups in aromatic PAs increase the T<sub>m</sub>. The polarity of the amide group and the length of the hydrocarbon chain affect the properties of PAs. Aliphatic PAs are good electrical insulators at room temperature, low frequencies and in dry conditions. High frequency electrical insulation is not counted among the pros of PAs due to the polarity of the polymers. (Ashter 2014)

Degree of crystallinity influences the properties of PAs greatly. Due to the linearity of aliphatic PAs they're easy to crystallize up to 50–60 % crystalline content with slow cooling and only to 10 % crystalline content with rapid cooling. Morphology of the resulting polymer depends on the processing method – fine aggregates form with rapid cooling and spherulites with slow cooling. (Brydson 1999)

PAs are hygroscopic and must therefore be dried before processing similar to PET. Moisture levels should be kept between 0.05–0.2 % to avoid undesirable viscosities and hydrolysis (Ashter 2014). Due to the hygroscopic behavior of PAs they are often combined with other materials to achieve the required gas and water vapor barrier properties (Massey 2004).

The high solubility parameters of PAs make them soluble only to a few liquids with equally high solubility parameters, such as formic acid, glacial acetic acid, phenols and cresols. They exhibit good resistance against hydrocarbons and are nonreactive with alkyl halides, glycols and esters. They are susceptible to mineral acids and tend to swell when in contact of alcohol. PAs also have an excellent alkali resistance at room temperature. (Brydson 1999)

Shrinkage can be observed post-molding due to relief of stresses during molding. Moisture absorption is responsible for additional dimensional changes. Annealing can be used for increased crystallinity for applications where dimensions are important. Molded PA's mechanical properties depend on molecular weight distribution, crystallinity, moisture content and conditioning. Before conditioning the samples are hard and brittle, but afterwards they become tough and wear resistant. (Ashter 2014) PAs have a particularly good abrasion resistance which can be further improved by utilization of external lubricants and processing conditions that support the development of a highly crystalline hard surface (Brydson 1999).

PA-6 exhibits limited water barrier properties, but it's resistant to oils and fats and most flavors and gases. It's difficult to process but used in multilayer packages for medical, food and pouch applications. PA-6 can be used together with polyolefins or foils to increase the moisture barrier. It can be used in both freezing low and boiling high temperatures still retaining 90 % of its tensile strength and all of its elongation properties. (Massey 2004)

PA-6,6 is one of the most used PAs and it can be oriented monoaxially in machine or transverse direction. Toughness and gas permeability can be improved via orientation. Applications include food packaging for greasy products such as cheese and meat. It may be treated for inking or improvement of coating receptivity. (Massey 2004)

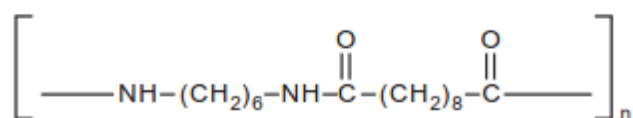
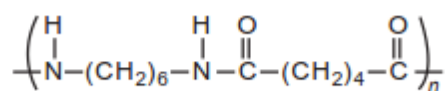


**Figure 5.** Chemical structure of PA-6,6 (upper) and PA-6,10 (lower) (Ashter 2014).

PA-6,66 combines properties of PA-6 and PA-6,6 providing good toughness and strength in combination with excellent resistance to chemicals, heat and abrasion. It's used in multilayer films to provide gas barrier properties. (Massey 2004).

Additives for PAs aim to suppress hydrolysis, thermal and thermo-oxidative degradation. Carboxylic acid in place of primary amino end groups increases thermal and thermo-oxidative degradation whereas incorporating lubricants decreases them. Yellowing can be controlled by incorporating optical brighteners or phosphites. Aromatic amines, copper salts and phenolic antioxidants are used to improve stability during service life of PA. (Keck-Antoine et al. 2010)

In multilayer structures, PAs provide oil resistance and flavor/aroma barrier properties. (Butler & Morris 2010) PA also features good thermoformability, toughness, abrasion resistance and optics (Ashter 2014). Orientation improves the basic barrier and mechanical properties. Oxygen and aroma-barrier properties can be improved significantly via biaxial orientation. OPA-films are used together with PVDC, aluminum foil and ionomer or PE films. (Massey 2004)

### 2.2.5 Ethylene vinyl alcohol

EVOH is a thermoplastic crystalline copolymer that is produced with varying levels of ethylene and vinyl alcohol which in turn determines the oxygen barrier properties of EVOH. Chemical structure of EVOH is depicted in Figure 6. Ethylene content varies between 27–48 %. It can be coextruded with all types of polyolefins, PA, PS, polyesters and PVC. EVOH exhibits antistatic behavior and finished products have a high gloss and low haziness. It also has good printability due to the alcohol group in the molecular chain and a good resistance to oils and organic solvents in addition to excellent weather resistance. EVOH is also an excellent barrier material against gases. (Massey 2004) EVOH is stiff but sensitive to thermal exposure and flex cracking (Wagner Jr. & Marks 2010).

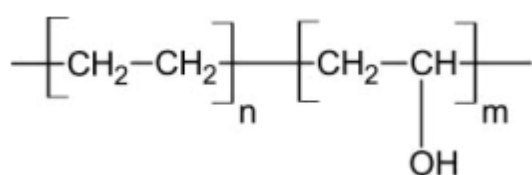


**Figure 6.** Chemical structure of EVOH (Mokwena & Tang 2012).

Increasing the ethylene content in EVOH produces a more stretchable resin for orientation process in order to increase the barrier properties. However, increasing the ethylene content too much also decreases the barrier properties significantly. Ethylene content of 33 % and below produces a good oxygen barrier within a thin (2 μm) layer. (Breil 2010) Decreasing the ethylene content leads to increases in tensile strength, tensile modulus and crystalline melting point (Brydson 1999). EVOH has a  $T_m$  range of 155–193 °C,  $T_g$  range of 44–72 °C and decomposition temperature of >245 °C (Wypych 2012).

EVOH can be blended together with HDPE, PA and PP (Wypych 2012). Among the polymers used for multilayer structures, EVOH has an extremely low oxygen permeability coefficient, making it ideal as a barrier material against oxygenation. While this is true, it has a high moisture vapor transmission rate compared to many polymers. (Butler & Morris 2010) It is also used as a flavor/aroma barrier layer and requires tie layers except when used with PAs. (Wagner Jr. & Marks 2010) Some examples of multilayer structures involving EVOH include PS/EVOH/PS for coffee and cream packages and HDPE/EVOH/EVA as a barrier film for cereal packages (Brydson 1999).

## 2.2.6 Ethylene vinyl acetate

EVA is a rubbery copolymer of ethylene and vinyl acetate, with the vinyl acetate content varying between 7.5 and 33 weight-%. Chemical structure of EVA is depicted in Figure 7. The incorporation of vinyl acetate into PE provides the copolymer with increased flexibility, improved optical properties, lower sealing temperature, better adhesion, increase in both impact strength and puncture resistance. Lower vinyl acetate content provides the copolymer with increased crystallinity and stiffness, while higher vinyl acetate content increases the gas permeability, optical qualities, impact strength and flex-crack resistance. Vinyl acetate addition in any amount decreases the sealing temperature. (Massey 2004)

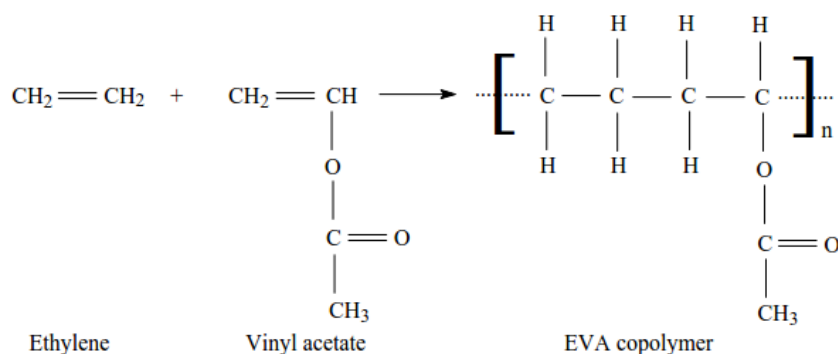


**Figure 7.** Chemical structure of EVA (Andersen 2004).

Physical properties of EVA include a  $T_m$  range of 58–112 °C,  $T_g$  range of -38 to -42 °C, crystallization temperature range of 52–76 °C and decomposition temperature range of 221–240 °C. EVA's color ranges from colorless to white. EVA can be blended with LDPE, LLDPE, HDPE, PP and PA among others. (Wypych 2012)

EVA blended with LLDPE provides sealability and good optics in a multilayer structure (Wagner Jr. & Marks 2010; Butler & Morris 2010). EVA with an ethylene content of ~97 mole % can be used as a modifier for LDPE to reduce crystallinity and increase

softness and flexibility (Brydson 1999). EVA is also used as a tie layer to provide adhesion between dissimilar components (Wagner Jr. & Marks 2010).

### 2.2.7 Additives

Different types of additives to modify the base properties of a polymer include modifiers, fillers and stabilizers. Modifiers are used to alter or enhance the base material properties. Stabilizers maintain the original mechanical, organoleptic and optical properties of a polymer during the polymer's life cycle. Fillers reduce the costs or improve the physical properties of a polymer. Additives are incorporated into the polymer after synthesis or they can be added in the multilayer film layers. (Keck-Antoine et al. 2010)

Modifiers can be further divided into antiblock additives, antistats, slip additives and optical brighteners. Optical brighteners re-emit absorbed light in the ultraviolet (UV) range at a higher wavelength, thus increasing the amount of reflected bluish light. They are used in very low concentrations ( $\leq 10$  ppm). Slip additives are used to modify the friction between layers. Slip is quantified by the coefficient of friction. Slip additives are divided to migrating and non-migrating, where the former migrates to the surface of the polymer matrix upon crystallization. Typical migrating slip additives are fatty acid amides. They can be incorporated during extrusion, compounding or conversion. (Keck-Antoine et al. 2010)

Antiblock additives are used to prevent two adjacent films layers from sticking to one another. They can be divided to inorganic and organic, where inorganic are most commonly used. Inorganic antiblock additives must not interact with the polymer. They are typically incorporated during conversion, compounding and/or extrusion. Antistats are used to prevent electrostatic charges from building up between two substrates due to friction. Electrostatic charges can be decreased with an external or internal antistat or a conductive filler. Antistatic properties increase with higher relative humidity. They are typically incorporated during compounding. (Keck-Antoine et al. 2010)

Stabilizers can be further divided into UV stabilizers and antioxidants. Antioxidants provide the organic substrates with protection against thermal and thermo-oxidative degradation when UV light is not present. Various types of antioxidants are used depending on the polymer resin. Incorporation of antioxidants happens typically during the extrusion process, while UV stabilizers are typically incorporated during conversion or compounding. UV stabilizers work by absorbing UV light and dissipating it as heat or by free radical scavenging. (Keck-Antoine et al. 2010)

Important factors to consider when choosing an additive include the primary effect of the additive (e.g. reinforcement, a functional property), suitability for industrial purposes, residues in the substrate material and secondary effects (e.g. discolorations, interactions with other additives) and cost. (Keck-Antoine et al. 2010)

Additives can be added to individual layers in a multilayer structure to achieve a certain property. Additive migration from one layer to another may occur depending on the solubility and concentration difference between phases. In most additives, concentration affects the overall effectiveness of an additive until a saturation point is reached. (Keck-Antoine et al. 2010)

## **2.3 Methods of composition analysis**

This section covers the theory behind the analysis methods for various multilayer film structures in this thesis, including polarized light optical microscopy, differential scanning calorimetry (DSC) and Fourier transform infrared spectroscopy (FTIR). Basics of each method are explained.

### **2.3.1 Polarized light optical microscopy**

Optical microscopy is based on the interaction between light and materials. As light comes into contact with an object, it can be transmitted, reflected and/or absorbed. The use of polarized light exploits a phenomenon called birefringence, where one ray of light splits into two sister rays due to refraction. Birefringence can be defined as the difference between lowest and highest refractive indices of a material. Some materials that exhibit birefringence and thus have an ordered structure (such as crystalline materials) produce interference colors when utilizing linearly polarized light which are then detectable with an optical microscope. The interference colors are a result of the recombination of the split sister rays. (Carlton 2011) Thickness, birefringence and the orientation of a sample affect the interference colors. The colors vary between white, gray, red, yellow, blue and their combinations. (Carl Zeiss 2001)

Some characteristics that can be identified by a polarized light optical microscope include morphology, transparency, reflectivity, color, pleochroism, fluorescence and refractive index or indices of a sample. Polarized light is light that is essentially vibrating in only one direction. To be able to detect birefringence, an optical microscope must be equipped with two polarizers. The vibration directions of the polarizers must be 90 degrees in relation to one another. The second polarizer is also known as analyzer. In order for a material to exhibit birefringence it must be anisotropic, since isotropic materials only have one refractive index. (Delly 2008) Figure 8 illustrates the principle of how a polarized light optical microscope functions.

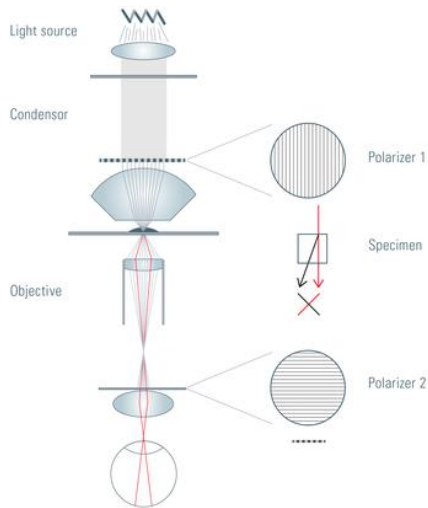


**Figure 8.** Principle of a polarized light optical microscope (Ockenga 2011).

Unpolarized light travels through the first polarizer and then the condenser focuses the polarized light on the sample. Birefringent samples cause a portion of the light's polarization plane to twist by 90 degrees, illustrated by the red lines in the figure. Objective magnifies the image of the sample and the light passes the analyzer. If the analyzer is configured to be in a position of 90 degrees relative to the first polarizer, only the light that passes through birefringent material can be seen in the image. (Ockenga 2011)

### 2.3.2 Differential scanning calorimetry

DSC is a method of thermal analysis where the temperature difference between the reference and a sample is measured against time (isothermal) or temperature (scanning). The temperature conditions are controlled. Heat flux is calculated as energy input per unit of time. The change in the heat flux is proportional to the temperature difference. The measuring cell of a heat-flux DSC system is illustrated in Figure 9. It consists of a furnace and holders for a reference material and a sample material. The reference material is thermally inert over the experiment's temperature range. Thermocouples that measure the temperature difference between the reference and the sample are connected to the base of the reference and sample holders. The temperature of the furnace and the heating block under the reference and sample holders is measured by a second set of thermocouples. (Hatakeyama & Quinn 1999)

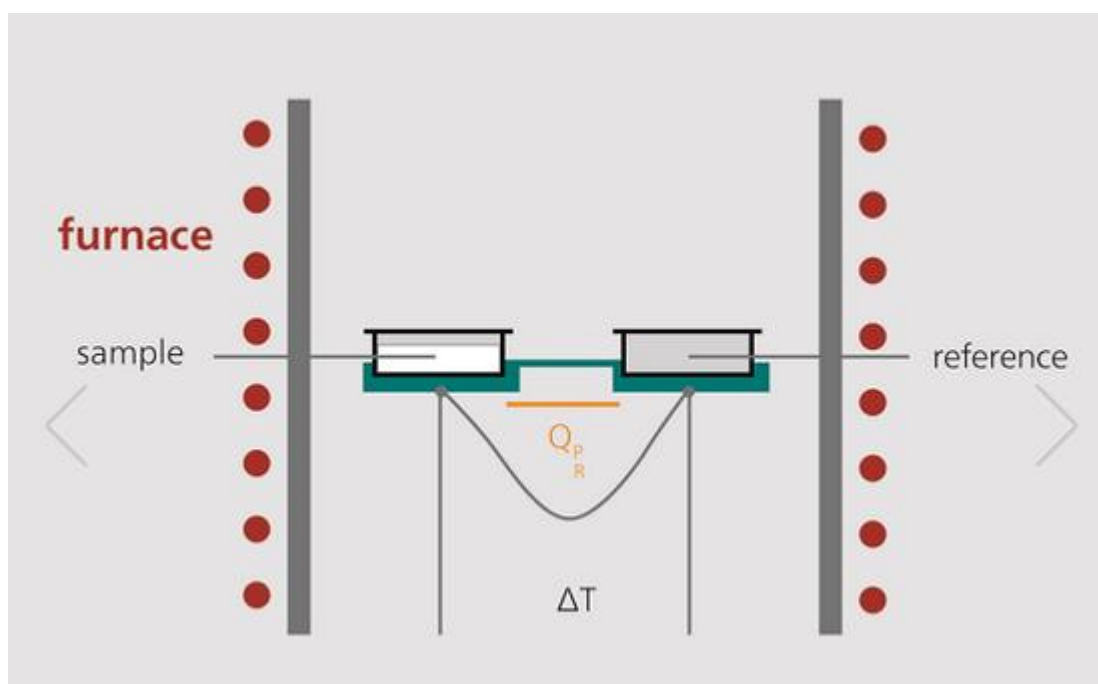


**Figure 9.** The measuring cell of a heat-flux DSC system (Netzsch 2016).

Heat is applied to the measuring cell at a programmed rate, leading to uniform increase of the temperature of both reference and sample. A phase change in the sample releases or absorbs heat which causes variations to the heat flux through the heating block. This results in an incremental temperature difference between the furnace and the heat-sensitive plate which can be measured. Enthalpy of transition can then be estimated from the incremental temperature fluctuation. (Hatakeyama & Quinn 1999) A constant-an body that is connected to the base of a silver measuring chamber allows conditioned purge gas to flow through the system. Nitrogen is often used. DSC consists of two calorimeters, one for the sample and one for the reference. Sample calorimeter consists of the sample and a pan while the reference calorimeter usually consists of an empty pan. (Wunderlich 2005)

Sample masses can vary between 0.05 and 100 mg depending on the goal of the study. Small masses are used to determine large heat effects such as phase transitions or chemical reactions. Glass transition and heat capacity measurements utilize larger sample masses. (Wunderlich 2005) Hatakeyama and Quinn (1999) suggest that the sample should weigh less than 10 mg and that it should be placed uniformly on the base of the sample crucible to achieve optimum results.

DSC curves typically have a baseline and various peaks of endo- or exothermic processes. There are also characteristic temperatures which can be differentiated from the curves, such as the beginning of melting, the peak temperature and the end of melting where the curve returns to the baseline. The point where melting begins is dependent on the sample purity and the equipment's sensitivity among others. A broad melting range is often characterized by a peak melting temperature, where the melting rate is the high-



est. A DSC-curve for a 10 mg sample of PET in nitrogen atmosphere is illustrated in Figure 10. (Wunderlich 2005)

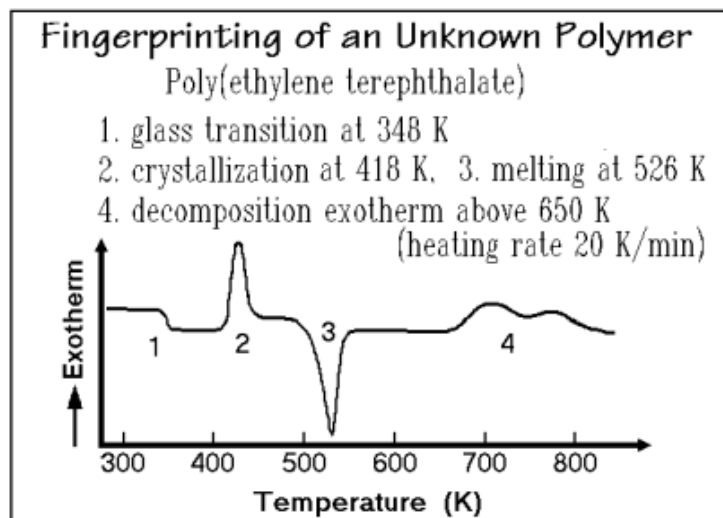


**Figure 10.** Fingerprinting of an unknown polymer, DSC curve for PET (Wunderlich 2005).

Fingerprinting of a polymer refers to identifying them by inspecting their characteristic phase transitions or chemical reactions. Typical exothermic reactions for polymers that can be seen in Figure 10 include the glass transition (1), crystallization (2) and decomposition (4), while melting (3) is endothermic. The baseline shifts towards the crystalline level after crystallization. (Wunderlich 2005)

Polymers have thermal histories that influence the characteristic temperatures for crystallization and melting. Thermal history can be a result of processing, ageing, curing and/or annealing among others. Due to the thermal history an extra heating cycle is often recommended to remove the previous thermal history from a sample. During this cycle the sample is heated above its  $T_m$ . Care must be taken so that the sample doesn't decompose or sublime due to prolonged exposure to high temperature. (Hatakeyama & Quinn 1999)

### 2.3.3 Fourier transform infrared spectroscopy

IR spectroscopy measures a material's IR radiation transmission or absorption as a function of wavelength or frequency. An IR spectrum consists of a plot of absorption/transmission against wavelength/frequency. Functional groups within a molecule vibrate and these vibrations can be associated with absorption bands. Identifying these bands can be used to identify particular molecules that construct a material. FTIR can be used to analyze various types of samples, including solids, gases, liquids, powders and thin films. Identifying functional groups in organic polymers is one of the possible applications. Reflectance spectroscopy can be used for samples that are highly absorbent,

typically opaque solids. Transmission spectroscopy can be used for weakly absorbing samples. (Gaffney et al. 2012)

The IR spectral region spans from the wavelength of 0.78 to the wavelength of 1000  $\mu\text{m}$ . This spectral region can be further divided into near infrared NIR (0.78–3.0  $\mu\text{m}$ ), mid-infrared MIR (3.0–50  $\mu\text{m}$ ) and far infrared FIR (50–1000  $\mu\text{m}$ ) spectral regions. When operating in the MIR region, wavenumber [ $\text{cm}^{-1}$ ] is commonly used instead of wavelength. The range of MIR spectral region in wavenumbers corresponds to 4000–200  $\text{cm}^{-1}$ . (Gaffney et al. 2012)

IR radiation absorption leads to transitions between a molecule's quantized vibrational energy states. A molecule exposed to IR radiation absorbs an equal amount of energy from the radiation that is required for a vibrational transition of the molecule. The shape of an IR absorption band is dependent not only on the vibrational energy transitions but also on rotational energy states. Geometry and force constants of a molecule's bonds in addition to the relative masses of the atoms within the molecule are responsible for the wavelength of absorption. The bonds within a molecule restrict the vibrational motions of the atoms. Transition from the vibrational ground state to the lowest energy vibrational state is known as the fundamental transition. The fundamental transition is typically observed for most molecules in the MIR spectral region due to its intensity. (Gaffney et al. 2012)

All absorption bands cannot be observed in an IR absorption spectrum due to limiting factors such as non-IR active bands, very low intensity bands and band degeneracies. For a molecule to be IR-active, a change in dipole moment is required, which in turn requires a molecule to have more than two atoms or the molecule to be asymmetric. A molecule may possess multiple normal modes of vibration that appear at the same energy, generating absorption bands at identical frequencies. These degenerate modes have the appearance of a single band in an IR absorption spectrum. (Gaffney et al. 2012)

The most common application of FTIR is the identification of compounds. IR spectrums of unknown materials may be compared with those of known materials that possess similar structures. Structure of an unknown material can be identified by combining the known frequencies of certain functional groups. Functional groups which consist of bonded groups of atoms absorb IR radiation in a frequency range that is characteristic to each functional group. The locations of functional groups within a molecule do not affect the characteristic frequency ranges and neither does the chemical environment of a functional group. 4000–1300  $\text{cm}^{-1}$  is the typical range for many fundamental vibrational transitions of functional groups. 1500–1300  $\text{cm}^{-1}$  is known as the fingerprint region due to the fact that the peaks there are often due to individual compounds. (Gaffney et al. 2012) Infrared bands for polymers are illustrated in Figure 11.

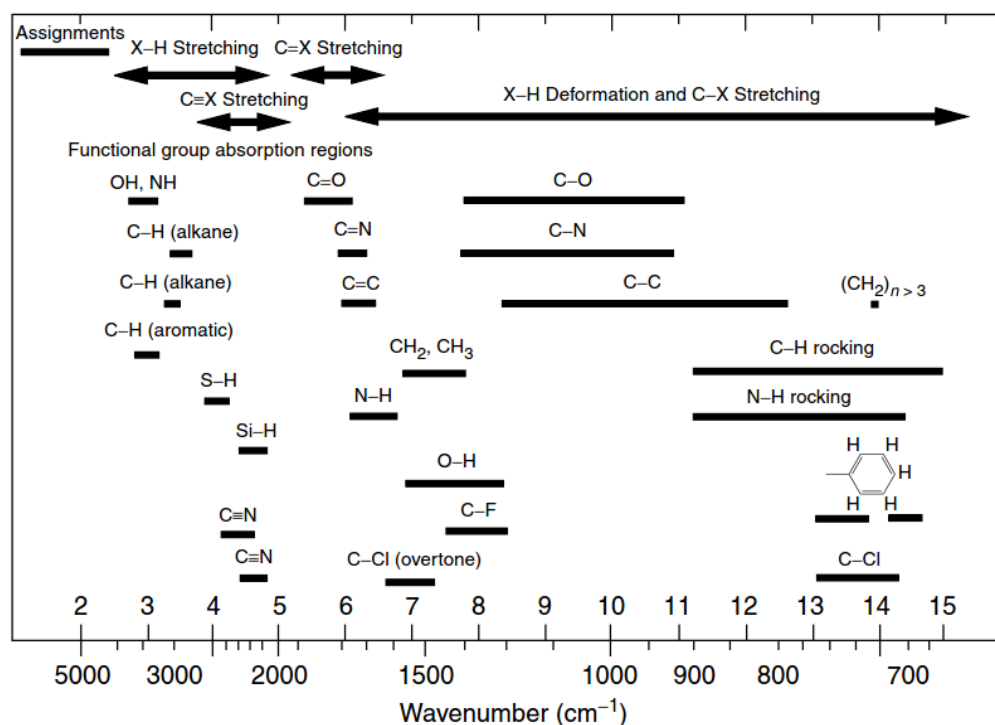


**Figure 11.** Infrared bands of polymers (Stuart 2004).

An optical spectrometer comprises of a spectral analyzer, a radiation detector, a source for electromagnetic radiation and optical elements that direct the beams. FTIR instruments also employ interferometers to determine interferograms. Interferogram is a plot of retardation against the detector signal. A Fourier transform is applied on the interferogram for the IR spectrum. The optical elements of an IR device are responsible for directing the beam from the source through the interferometer, focusing it on the sample, collecting the beam and then refocusing it on the detector. These tasks are accomplished by employing off-axis parabolic mirrors. The IR detectors convert the measured intensity of radiation into an electrical signal which is then processed into a spectrum. Thermal and quantum detectors exist, with thermal detectors being the more common ones in the MIR region. (Gaffney et al. 2012)

Figure 12 illustrates a basic design of an interferometer employed in modern FTIR instruments. M1 denotes a fixed mirror, M2 a movable mirror, BS a beam splitter and D detector. Half of the radiation is directed by the beam splitter to M1 and half to M2 and then recombined through the beam splitter on the mirror next to the detector. The detector signal will be at its maximum when the two paths (a) and (b) are equal. Several factors influence the final quality of the IR spectrum including mirror velocity, spectral resolution, background correction, signal averaging, apodization and phase correction. Spectral resolutions of 4 or 8  $\text{cm}^{-1}$  are often used for solids and liquids in FTIR. (Gaffney et al. 2012)

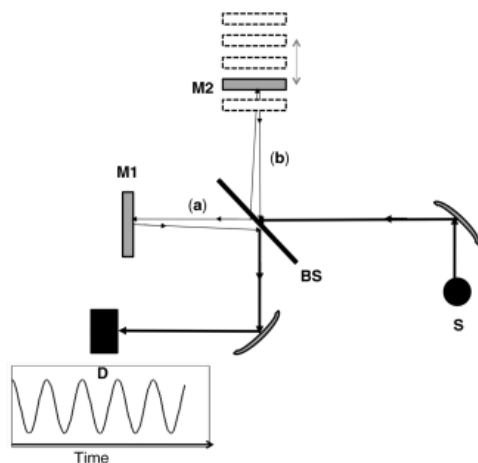


**Figure 12.** Basic design of a "Michelson" interferometer (Gaffney et al. 2012).

An IR spectrum may be processed for ease of analysis and interpretation. A baseline correction can be applied to a spectrum so that the baseline lies at zero absorbance or transmittance. Spectral smoothing can be used to manipulate the signal-to-noise ratio before obtaining the spectrum or by mathematical smoothing after the spectrum has been obtained. Peak fitting separates overlapping bands, but the knowledge of the amount of overlapped bands and their locations is required for successful utilization of peak fitting. (Gaffney et al. 2012)

Each polymer's IR spectrum has various characteristic peaks, which can be analyzed to identify the correct polymers or polymer blends. PE's strongest vibrations occur at 2927, 2852, 1475, 1463, 730, and 720  $\text{cm}^{-1}$ . Weaker vibrations in the fingerprint region occur at 1370, 1353 and 1303  $\text{cm}^{-1}$ . LDPE, LLDPE and HDPE can be further differentiated from an IR spectrum due to small differences in the spectra. LDPE has three peaks in the 1400–1330  $\text{cm}^{-1}$  range while HDPE only has two, lacking the 1377  $\text{cm}^{-1}$  peak. LLDPE exhibits two peaks at 890 and 910  $\text{cm}^{-1}$  which are weak and almost equal in intensity while LDPE only has the 890  $\text{cm}^{-1}$  peak. LLDPE can be polymerized using various comonomers; however the most common is butene-1. This type of LLDPE produces a peak at 775  $\text{cm}^{-1}$ . (Lobo & Bonilla 2003)

Ethylene-propylene copolymers have characteristic peaks at 1150.7 and 936.7  $\text{cm}^{-1}$  due to methyl branching. Use of 4-methyl-pentene-1 comonomer produces peaks of 1383 and 1370  $\text{cm}^{-1}$ , the latter overlapping the 1368  $\text{cm}^{-1}$  peak. Ethylene-propylene copolymer's IR spectrum reflects the respective amounts of the two polymers present. Characteristic peaks of each polymer differ in intensity in relation to the amount of polymers present, which leads to the features of the major component showing prominence. This is illustrated in Figure 13. Isotactic PP has crystallinity sensitive characteristic peaks at 1167, 998, 899 and 842  $\text{cm}^{-1}$ . Peaks at 948, 844 and 810  $\text{cm}^{-1}$  are associated with isotacticity. Due to lack of crystallinity, atactic PP doesn't have peaks at 1167, 998 or 875  $\text{cm}^{-1}$ . (Lobo & Bonilla 2003)

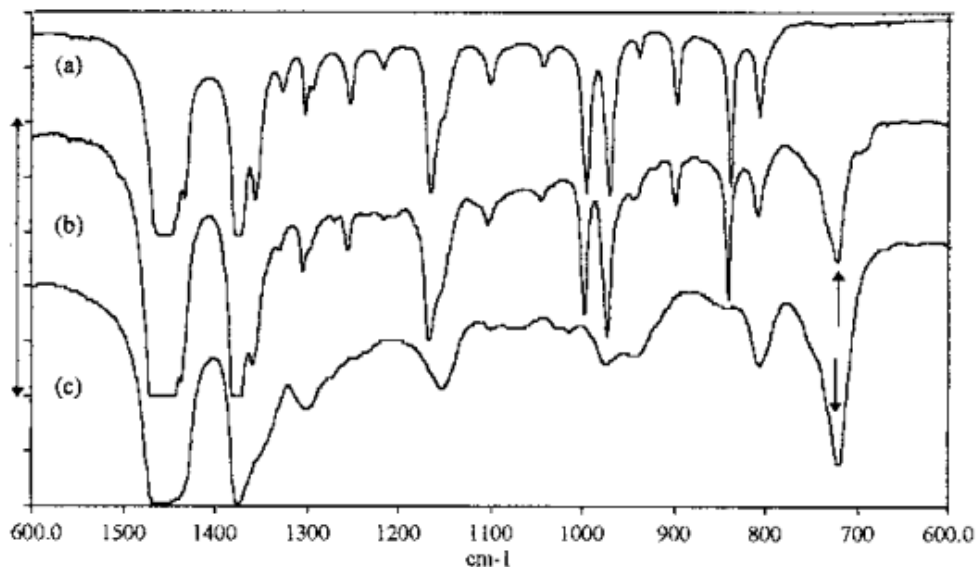


**Figure 13.** Ethylene-propylene copolymer with varying amounts of ethylene: (a) 0 %, (b) below 10 % and (c) 68 % (Lobo & Bonilla 2003).

PAs have characteristic peaks associated with amine groups at 3300, 3050, 1630 and 1550  $\text{cm}^{-1}$ . Each type of PA also has its own characteristic peaks in the fingerprinting region, which are 1465, 1265, 960 and 925  $\text{cm}^{-1}$  for PA-6, 1480, 1280 and 935  $\text{cm}^{-1}$  for PA-66, 1480, 1245 and 940  $\text{cm}^{-1}$  for PA-6,10 and 1475, 940 and 720  $\text{cm}^{-1}$  for PA-11. PET has a large amount of characteristic peaks due to both ester functionality and aromatic rings. These include 3054, 1718, 1615, 1578, 1505, 1126, 1099, 1021, 848 and 728  $\text{cm}^{-1}$ . Peaks at 1340, 1280, 1260, 1020 and 988  $\text{cm}^{-1}$  are associated with the crystallinity of PET. (Lobo & Bonilla 2003)

## 2.4 Compatibilization

Polymer blends are very often immiscible and to improve their performance, compatibilization is required. Compatibilization aims to solve three problems in the blending of polymers: morphology stability, degree of dispersion and solid state adhesion between phases. (Utracki 2003)

Interfacial tension between polymers can be reduced by compatibilizers. Block or random copolymers can contain two functionalities, each miscible with one of the blended polymers. Functional groups that react with a specific polymer may also be added to the compatibilizers. (Morris 2010) The goal of these copolymers is to reduce the interfacial tension and the size of the dispersed particles. Too high concentration of these copolymers may cause the formation of unwanted micelles. (Utracki 2003)

Immiscible two-component polymer blends may be compatibilized by exploiting a co-solvent – usually a polymeric substance that is miscible with both of the immiscible polymers. It induces interactions between the polymers, leading to a compatibilized two-phase structure. Common co-solvents include polymethylmethacrylate (PMMA), polyphenyl ether (PPE), phenoxy, polycaprolactone (PCL) and polycarbonate (PC). Adding too much co-solvent may lead to a miscible blend, reducing the mechanical performance of the blend. Typical amount of a co-solvent is 0.5–2 weight-% of the blend. Degree of dispersion can be improved by introducing a third immiscible polymer to a two-component immiscible polymer blend. This is due to the reduction of coalescence of the dispersed phase attributing to the migration of the immiscible third polymer to the interface between the two main resins. (Utracki 2003)

### 2.4.1 Blending and miscibility

Polymer blending is used to improve processing, enhance properties or to reduce overall costs. Final properties of a blend are dependent on the flow and stress history. Ingredients in polymer blends include additives, pigments and various polymers. (Morris 2013) Factors that determine which polymer will be the matrix or the dispersed phase include relative viscosities and relative volume proportions of the polymers. The more viscous polymer is more likely to form the dispersed phase of the blend. (Utracki 2003)

A polymer blend is immiscible if the blended polymers form multiple phases over their entire composition at a specified temperature. Immiscibility of many polymer blends causes the minor component(s) in a polymer blend to form a separate dispersed domain or phase within the polymer matrix. Blends can be mixed via distributive or dispersive mixing. Distributive mixing rearranges and separates the flow and utilizes kneading, whereas dispersive mixing breaks up the particles by utilizing shear stress. Blending can be used to introduce tailored properties such as barrier properties to layers in a multi-layer structure. It may also be exploited in improving processability by blending miscible polymers with dissimilar flow properties together. Typical example of this is blending LDPE into LLDPE. (Morris 2010)

Microscopy, various spectroscopy techniques, X-ray, neutron scattering, DSC and other thermal analyses can be used to determine the miscibility of a blend. In microscopy, large separate domains in a matrix that diffract light means that the blend is immiscible. DSC can be used to measure the  $T_g$  of a sample. A blend is miscible if only one  $T_g$  is present. The blend is partially miscible or immiscible if there are two or more glass transition temperatures. The glass transition temperatures in the cases of partial miscibility and immiscibility are different than the  $T_g$  values for the pure components. (Morris 2010; Sharma 2011)

Solubility parameter can be used to predict the miscibility of polymers to an extent. Miscibility of low molecular weight distribution additives in polymers may also be pre-

dicted. The compatibility is better when the solubility parameters of two polymers are close to each other. Solubility parameter is the square root of cohesive energy density. Cohesive energy density describes the forces required to hold the material together. Both polar and non-polar interactions contribute to the cohesive energy. Polymers may be miscible below critical solubility parameter difference, which is dependent on the present polar and non-polar interaction forces. (Morris 2010)

Examples of polymer blends include added rubber in PA for better low temperature toughness, cyclic olefins in aliphatic polyolefins to improve stiffness, HDPE in LDPE/LLDPE for moisture barrier, amorphous PA in PA-6 for better oxygen barrier at high relative humidity and EMA/EVA in PE for better adhesion to specific inks. (Morris 2010)

Pellets can be pre-mixed before processing in either an in-line mixer or in an off-line batch mixer. Batch mixers can feed more than one extruder. In-line mixer has an individual feeder for each ingredient and is usually positioned above the extruder hopper. Feeders can be either volumetric or gravimetric where gravimetric ones are more common. In-line mixers benefit from the ability of changing ingredient proportions during processing, but batch mixers are more inexpensive. (Morris 2010)

In extrusion, mixing elements in the screw design may be utilized to improve mixing. These elements include designs such as restriction rings and pins. Saxton, Maddock, Dulmage and pineapple are more specialized designs. Pins, kneaders and Saxton mixers are used for distributive mixing, while Maddock is used for both dispersive and distributive mixing. Twin-screw extruders are often used for compounding. (Morris 2010)

## 2.4.2 Incorporation of specific interacting groups

Minor amounts of specific interacting groups can be incorporated into a polymer blend thus improving the miscibility, dispersion and mechanical properties. These specific interactions include hydrogen and  $\pi$ -hydrogen bonding,  $n$ - $\pi$  and  $\pi$ - $\pi$  complexes, charge transfers and acid-base, dipole-dipole, ion-dipole and ion-ion interactions. Hydrogen bonding involves the interaction of two groups with one being an electron donor and the other an electron acceptor. Strong electron donors include anhydrides, tertiary amines, pyridine and sulfoxides. Some groups have the potential to be either electron donors or acceptors. When a stronger donor or acceptor is subjected to an interaction with a weaker donor or acceptor, the stronger one will retain its characteristic donor or acceptor behavior. (Robeson 2007)

Dipole-dipole interactions are typically weaker than hydrogen bonding. The specific interaction in this case is improved by the presence of strong dipole moments. Polar polymers and ionic polymers have the possibility for ion-dipole and ion-ion interactions. Examples of incorporating specific interacting groups include compatibilization

of PVOH (polyvinyl alcohol) and PE with the introduction of acrylic acid groups into PE and vinyl amine groups into PVOH. While PE and PVOH are normally immiscible, incorporating these groups makes the blend partially miscible and improves the mechanical properties significantly. (Robeson 2007)

### 2.4.3 Ternary polymer addition

This nonreactive method of compatibilization involves the addition of a ternary polymer into a binary polymer system, where the two main polymers are immiscible. The objective of the ternary polymer is to stabilize the interfacial area by providing an interfacial adhesion to both components and concentrating at the interface of the two immiscible polymers. This leads to better stress transfer across the interface and smaller particle size. Random copolymers, graft copolymers and polymers with good interfacial adhesion or miscibility to the blend components may be used in a ternary polymer system. The random copolymers comprise of structural units that are similar or the same as the blend components. Another possibility is utilizing specific interacting groups mentioned in Section 2.4.2 that have the capability of nonreactive interaction with at least one of the blend components. (Robeson 2007)

Graft copolymers utilized in ternary polymer addition consist of a main chain and a graft, each often being the respective immiscible polymers in the binary polymer system. The main chain or the graft may also be a polymer that exhibits good interfacial adhesion or miscibility to at least one of the components in the binary polymer system. An example of a ternary compatibilizer is EVA used in a system of PA-6 and LDPE leading to an improvement of toughness and dispersion. (Robeson 2007)

Block copolymer addition is a subset of the ternary polymer addition. In this method, the blocks of the copolymer consist of the same or similar components to those used in the binary polymer blend. Like in ternary polymer addition, the block copolymer concentrates at the interface of the two immiscible polymers. An example of this compatibilization method is adding SEBS (styrene ethylene butylene styrene) block copolymer to a blend comprising of PS and a polyolefin, improving the mechanical properties greatly. (Robeson 2007)

Addition of a block copolymer reduces the interfacial tension between immiscible polymers leading to an increased interface width and dispersion of phases, which in turn promotes adhesion. Block copolymer chains also reinforce the interface mechanically by joining the immiscible phases together. The degree of reinforcement depends on the molecular weight of the block polymer and the block copolymer's areal chain density at the interface. (Sabu et al. 2005) It has been demonstrated that fracture toughness increases by increasing interfacial width (Schnell & Stamm 1998).



#### 2.4.4 Polymer-polymer reactions

Typically phase separated polymers can be compatibilized and even be made miscible by polymer-polymer reactions. Most common reactions are transesterification and transamidation. Elevated temperature and longer reaction time during melt mixing promotes transesterification. Polycarbonates, polyesters and polyarylates demonstrate transesterification with polymers containing hydroxyl, resulting in cross-linking and miscibility. Esterification catalyst can be used in some blends such as PLLA (poly-L-lactic acid)/EVOH to achieve transesterification. Sometimes transesterification is unwanted due to a decrease in crystallinity and/or rate of crystallization and transesterification inhibitor agent can be used. (Robeson 2007)

PAs exhibit transamidation, which can result in a lower crystallinity and rate of crystallization on crystalline PAs in addition to improved miscibility. Transamidation occurs between different types of PA, such as PA-6 and PA-66. Other types of polymer-polymer reactions include ester-amide interchange between PET and PA-66 and acid-amine interchange between SAA (styrene-acrylic acid) and PAs. (Robeson 2007)

#### 2.4.5 Reactive compatibilization

Reactive compatibilization is a method where a compatibilizing copolymer (block, crosslinked, graft) is synthesized and added to the polymer blend during a molten state processing step such as extrusion. One advantage of reactive compatibilization is the automatic formation of the copolymer at the interface between two immiscible polymers, stabilizing the morphology. Another advantage is that the copolymer's two distinctive polymer segments generally have the same molecular weight as each individual bulk polymer phase, in which the corresponding segments must dissolve. This leads to optimal interfacial adhesion of the polymer blend. (Utracki 2003)

Several methods are available for the formation of a copolymer in extruding process. The most common ones include graft copolymer formation, producing block and random copolymers by redistribution, block copolymer formation, copolymer forming via covalent crosslinking and ionic bond formation. Coupling agents may be utilized to link two end-groups, whereas condensation agents are used to activate a reactive functionality of one polymer, thus making the reaction with the second polymer more efficient. Occurrence of a degradative process is possible in block copolymer formation, redistribution process and graft copolymer formations. (Utracki 2003)

Graft copolymer formation's direct process involves the reaction of the reactive sites of the two polymers, where one polymer's reactive sites lie at end-groups and the other's along its main chain. The obtained copolymer's molecular weight is the average of the two reacting participants. Degradative variant of graft copolymer formation has multiple reactive sites on one polymer chain, which react with the linkages of the second poly-

mer chain. The molecular weight of a copolymer created this way is less than the average of the participants, potentially leading to insufficient physical properties. (Utracki 2003)

Producing block and random copolymers by redistribution reactions is achieved by chemically interchanging block segments of a polymer chain for the segments that correspond with the second polymer chain. This type of copolymer formation is common for polymers produced via condensation such as PA and PC. For the best compatibilization a high degree of block copolymer formation and thus minimizing random copolymer formation is desired. Controlling a thermally initiated redistribution process is extremely important, whilst prolonged reaction times combined with too high a temperature might lead to random copolymer formation. Catalyst initiation may sometimes be utilized to control the process, quenching the catalyst after a desired point. Molecular weight distribution of the formed block copolymer varies between segments, with at least one segment of the initially formed block copolymer having a lower molecular weight than the original bulk polymer phase. (Utracki 2003)

Compatibilizing a polymer blend via block copolymer formation exploits functionalized end-groups on some chains of each of the polymer. The end-groups form a block copolymer by reacting across a melt phase boundary, resulting in A-B-A, A-B or a combination of these block copolymer structures. Resulting copolymer has an average molecular weight that corresponds with the reacting polymers' sum of average molecular weights. Another method to produce a block copolymer involves using a condensing agent, which activates an end-group of one polymer for reacting with a nucleophilic end-group of the second polymer. Phosphite esters that react with condensation polymers' hydroxy and acid end-groups are typically used. Condensation agents form by-products that are often removed via devolatilization of the molten blend. Coupling agents that are incorporated into the copolymer, such as carbodiimides, isocyanates, multifunctional epoxy resins and oxazolines, may also be used to form block polymers. Degradative variant of the block copolymer formation involves transreaction between linkages in the main chain on one polymer and the end-groups of the second polymer. Resulting block copolymer has a lower average molecular weight compared to the conventional block copolymer formation processes. (Utracki 2003)

Crosslinked copolymers may be utilized as compatibilizing agents for compatibilizing immiscible polymer blends. In a common crosslinking method functionalities on two polymers can be crosslinked directly by covalent bond formation without degradation. In this method the pendent, electrophilic sites react with the pendent, nucleophilic sites of each polymer. Less common method uses radical generation and recombination between two immiscible polymers to achieve covalent bonds. Crosslinking may also be generated by a third reagent, which acts as a condensing or coupling agent or as an activator. Ionic crosslinking is a less frequently used method, where instead of covalent

bonding ionic bonding happens. It requires the polymers to have ionizable groups such as phosphonic, carboxylic or sulfonic acid. (Utracki 2003)

#### **2.4.6 Compatibilization of recycled & commingled polymers**

Post-consumer polymeric waste (PCW) contains metals, heavy elements, paper and other impurities mixed with polymers. To produce plastics with good performance, the waste must be sorted, washed, impurities removed and afterwards dried and grounded. PCW can be recycled either in solid or molten state. It's possible to achieve adequate compatibilization by using intensive mechanical mixing. During intensive mixing, free radicals are generated via mechano-chemical means. The recombination of these free radicals produces a copolymer for the compatibilization of the system. Different methods of mechanical mixing include ball-milling and solid-state shear extrusion. (Utracki 2003)

Stabilizers are usually incorporated into the polymer blend during the first compounding and forming cycle. Recycled polymer blends must be re-stabilized – there may be residues from the earlier stabilizers that react with the new stabilizers and stabilizer deactivation products, which must be taken into account. Stabilizing a system comprising of multiple polymers is particularly challenging due to a stabilizer having a positive effect on one polymer having a detrimental effect on another. (Utracki 2003)

Polymer families with similar chemical structures, such as polyolefins and styrenics, require less compatibilization than if they are reprocessed with polymers of the same chemical family. When combining different polymer families, e.g. PAs with polyolefins, extensive compatibilization is required. Impact modification and ‘molecular repair’ might also be needed due to degradation of the polymers. (Utracki 2003)

Commonly used compatibilizers include PE and PP grafted with reactive maleic anhydride. Grafting maleic anhydride into these basic polymers provides reactive sites for other polymers to interact with, which in turn leads to hydrogen or covalent bonds. A maleic anhydride grafted polymer has both carboxyl and anhydride groups. The compatibilization is often carried out during melt processing in the presence of peroxide initiator. Peroxide is unnecessary when a polymer is unsaturated. The reaction of a polymer, maleic anhydride and peroxide has been used in compatibilizing polymer scrap consisting of multiple incompatible polymers. (Salamone 1999)

SEBS and styrene butadiene rubber (SBR) have been found to be effective in compatibilizing blends of polyolefins and styrenics. Polar polymers such as PA and ABS have been compatibilized by two copolymers as compatibilizers, which contain anhydride and vinyl alcohol respectively. A commingled polymer blend comprising of PET, PE, PP, PVC and PS has been compatibilized using either maleated SEBS or HDPE. Reactive compatibilizers are usually taken advantage of when compatibilizing commin-

gled polymer waste. Use of a toughening agent is often advisable because of the brittleness due to degradation and immiscibility. (Utracki 2003) PP and PET have been effectively compatibilized with maleated SEBS (Tekkanat et al. 1993).

### 3. THE SAMPLE POOL

A total of 121 samples of recycled plastic multilayer films were a part of this analysis after the initial screening of the sample pool by Arcada University of applied sciences. The samples examined in this thesis represent a larger amount of samples. The samples were analyzed by optical microscope (OM) and FTIR in addition to 77 DSC measurements on samples with undefined composition. The composition of samples 1-37 were identified from the packages. An article related to the origin of these samples is due to be published later this year. Table 4 contains the analyzed samples. Initial known material combinations have been presented in addition to the various package types and how many samples have been analyzed by OM and DSC.

**Table 4.** *The sample pool (Original table provided by Arcada University of applied sciences).*

Sample number	Material combination	Package type	OM samples	DSC samples
1	PE/PP	Processed meat	1	0
2	PE/PP	Processed meat	1	0
3	PE/PP	Frozen product	1	0
4	PE/PP	Frozen product	2	0
5	PE/PP	Frozen product	1	0
6	PE/PP	Dry product	2	0
7	PE/PP	Dry product	1	0
8	PE/PP	Dry product	3	0
9	PET/PE	Convenience food	1	0
10	PET/PE	Processed meat	1	0
11	PET/PE	Processed meat	2	0
12	PET/PE	Dry product	1	0
13	PA/PE	Processed meat	1	0
14	PA/PE	Processed meat	1	0
15	PA/PE	Processed meat	1	0
16	PA/PE	Cheese	1	0
17	PA/PE	Cheese	1	0
18	PA/PE	Varied	1	0
19	PA/PP	Chilled product	1	0
20	PA/PP	Fresh meat	1	0
21	PET/PP	Chilled product	1	0
22	PET/PP	Chilled product	1	0
23	PET/PP	Fresh meat	1	0
24	OPP	Convenience food	1	0

25	OPP	Dry product	2	0
26	PA/PP/PE	Processed meat	2	0
27	PA/PP/PE	Dry product	1	0
28	PET/PA/PE	Cheese	1	0
29	PET/PA/PE	Convenience food	1	0
30	PET/PE/ PP	Varied	1	0
31	PET/PE/ PP	Fresh meat	1	0
32	PA/PE/ EVOH	Fresh meat	1	0
33	PET/PE/ EVOH	Processed meat	1	0
34	PE/PP/PA/EVOH	Processed meat	1	0
35	PE/PP/PA/EVOH	Processed meat	1	0
36	PE/PP/PA/EVOH	Processed meat	1	0
37	PET/PE/PA/EVOH	Processed meat	1	0
38	Undefined	Frozen product	1	1
39	Undefined	Frozen product	3	3
40	Undefined	Frozen product	2	2
41	Undefined	Dry product	2	2
42	Undefined	Dry product	5	5
43	Undefined	Dry product	2	2
44	Undefined	Dry product	2	2
45	Undefined	Dry product	3	3
46	Undefined	Fresh meat	3	3
47	Undefined	Fresh fish	2	2
48	Undefined	Processed meat	3	3
49	Undefined	Processed meat	2	2
50	Undefined	Fresh meat	3	3
51	Undefined	Processed meat	1	1
52	Undefined	Processed meat	1	1
53	Undefined	Processed meat	1	1
54	Undefined	Milk products	1	1
55	Undefined	Chilled product	1	1
56	Undefined	Processed meat	1	1
57	Undefined	Processed meat	2	2
58	Undefined	Processed meat	1	1
59	Undefined	Convenience food	3	3
60	Undefined	Cheese	1	1
61	Undefined	Cheese	1	1
62	Undefined	Cheese	1	1
63	Undefined	Cheese	1	1
64	Undefined	Cheese	1	1
65	Undefined	Cheese	2	2

<b>66</b>	Undefined	Cheese	1	1
<b>67</b>	Undefined	Cheese	2	2
<b>68</b>	Undefined	Cheese	1	1
<b>69</b>	Undefined	Cheese	1	1
<b>70</b>	Undefined	Cheese	3	3
<b>71</b>	Undefined	Transparent	17	17
<b>Total</b>			<b>121</b>	<b>77</b>

In total there were 10 frozen product package samples, 4 chilled product packages, 27 processed meat packages, 12 fresh meat/fish packages, 24 dry product packages and 18 cheese packages. The rest of the packages were labeled under miscellaneous. The material proportions for every package type are calculated in Section 5.3.

## 4. RESULTS FROM THE COMPOSITION ANALYSIS METHODS

This section covers the preparation of samples and the measurement data gathered by optical microscopy, DSC and FTIR. The data is further analyzed in Chapter 5. Cross-sections by optical microscopy provided for thicknesses and amounts of layers in multi-layer film samples. DSC was used to ascertain the composition of samples with unknown composition. FTIR data was used to identify the top and bottom layers from each sample. All cross-section images by microscope can be found in APPENDIX A: Cross-section figures. 14 DSC figures and 16 FTIR spectra can be found in Appendixes B and C respectively. Only the most common DSC figures and FTIR spectra are listed in the appendixes.

In both the cross-sections by optical microscopy and FTIR, the top side of a sample can be identified as the side with a print, essentially what a customer sees on a package. Bottom side is the inner side of the package that is in direct contact with the packaged goods. This does not necessarily hold true for the transparent samples labeled as 71- due to the fact that there was no printing left to determine the top side of a sample.

### 4.1 Cross-section images from polarized light optical microscopy

The microscope samples were prepared and analyzed at Tampere University of Technology (TUT). The microscope for producing the cross-section images of samples was Zeiss Axioskop 40 equipped with Axiocam MRC camera. A piece of tape was applied on the bottom side of a cut sample and two pieces of tape were applied on the top side of the sample to make the top and bottom sides easier to distinguish under microscope. The sample was then inserted in the microtome between two flat silicone pieces. Sample was trimmed with a Microm HM 325 microtome and then an impression of the cross-section was produced on the adhesive side of the tape by pressing hard on the trimmed sample. A droplet of oil was applied on a microscope slide, the impression tape placed on the oil and then another droplet of oil was applied on top of the impression tape. The slide was then covered with a glass cover slip and analyzed with AxioVision 3.1 software. 400 fold magnification of the samples resulted in measurements in the micrometer region.

Samples 1–37 with known material combinations were first analyzed to match the correct interference colors of the various polymers in the multilayer film cross-sections. A



simple cross-section of sample 1 is illustrated in Figure 14. The brown and/or blue layers above and below the annotations are from the tape and tape adhesive respectively. The lower blue and brown tape layers have been removed from the images if it was possible so that only the plastic layers are visible. The top layer of a multilayer film is always the topmost layer in a cross-section and the bottom layer is at the bottom of the image above the blue tape adhesive layer (if visible). The multilayer film in Figure 14 consists of five layers: a 19.57  $\mu\text{m}$  thick top layer made of PP, 6.07  $\mu\text{m}$  print layer, 30.04  $\mu\text{m}$  LDPE layer, 3.37  $\mu\text{m}$  tie layer and a 23.29  $\mu\text{m}$  LDPE layer. After several analyses of the various cross-sections the most common interference color of PE was determined to be hues of brown while PP had an interference color of a darker shade of brown or a grayish.

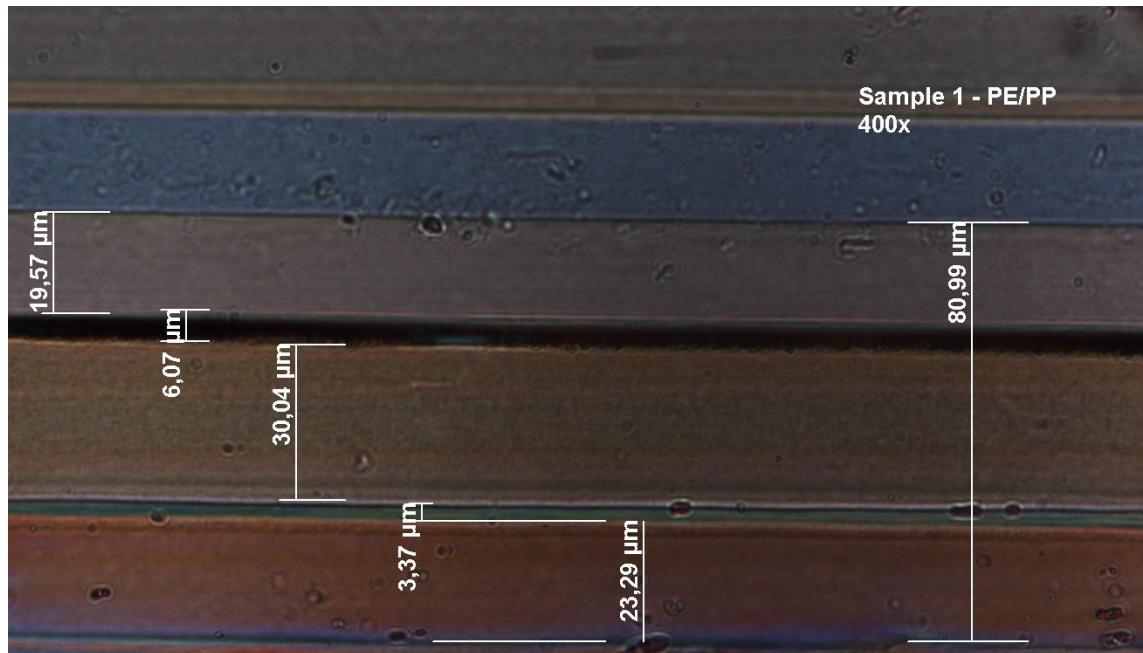


**Figure 14.** Cross-section of sample 1.

The interference color of PA-6 was identified to be often greenish or blueish with many variations. Sometimes PA-6 occurred in a shade of gray. An example of the green shade can be seen in the cross-section of sample 15 in Figure 15. Some examples of the other interference colors of PA-6 can be seen in the cross-sections of samples 13 and 32.

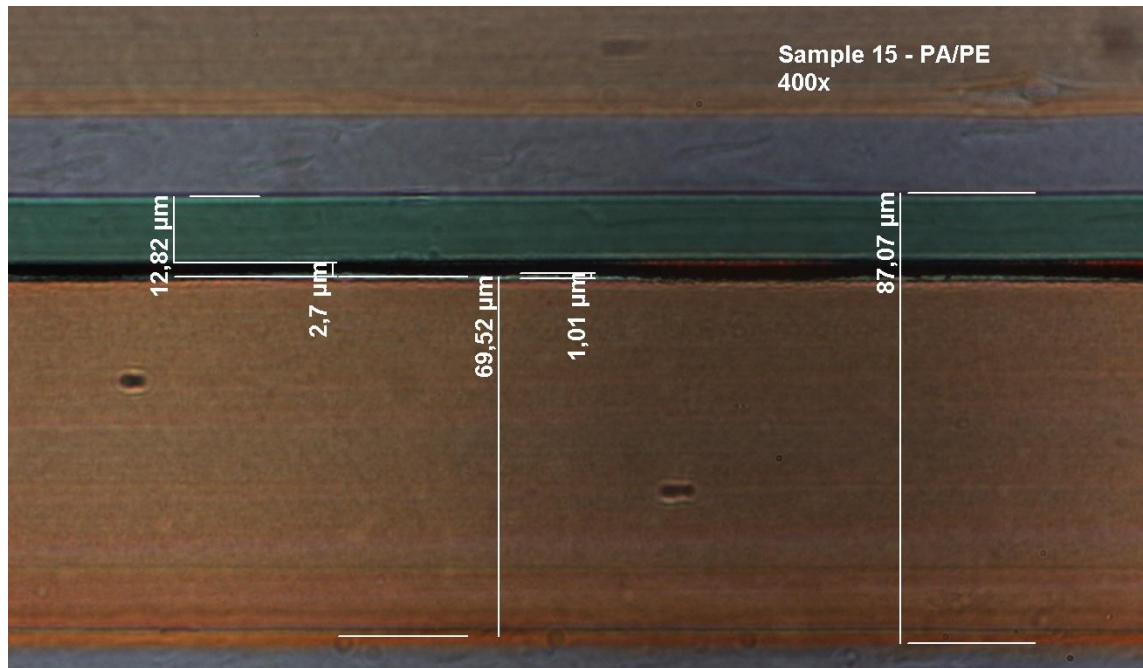


**Figure 15.** Cross-section of sample 15.

PET also exhibited various interference colors with hues of violet being the most common followed by hues of green. Sample 23 in Figure 16 has a violet top layer made of PET, bottom and bulk layer made of PP and in the middle a small layer of likely EVOH between two green tie layers. EVOH's interference color is also often grayish. Examples of the greenish hue of PET can be found in samples 10 and 11-2.

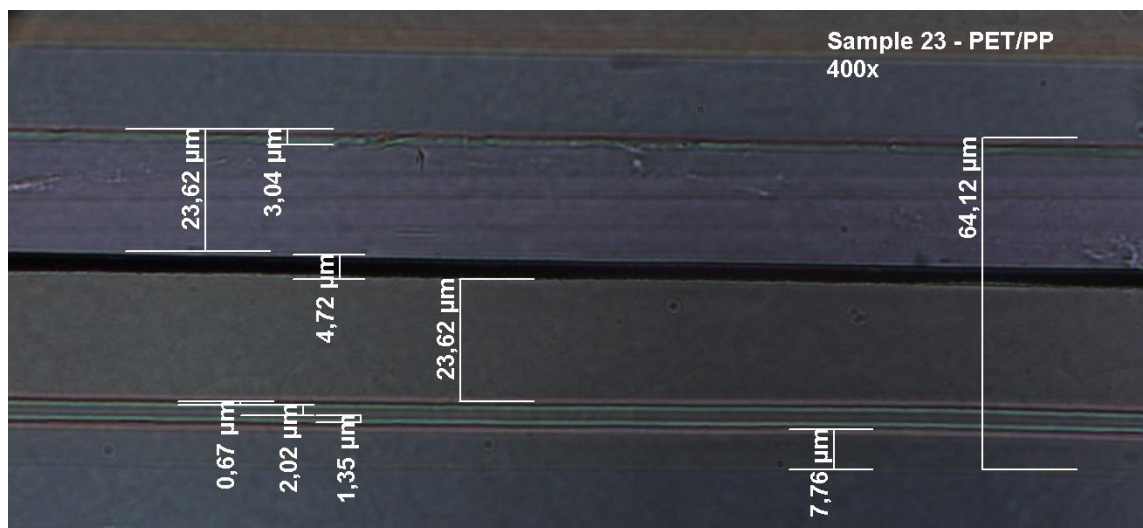


**Figure 16.** Cross-section of sample 23.

Several layers didn't exhibit interference colors at all due to color pigments or other additives. These black layers in the middle of a sample make it practically impossible to determine the exact polymer apart from making an educated guess based on the position of the layer in comparison to the other plastic layers in a multilayer structure. Many of the black layers were identified as either LDPE or PP by FTIR if they were the top or

bottom layer. An example of a black layer is seen in Figure 17, which is highly likely made of LDPE. OPP also often exhibits a degree of black as can be seen from the cross-sections of samples 25-1 and 25-2. The print layers under the top layers were almost always black as can be seen in Figure 15, Figure 16 and Figure 17.

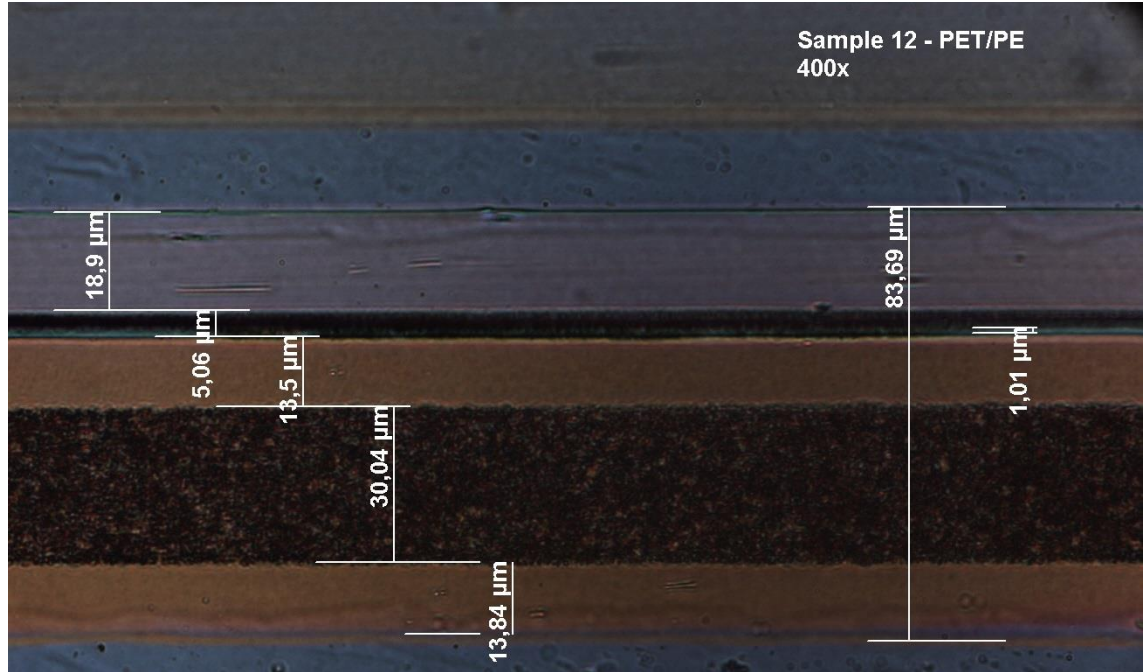


**Figure 17.** Cross-section of sample 12.

Figure 18 illustrates a complex multilayer structure with many layers. Top and bottom layer consist of a copolymer of PE and PP, the gray layers were identified as EVOH with small layers of PA-6 on both sides. The orange layer was identified as aPP and the bulk layer in the middle as LLDPE (black layers) and LDPE. In the case of this multilayer film, it is impossible to say for certain if the black layers are LLDPE or not, but this is an assumption based on the DSC data.

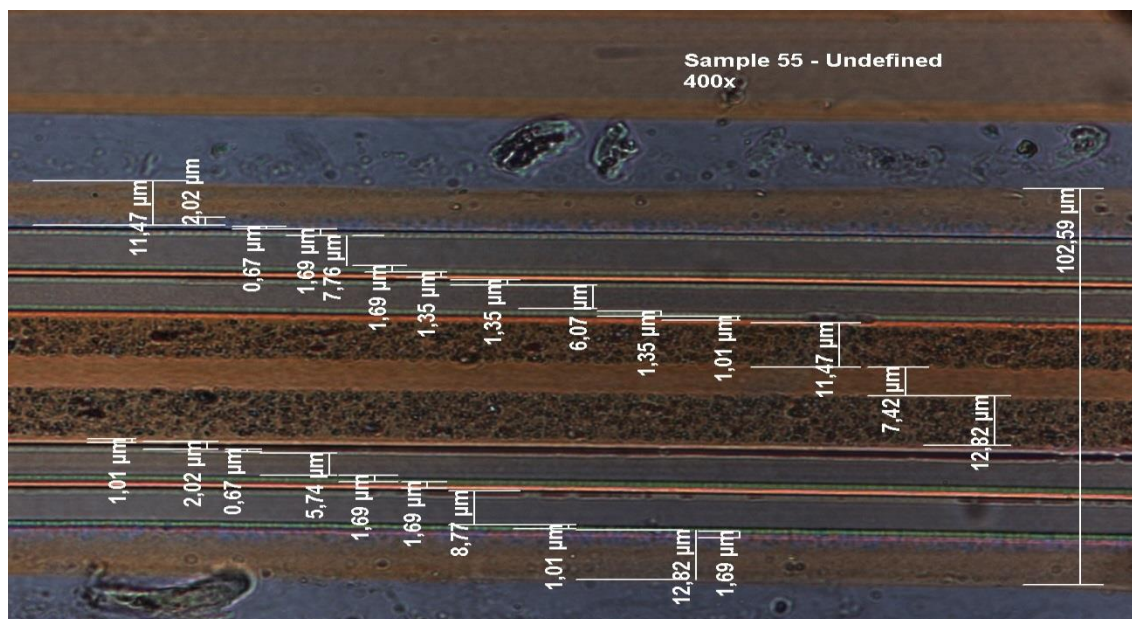


**Figure 18.** Cross-section of sample 55.

Complete list of the 124 cross-section images by polarized light optical microscopy can be found in APPENDIX A: Cross-section figures. Some samples required multiple images due to their large thickness.

## 4.2 DSC sample preparation & measurements

The DSC measurements were performed at TUT with Netzsch DSC 204 F1 equipment. The reference was an empty crucible made of aluminum with a pinhole inserted in the top center of the crucible. The sample crucibles followed the same logic with sample masses varying between 7 and 15 mg. Variation of the sample masses is due to varying thicknesses of the samples and thick films being easier to make into DSC samples. The samples were prepared using a perforator on the multilayer films. The samples were processed using an integrated and automatic sample changer. Liquid nitrogen which had been converted into gas by the DSC machine was used as a cooling medium. Netzsch Proteus Thermal Analysis software was used to analyze the resulting DSC curves. DSC analysis was carried out for samples 38–71 since they had unknown composition for a total of 77 measurements.

Samples were heated two times from 20 °C to 280 °C with a heating rate of 10 °C/min to remove thermal history. Figure 19 illustrates the temperature program used for all the samples. Initially the samples were heated from room temperature to 280 °C, then cooled down to 20 °C at a rate of 20 °C/min and kept there for 5 minutes, again heated to 280 °C and cooled down to 20 °C.

Num	Mode	°C	K/min	pts/min	hh:mm	STC	Co	P1:--	P2:N2	PG:N2	LN2	GN2
●	Initial	30,0				1	0	0,0	20,0	50,0	Off	Off
▲	1 Dynamic	280,0	10,000	100,00	00:25	1	0	0,0	20,0	50,0	Off	Off
▼	2 Dynamic	20,0	20,000	100,00	00:13	1	0	0,0	20,0	50,0	Off	5,0
→	3 Isothermal	20,0		20,00	00:05	1	0	0,0	20,0	50,0	Off	5,0
▲	4 Dynamic	280,0	10,000	100,00	00:26	1	0	0,0	20,0	50,0	Off	Off
▼	5 Dynamic	20,0	20,000	100,00	00:13	1	0	0,0	20,0	50,0	Off	5,0
⊕	6 Emergency	290,0					0	0,0	0,0	0,0	Off	Off

**Figure 19.** The temperature program for DSC samples.

Typical DSC curve is illustrated in Figure 20. Black curve presents the first heating and the red curve the second heating. Cooling curves were left out in these images. The crystallization temperature peaks in cooling curves were used to confirm the existence of some polymers that were hard to identify only by the melting DSC peaks. Figure 20 confirms the existence of LDPE (peak at 110 °C), LLDPE (126 °C) and PP (162–166 °C). The small peak at 66.8 °C is possibly EVA and due to its low decomposition temperature, it doesn't appear in the second heating. The melting peak temperature of EVA and EVOH varies due to the different relative amounts of the monomers in the copolymers. Small DSC peaks during the first heating between 60 and 90 °C were attributed to EVA in this thesis.

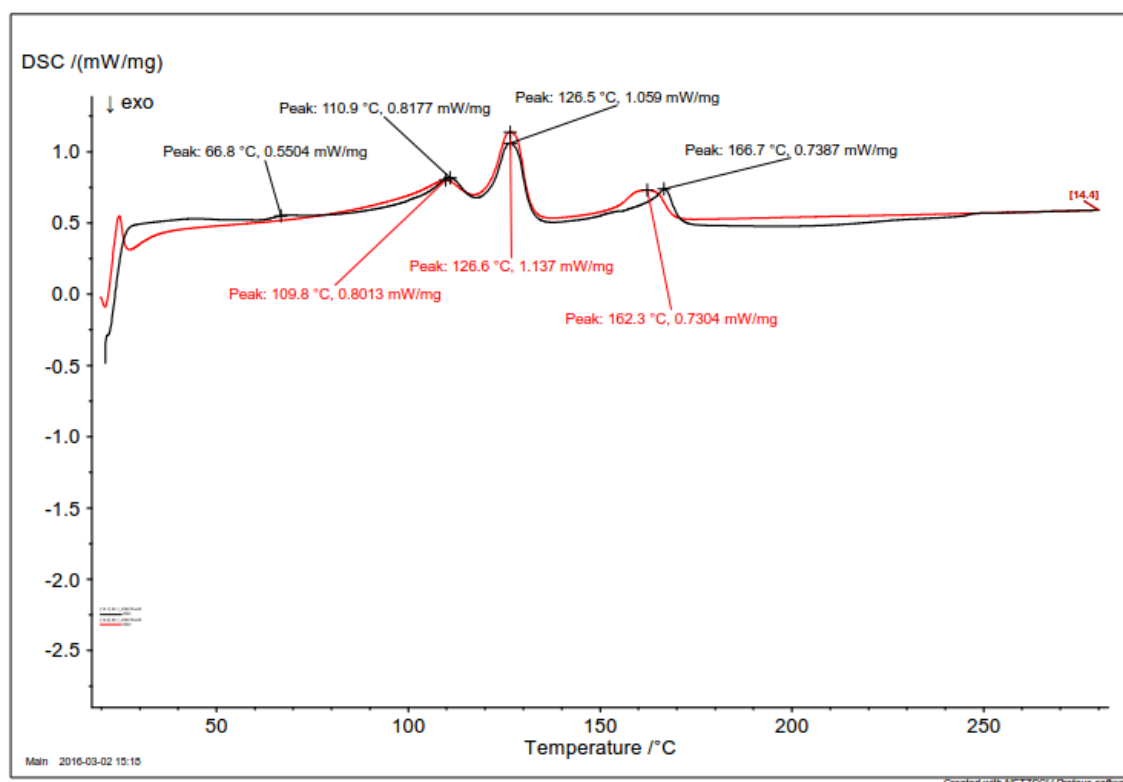


**Figure 20.** DSC curve for sample 43-1.

Figure 21 illustrates a more complex multilayer film with multiple peaks. In this sample, peaks for EVA (81.9 °C), LDPE and LLDPE can again be identified. The recurring

peak at around 140 °C is likely due to atactic PP, the peak at 171.9 °C is EVOH and the last peak around 220 °C is PA-6.

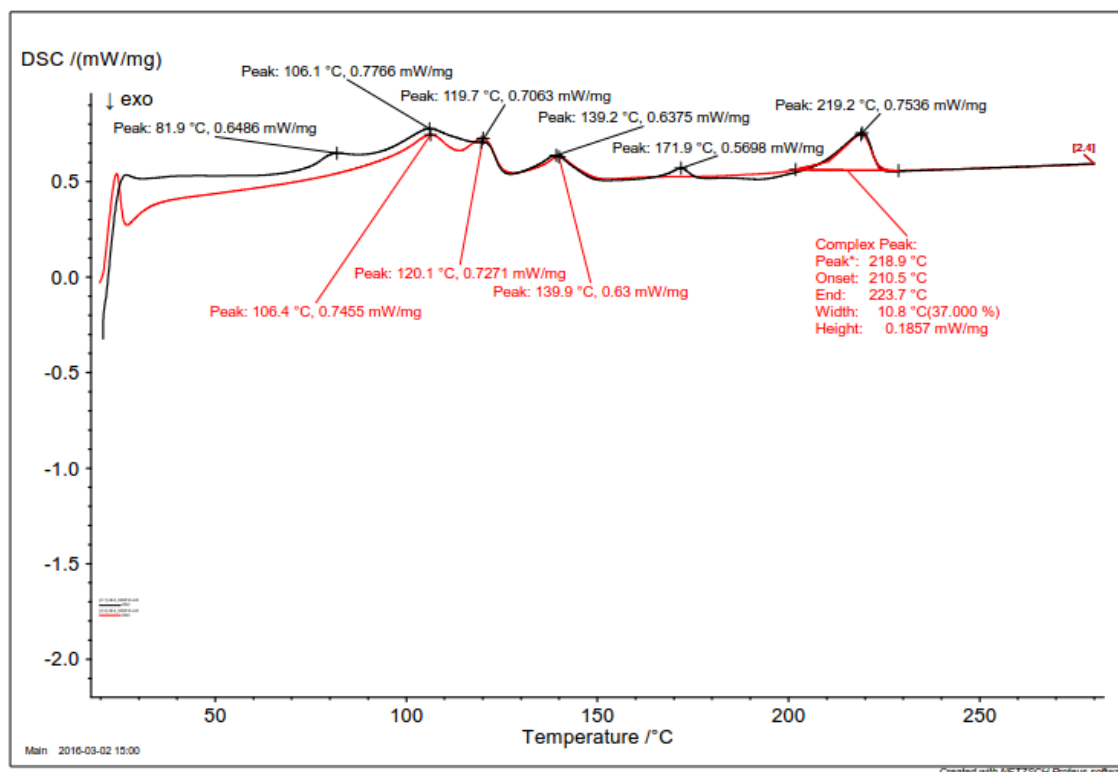


**Figure 21.** DSC curve for sample 46-2.

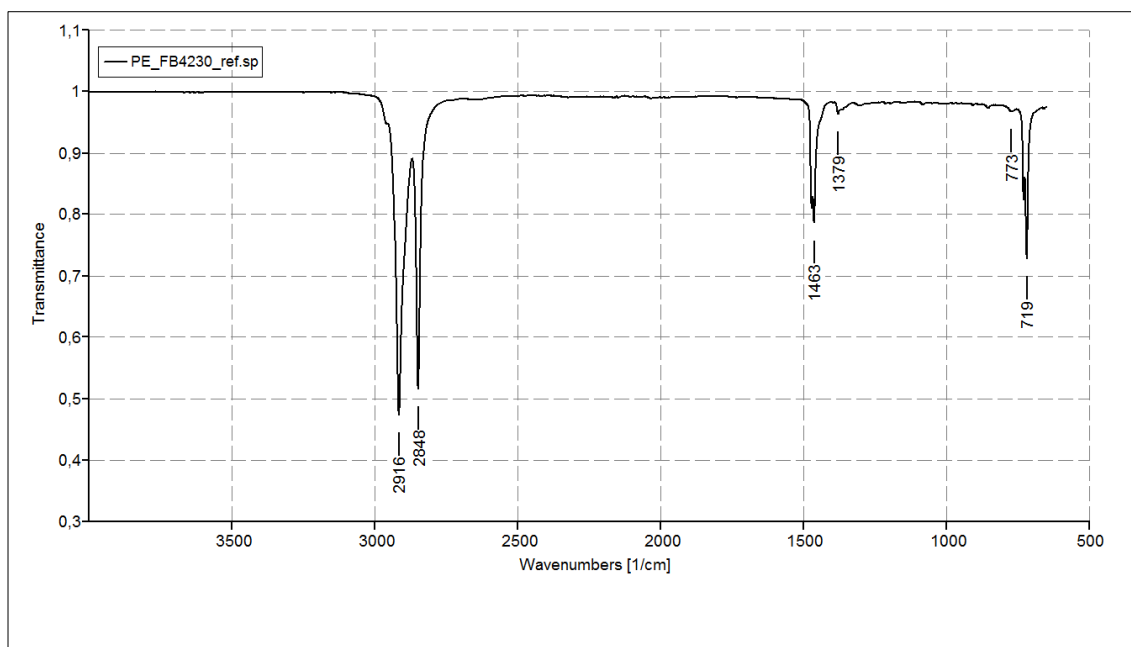
EVOH decomposes over temperatures of 245 °C so that is likely why the peak doesn't occur during the second heating. Similar melting peaks were observed in many samples in the range of 170–186 °C and they were attributed to EVOH. Recurring DSC peaks at over 250 °C were attributed to PET. An example of this can be found in Figure B-3 in Appendix B.

### 4.3 FTIR measurements

The FTIR measurements were performed by Arcada University of applied sciences with a Perkin Elmer spectrometer and the raw data was further processed and analyzed at TUT. Both the top and the bottom side of the sample films were measured and then analyzed, resulting in over 240 FTIR spectra in addition to five reference spectra. Two of the reference samples were PE and the rest were PP, PA and PET. Spekwin32 spectroscopy software was used to convert the raw data into image files containing peak labels. The spectra were normalized to 1 at their maximum wavelength in the x-axis range to make the comparison of the spectra easier. A 5% threshold value and a prominence value of 3 or 4 were used for automatic determination of the peak label values. The polymers were identified by comparing the FTIR spectra to the reference polymers' spectra.

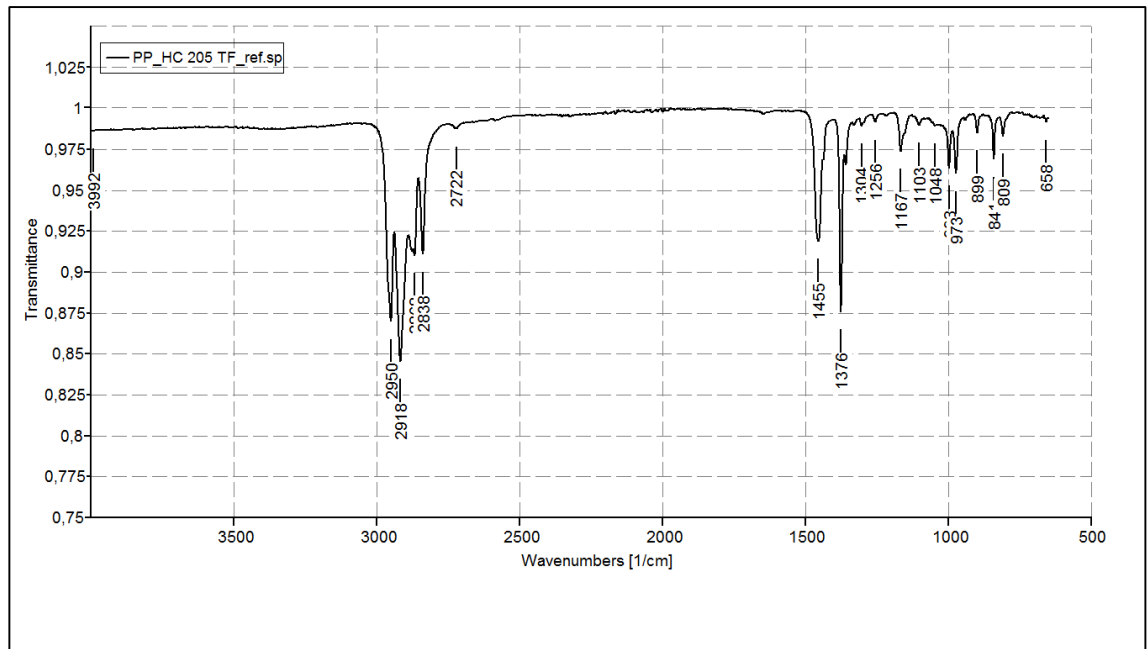
The most intense peaks in the reference spectra were the most important guideline in determining the correct polymer(s).

Figure 22 illustrates an FTIR spectrum for the reference LDPE. The spectra identified as PE had common peaks at 2916, 2848, 1463, 1379, 773 and 719  $\text{cm}^{-1}$ . Peaks with weaker intensities such as 1379 and 773  $\text{cm}^{-1}$  were not present on all spectra due to overlapping peaks. Due to normalization of the spectra, the baseline lies at transmittance of 1 for all samples. Spectra with peaks different to the common peaks were attributed to various additives in polymers. Due to the use of additives it makes it exceedingly hard to differentiate between the types of PE used. Common peaks for additives in PE were found in the region of  $>1700 \text{ cm}^{-1}$  and  $>1500 \text{ cm}^{-1}$ .



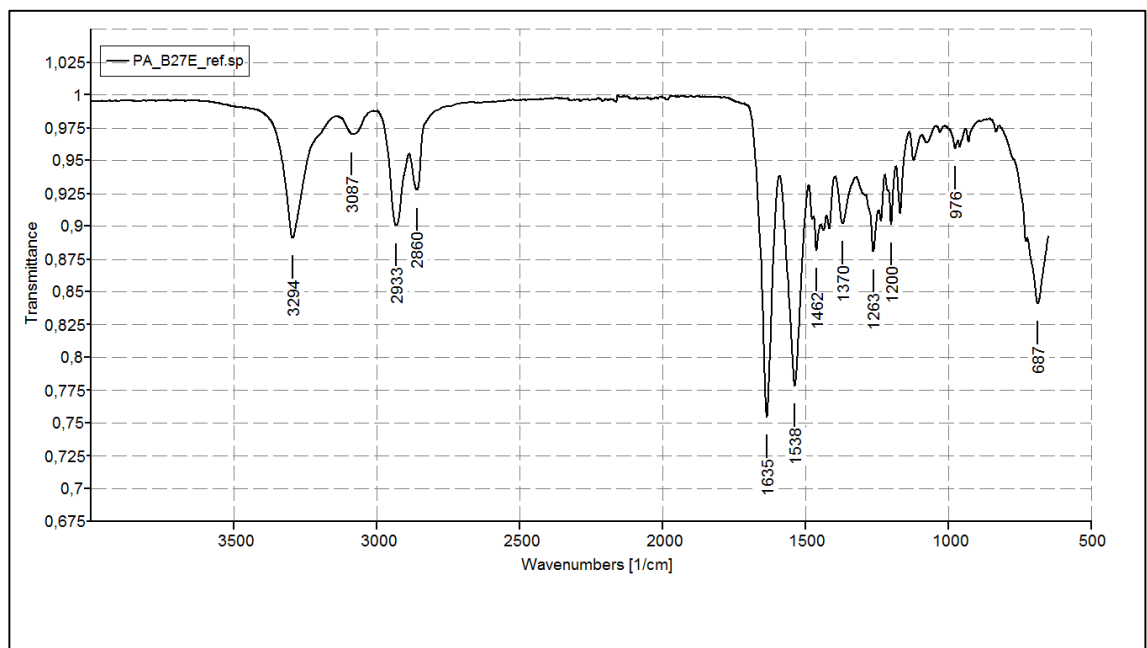
**Figure 22.** FTIR spectrum of a PE reference sample.

Figure 23 is an FTIR spectrum for the reference PP sample. Typical peaks for PP in this spectrum and the spectra identified as PP include the peaks of 1455, 1376, 1167, 998, 973, 899, 841 and 809  $\text{cm}^{-1}$ . Due to use of additives, these peaks shift and vary in intensity. This holds true for all the reference spectra peaks. PP spectra also often had the same additive peaks as PE at  $>1700$  and  $>1500 \text{ cm}^{-1}$  in addition to others. Smaller characteristic peaks in the region below  $1300 \text{ cm}^{-1}$  were often overlapping with peaks from additives, which made polymer identification more difficult.



**Figure 23.** FTIR spectrum of the PP reference sample.

PA spectra shared unique characteristic peaks in the region above  $2860\text{ cm}^{-1}$  as can be seen in the PA reference sample spectrum in Figure 24. The peaks at  $1635$ ,  $1538$ ,  $976$  and  $687\text{ cm}^{-1}$  were also very common and helpful in identifying the plastic as PA.



**Figure 24.** FTIR spectrum of the PA reference sample.

The FTIR spectrum of PET as illustrated in Figure 25 has strong peaks at  $1712$ ,  $1410$ ,  $1341$ ,  $1241$ ,  $1095$ ,  $1018$ ,  $871$  and  $721\text{ cm}^{-1}$ . The spectra identified as PET shared similar peaks to the peaks in the reference spectrum. These peaks are quite different to the other polymers in multilayer films, thus PET was quite easy to distinguish.



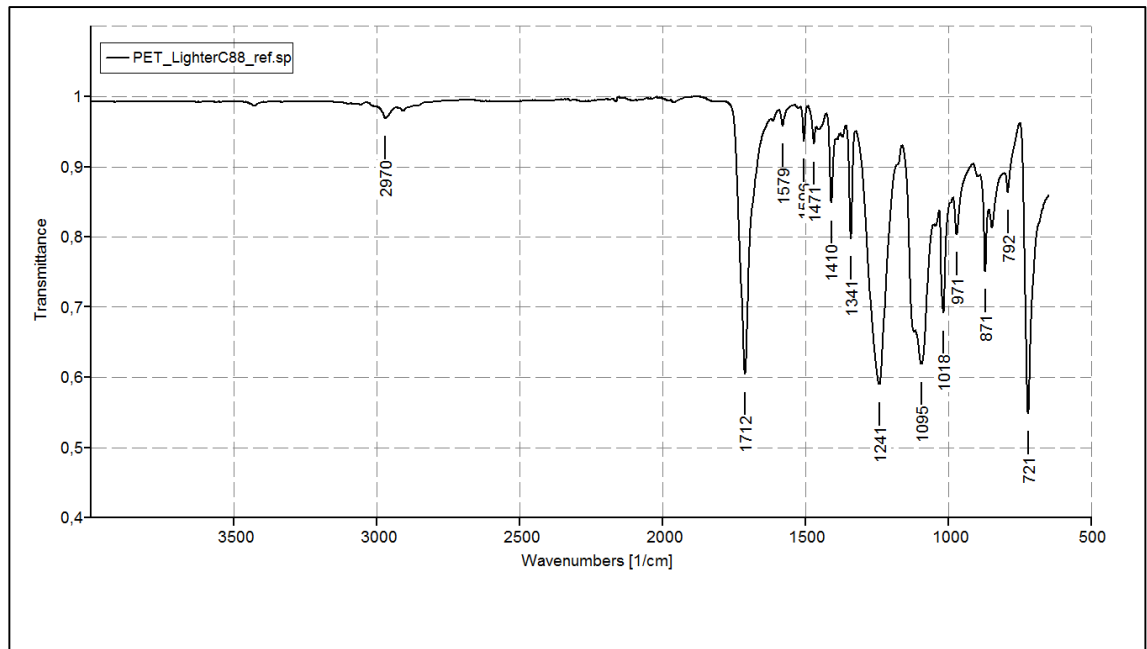


**Figure 25.** FTIR spectrum of the PET reference sample.

Figure 26 illustrates the toughness in determining the correct polymer(s) in question. It exhibits characteristics from both PE and PP with very strong peaks from additives. In this case, the top layer of sample 38 was identified as a copolymer of LDPE and PP.

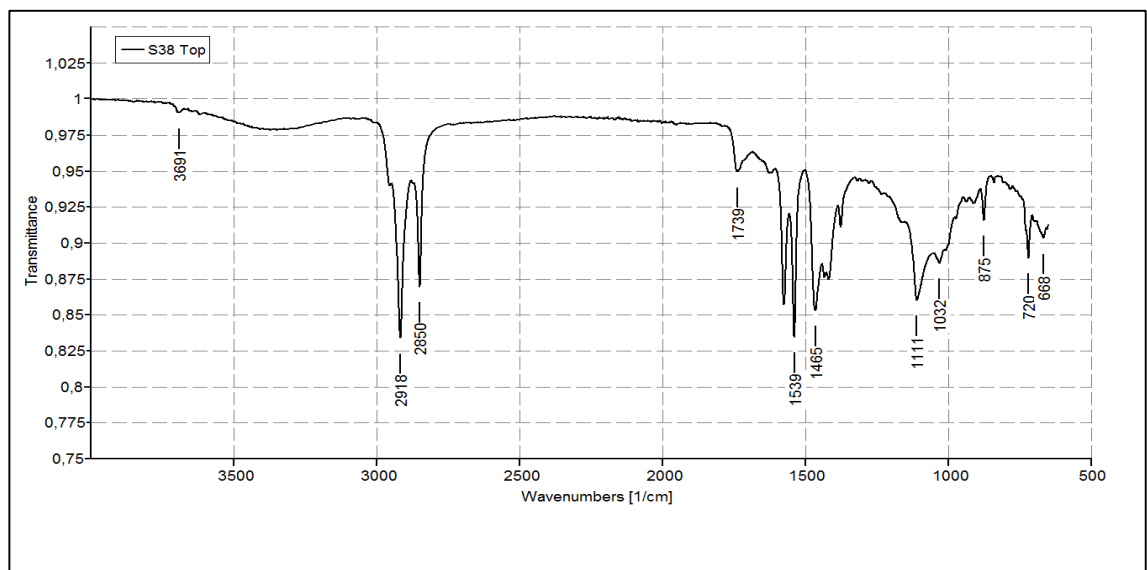


**Figure 26.** FTIR spectrum of the top layer of sample 38.

List of the most common FTIR spectra can be found in APPENDIX C: FTIR spectra. Not all spectra are listed due to the sheer amount of the spectra.

## 5. COMPOSITION ANALYSIS

This section covers the analysis of the gathered data via optical microscopy, DSC and FTIR. The data is used to calculate material proportions in relation to the thickness of the layers for each material found in the pool of samples. Different polymers are identified by analyzing the thermal data provided by DSC data in samples where the polymer composition was unknown. FTIR has been used to ascertain the bottom and top layer of a multilayer film, while the microscope cross-sections provide layer thicknesses and layer identification based on the layer color and the layer position in the multilayer film structure.

### 5.1 Polymer identification from DSC data

The following DSC peak temperature ranges listed in Table 5 were the main guideline in identifying the corresponding polymers in samples 38–71. 14 common DSC curves that are the base of these results can be found in APPENDIX B: DSC figures.

*Table 5. Temperature ranges for peaks observed from DSC curves.*

Polymer	Temperature range [°C]
EVA	60-100
LDPE	105-115
LLDPE	115-125
aPP	139-145
iPP	160-168
EVOH	170-190
PA-6	218-225
PET	250-260

The polymers identified from the DSC curves are listed in Table 6 from lowest melting peak to the highest (left to right). PP is isotactic unless otherwise denoted.

*Table 6. Polymers identified from DSC measurements.*

Sample	Polymer 1	Polymer 2	Polymer 3	Polymer 4	Polymer 5	Polymer 6
38	EVA	LDPE	PP			
39-1	LDPE	LLDPE	PP			
39-2	EVA	LDPE	PP			
39-3	EVA	LDPE	PP			
40-1	EVA	LDPE	LLDPE	PET		
40-2	EVA	LDPE	PP			
41-1	EVA	LDPE	LLDPE	EVOH	PET	
41-2	EVA	LDPE	PET			
42-1	PP					
42-2	PP					
42-3	EVA	LDPE	LLDPE	EVOH	PET	
42-4	EVA	LDPE	PET			
42-5	EVA	LDPE	PP			
43-1	EVA	LDPE	LLDPE	PP		
43-2	EVA	LDPE	LLDPE	PP	PET	
44-1	LDPE	EVOH	PA-6	PET		
44-2	LDPE	LLDPE	EVOH	PA-6	PET	
45-1	PP					
45-2	PP					
45-3	LDPE	PP				
46-1	EVA	LDPE	LLDPE	PA-6		
46-2	EVA	LDPE	LLDPE	aPP	EVOH	PA-6
46-3	EVA	LDPE				
47-1	EVA	LDPE	LLDPE	PA-6		
47-2	EVA	LDPE	PP			
48-1	EVA	LDPE	EVOH	PET		
48-2	EVA	LDPE	LLDPE	EVOH	PET	
48-3	EVA	LDPE	EVOH	PET		
49-1	EVA	LDPE	EVOH	PET		
49-2	EVA	LDPE	PA-6			
50-1	PP	PA-6	PET			
50-2	PP	PET				
50-3	EVA	LDPE	LLDPE	EVOH	PET	
51	LDPE	EVOH	PET			
52	EVA	LDPE	EVOH	PET		
53	EVA	LDPE	EVOH	PET		
54	PET					
55	LDPE	LLDPE	aPP	EVOH	PA-6	
56	EVA	LDPE	PA-6			
57-1	EVA	LDPE	PA-6			
57-2	EVA	LDPE	LLDPE	EVOH	PET	

58	EVA	LDPE	PP			
59-1	EVA	LDPE	EVOH	PET		
59-2	EVA	LDPE	EVOH	PET		
59-3	LDPE	aPP	PA-6			
60	EVA	LDPE	PA-6			
61	EVA	LDPE	LLDPE	PA-6		
62	EVA	LDPE	LLDPE	PA-6		
63	EVA	LDPE	LLDPE	PA-6		
64	EVA	LDPE	LLDPE	PET		
65-1	EVA	LLDPE	PET			
65-2	EVA	LDPE	EVOH	PET		
66	EVA	LLDPE	PA-6			
67-1	EVA	LDPE	PA-6			
67-2	EVA	LDPE	EVOH	PET		
68	LDPE	EVOH				
69	EVA	LDPE	EVOH			
70-1	EVA	LDPE	PA-6			
70-2	EVA	LDPE	LLDPE	PA-6		
70-3	EVA	LDPE	LLDPE	PA-6		
71-1	EVA	LDPE	LLDPE	PA-6		
71-2	PP	PA-6				
71-3	EVA	LDPE	LLDPE	aPP	PA-6	
71-4	EVA	LLDPE	PA-6			
71-5	LDPE	aPP	PA-6			
71-6	EVA	LLDPE	PA-6			
71-7	EVA	LDPE	EVOH	PET		
71-8	LDPE	PA-6				
71-9	EVA	LDPE	LLDPE			
71-10	LDPE	PA-6				
71-11	LLDPE					
71-12	EVA	LDPE	EVOH	PA-6		
71-13	EVA	LLDPE	aPP	PP		
71-14	LDPE	PA-6				
71-15	LDPE	PA-6				
71-16	LDPE	LLDPE	PA-6			
71-17	EVA	LDPE	PA-6			

The results from these measurements were cross-referenced with the data from both optical microscopy and FTIR, which is further discussed in Section 5.2. This data was also helpful in identifying and correcting mistakes made in the analysis of the cross-sections of samples 1–37

## 5.2 Identification of different polymer layers

The interference colors discussed in Section 2.3.1 and Section 4.1 were used in identifying the various plastic layers. Samples 1–37 with known material combinations were first analyzed layer by layer and samples 38–71 in the same manner after the DSC measurements. After initial layer compositions were known the top and bottom layers were cross-referenced with the data from FTIR measurements. Bottom or top layers could then also be used as a reference in the analysis of the cross-sections if there were any layers with the same interference colors.

Table 7 shows the principle of the layer analysis. All samples aren't listed in Table 7 due to space limitations – there were a few samples with over 20 layers. The multilayer film cross-section was divided in individual layers from top to bottom belonging to a certain plastic and later confirmed by FTIR. Layer 1 in Table 7 is the top layer while the last layer on a row is the bottom layer. The values in the brackets correspond to the thickness of that particular layer. FTIR's limitations come apparent when analyzing multilayer films with a great amount of different layers, since its use is limited only to the top and bottom layers, identical layers in a cross-section notwithstanding.

**Table 7.** Analysis of layers of the multilayer films and their thicknesses [ $\mu\text{m}$ ].

Sample	Layer 1	Layer 2	Layer 3	Layer 4	Layer 5	Layer 6	Layer 7
38	LDPE+PP (22.61)	Print (4.05)	EVA (2.02)	LDPE (58.05)			
39-1	PP (21.26)	Print (5.74)	LDPE (9.11)	LLDPE (23.96)	LDPE (11.14)		
39-2	LDPE (34.42)	EVA (0.67)	Print (2.03)	EVA (1.01)	LDPE (27.68)	LDPE (9.11)	
39-3	LDPE+PP (20.92)	Print (3.03)	EVA (1.69)	LDPE (14.85)	LDPE (21.94)	LDPE (16.87)	
40-1	PET (13.16)	Print (3.71)	EVA (1.69)	LDPE (16.2)	LLDPE (21.94)	LDPE (22.95)	
40-2	PP (19.57)	Print/Tie (5.74)	LDPE (52.31)				
41-1	PET (13.84)	Print (4.05)	LLDPE (39.82)	EVA (1.01)	EVOH (3.04)	EVA (1.01)	LDPE (41.85)
41-2	PET (13.5)	Print (3.71)	EVA (1.35)	LDPE (74.92)			
42-1	PP (19.24)	Print/Tie (5.4)	OPP (17.55)	PP (4.05)			
42-2	PP (19.91)	Print (5.40)	PP (18.56)				
42-3	PET (12.49)	Print (6.07)	LLDPE (38.81)	EVA (0.67)	EVOH (4.39)	EVA (0.67)	LDPE (43.2)
42-4	PET (10.46)	Print (5.4)	EVA (2.7)	PET (10.12)	EVA (3.04)	LDPE (35.43)	LDPE (16.54)
42-5	LDPE+PP (17.55)	Print (2.36)	EVA (1.69)	LDPE (16.87)	LDPE (19.57)	LDPE (13.84)	

<b>43-1</b>	PP (20.25)	Print (4.4)	EVA (1.35)	LDPE (6.75)	LLDPE (31.72)	LDPE (9.78)	
<b>43-2</b>	PET (11.81)	Print (4.05)	EVA (1.35)	LLDPE (3.71)	OPP (30.37)	EVA (1.69)	LDPE (52.65)
<b>44-1</b>	PET (13.5)	Print (6.41)	LDPE (13.84)	PA6 (1.35)	EVOH (7.42)	PA6 (1.01)	LDPE (21.16)
<b>44-2</b>	PET (14.17)	Print (4.05)	LLDPE (22.79)	PA6 (1.01)	EVOH (1.01)	PA6 (1.01)	LDPE (22.11)

Some of the transparent multilayer films denoted 71- only had one layer, but most of the samples had at least three layers. Average number of layers per multilayer film was 6 and the maximum was 24 layers in sample 69. A total of 738 layers were analyzed across all the samples. Figure 27 depicts the amount of layers by material in comparison to the total 738 layers.

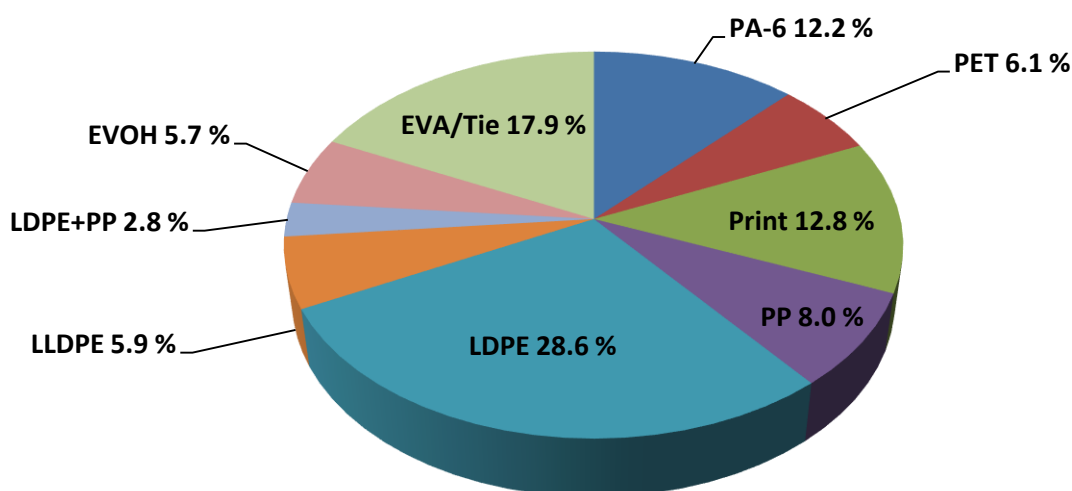


**Figure 27.** Amount of layers versus the type of material.

As can be seen from Figure 27, over one third of the layers were made of PE. This is due to large use of PE as bulk layers in the multilayer films. There were also relatively many tie layers in the films with a share of 17.9 %, which is highly likely due to the poor adhesion between many plastics without the use of compatibilizers. The tie layers were often very thin (as thin as 0.67  $\mu\text{m}$ ) and they were commonly found on both sides of incompatible layers, which explains their large amount. PA-6 layers were found both in the middle of the multilayer structure but also often as the top layer. PET was mostly used as a top layer. EVOH was always in the middle of the multilayer structure. The print layer was in most of the cases under the top layer but in rare cases the top layer. Both PP and PE were found in various locations within the multilayer structure.

### 5.3 Calculation of material proportions

The total thickness of the whole sample pool was calculated to be 9695  $\mu\text{m}$ . The average thickness of a multilayer film was therefore 81.06  $\mu\text{m}$ . The total thickness of the sample pool was calculated by measuring each individual layer in the cross-section images. The thickest multilayer film was sample 71-10 with a thickness of 184.93  $\mu\text{m}$  and the thinnest multilayer film was sample 24 with a thickness of 41.51  $\mu\text{m}$ . The total thickness for each type of polymer for the whole sample pool is shown in Table 8.

*Table 8. The thickness of each material for the whole sample pool.*

Material type	Total thickness [ $\mu\text{m}$ ]
PA-6	918.61
PET	759.62
Print	394.39
PP	1305.4
LDPE	4769.6
LLDPE	727.79
LDPE+PP	439.82
EVOH	184.95
EVA/Tie	194.67
	$\Sigma$ 9695

The data in Table 8 was further used to calculate the proportions of each material in the sample pool in relation to volume. For the calculation of volume the values of the other dimensions are assumed to be 1  $\mu\text{m}$ . This is depicted in Figure 28. Material proportion percentages were also calculated for the most common package types found in the sample pool (Figure 29–Figure 35).

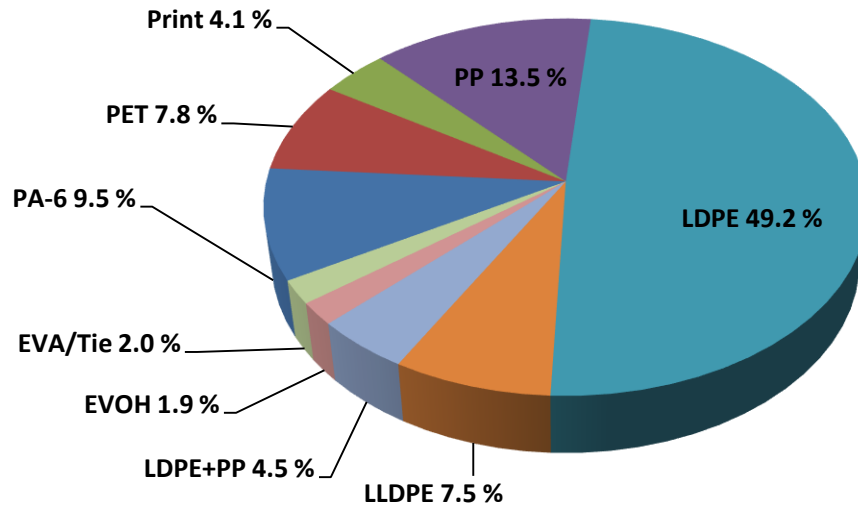


**Figure 28.** Volume percentages of materials in the sample pool.

As Figure 28 illustrates, LDPE and its variants are by far the most used plastic in multi-layer films, contributing to over half of the used material. Second most used is PP, followed by PA-6 and PET. EVA only contributes little to the total amount of material despite the fact that the tie layers in general were the second most used layer in these samples. Usage of EVOH was also relatively low.

Frozen product packages were the simplest packages and consisted of mostly PE and PP as shown in Figure 29. In addition to these polymers there were only minor amounts of tie materials and print. In contrast to the other package types, frozen product packages don't have any PA-6, PET or EVOH in them. There were a total of 10 frozen product package samples.



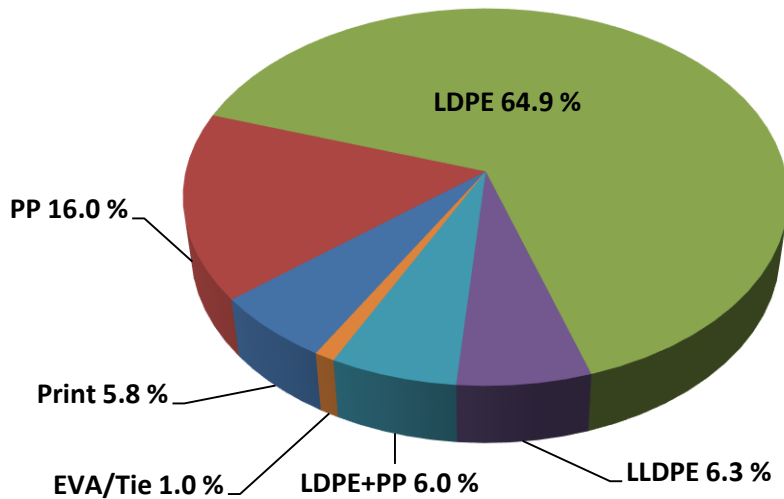


**Figure 29.** Volume percentages of materials for frozen product packages.

There were only 4 samples that were labeled as chilled product packages. Regardless to the fact that the sample amount was low, they were an exception to the dominating amount of PE in the multilayer films. PP was by far the most used polymer in these types of packages as illustrated in Figure 30. EVOH is used the most in chilled product packages when compared to other package types. Notable is also the very low amount of PET used.

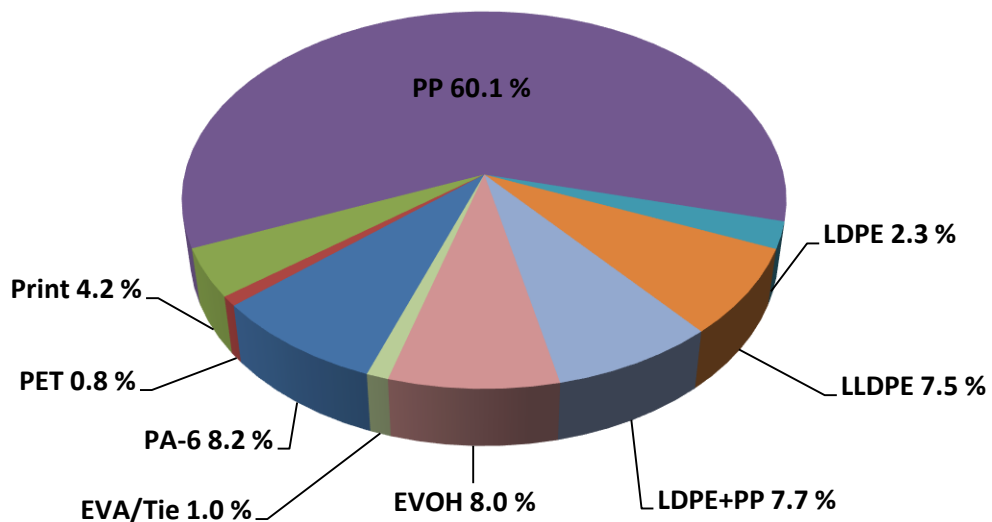


**Figure 30.** Volume percentages of materials for chilled product packages.

There were a total of 27 processed meat package samples, making it the most common package type in this thesis. PE is the dominating material in this package type, but vari-

ous other materials are also used as depicted in Figure 31. PET is the second most used plastic in this package type, followed by equal amounts of PA-6 and PP.

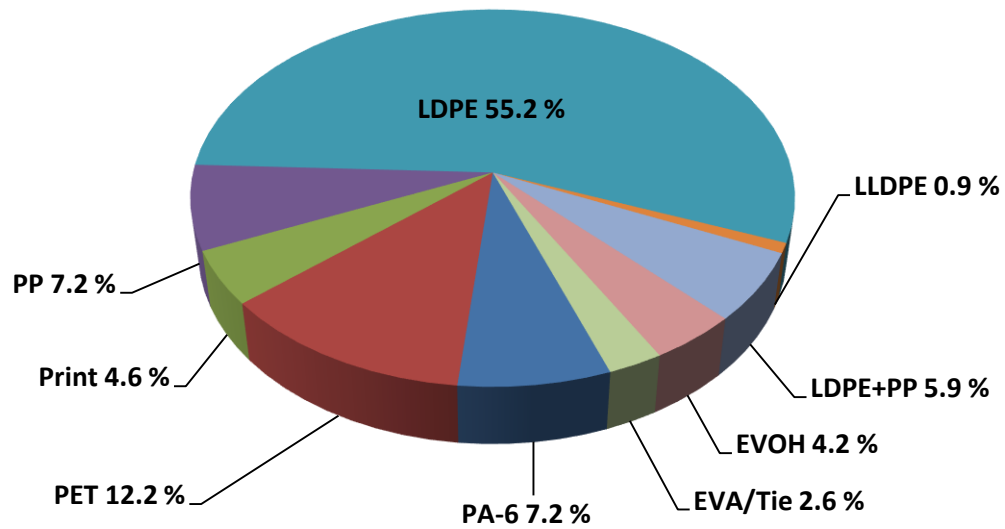


**Figure 31.** Volume percentages of materials for processed meat packages.

Fresh meat and fish packages amounted to a total of 12 samples. Material proportions for this package type are illustrated in Figure 32. Compared to processed meat packages, more PP and less PE is used. Changes in the proportions of the other materials are relatively low when compared to processed meat packages. Compared to the proportions of materials in the whole sample pool (Figure 28) the proportions are almost similar.

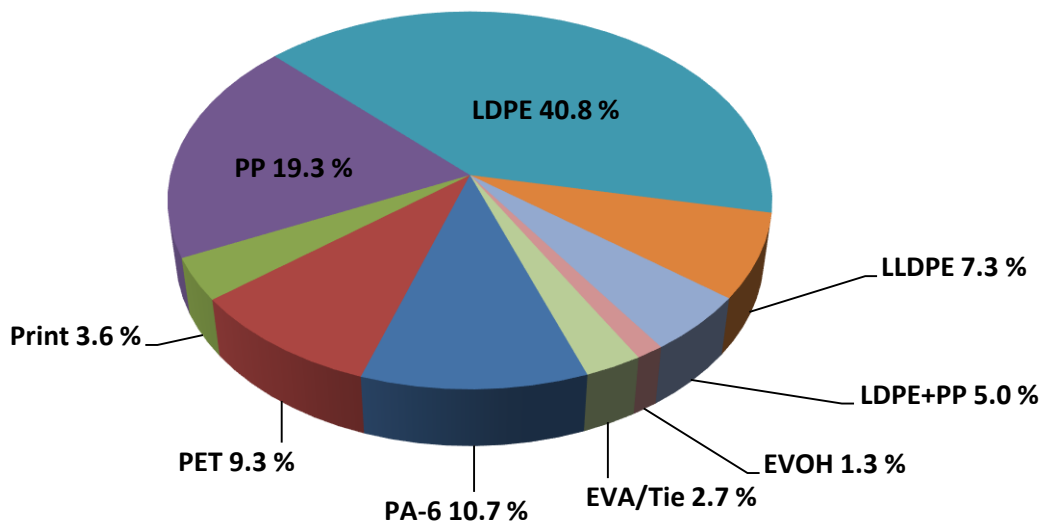


**Figure 32.** Volume percentages of materials for fresh meat and fish packages.

Dry product packages were quite simplistic compared to other types of packages, with over 80 % of the total material consisting of PE and PP. As illustrated in Figure 33,

PA-6 and EVOH contribute to very low amount of material in this package type. PET is used relatively much compared to the other non-bulk layer plastics. 24 dry product packages were analyzed.

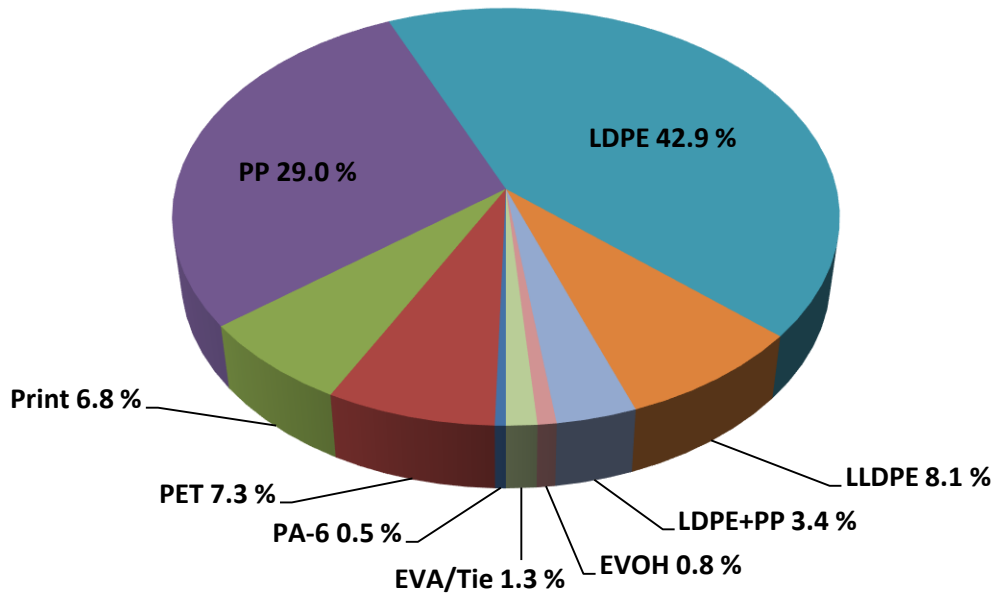


**Figure 33.** Volume percentages of materials for dry product packages.

PE was the most dominant polymer in cheese packages, accounting for over 70 % of the used material as seen in Figure 34. It is also the only package type with no PP. PET and PA-6 were the most used top layer material in this package type. Some of the multilayer films used in cheese packages were very thick, but the used material combinations were overall quite low. A total of 18 cheese packages were analyzed.

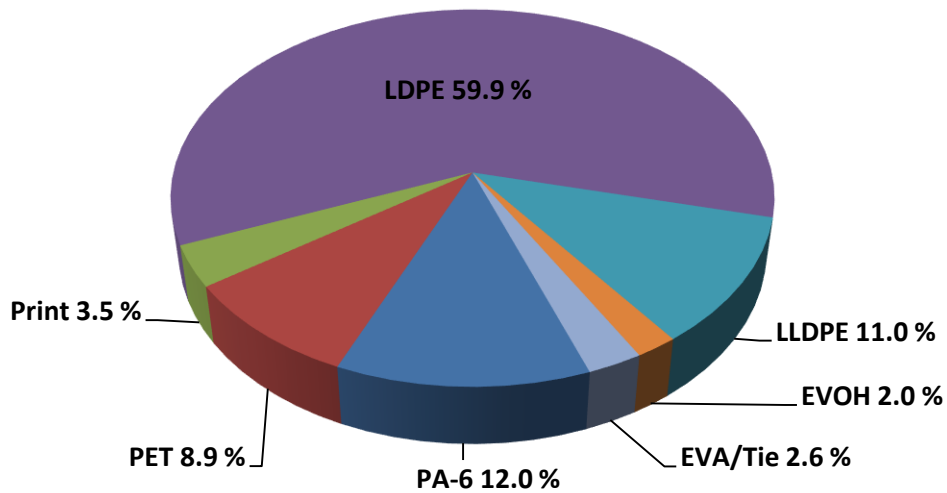


**Figure 34.** Volume percentages of materials for cheese packages.

The miscellaneous packages consist of package types that do not fit in the aforementioned categories, such as milk products, varied packages, convenience food packages and transparent multilayer films. Material proportions for miscellaneous packages are illustrated in Figure 35.

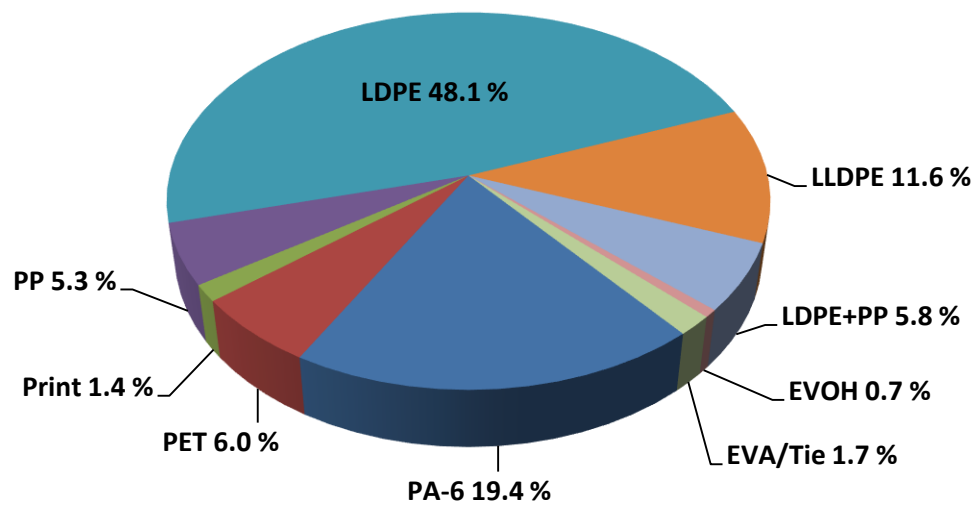


**Figure 35.** Volume percentages of materials for miscellaneous packages.

The most used plastic in miscellaneous packages is again PE. In contrast to the other package types, the miscellaneous packages have a very large proportion of PA-6. This was the case especially in the transparent films which had no print left. There were a total of 26 packages in this category.

## 5.4 Sources of error

Possible errors may have been made in identifying the correct layers in the middle of the cross-sections, but the errors are small in the scope of the whole composition analysis. This holds true especially for various layers identified as tie layers, since they were often very thin (0.67  $\mu\text{m}$ ). Educated guesses can be used to determine if tie layers were needed in the structure based on the identified polymers, but these assumptions are not always valid if the polymers were modified with compatibilizers to begin with. The black layers in the cross-section images also pose another cause for error. They were usually identified as either LDPE or PP based on the identified polymers via DSC or package inspection. If both polymers existed in a multilayer film, it was purely guesswork as both polymers are used as bulk layers, albeit the proportions of LDPE are much larger.

A possible error in the analysis of DSC curves includes the misidentification of EVA, since the melting peaks for EVA were quite small. Nonexistent peaks for EVOH and EVA on the second heating curve may also be a source of error. This behavior was attributed to the low decomposition temperature of both copolymers. A measure to confirm decomposition would have been to measure the weights of the samples after the DSC measurements and compare them to the original weights. Another option would have been to do DSC measurements with lower temperatures than the decomposition temperatures for these samples, but that would have required extensive resources.

Identifying the correct top and bottom layers from FTIR images was not always straightforward due to various reasons. Main error source here was the presence of additives in the films, which often obscured characteristic peaks or reduced the intensities of the peaks. Errors in misidentifying the layers this way were relatively small due to cross-referencing with the cross-sections, the DSC data and the initial material combinations inspected from the packages. Largest errors were possibly made in misidentifying the type of PE. While DSC provided information about the existence of LLDPE, it was often impossible to confirm the existence of LLDPE from FTIR spectra due to a variety of additives. There was also no distinct difference in the interference colors of LDPE and LLDPE. LDPE can be blended together with LLDPE, which further complicated the identification.

## 6. CONCLUSION

The composition analysis of multilayer plastic films was carried out by FTIR, DSC and polarized light optical microscopy. The most important result in this thesis was the material proportions of the sample pool shown in Figure 28. Over half of the materials in multilayer films are various types of PE in relation to thickness. Following PE is PP with a 13.5 % portion of the total thickness. These two polymers often formed the bulk of a multilayer film. PA-6 had the third largest share with 9.5 %, followed by PET at 7.8 %. Both PA-6 and PET were often found to be the top layer in a multilayer structure, providing functional properties such as barrier properties or printability. Print layers had a share of 4.1 %. EVA and other tie material layers accounted for 2.0 % of the total thickness and lastly EVOH had a share of 1.9 %.

While these results give a general understanding about the material proportions in multilayer plastic films, more research would be needed before applying them in large scale. For example these results don't take into account the large amount of additives that are embedded in many multilayer films, which makes the compatibilization of the post-consumer waste even more challenging. The next logical step in the direction of recycling multilayer plastic films would be to try to compatibilize neat materials consistent with the composition in this research. Maleic anhydride with a peroxide initiator could possibly prove successful in this.

## REFERENCES

- Andersen, B. (2004). Investigations on Environmental Stress Cracking Resistance of LDPE/EVA Blends, Doctorate, pp. 31-32. Available: <http://sundoc.bibliothek.uni-halle.de/diss-online/04/04H140/prom.pdf>.
- Ashter, S.A. (2014). 3 - Review of Characteristics of Common Plastics for Thermoforming, in: Ashter, S.A. (ed.), Thermoforming of Single and Multilayer Laminates, William Andrew Publishing, Oxford, pp. 39-63.
- Breil, J. (2010). Chapter 16 - Multilayer oriented films, in: Wagner, J.R. (ed.), Multilayer Flexible Packaging, William Andrew Publishing, Boston, pp. 231-237.
- Brydson, J.A. (1999). Plastics Materials, 7th ed., Butterworth-Heinemann, Oxford, 920 p.
- Butler, T.I. & Morris, B.A. (2013). 3 - PE-Based Multilayer Film Structures, in: Ebnasajjad, S. (ed.), Plastic Films in Food Packaging, William Andrew Publishing, Oxford, pp. 21-52.
- Butler, T.I. & Morris, B.A. (2010). Chapter 15 - PE based multilayer film structures, in: Wagner, J.R. (ed.), Multilayer Flexible Packaging, William Andrew Publishing, Boston, pp. 205-230.
- Calhoun, A. (2010). Chapter 3 - Polypropylene, in: Wagner, J.R. (ed.), Multilayer Flexible Packaging, William Andrew Publishing, Boston, pp. 31-36.
- Carl Zeiss (2001). Operating Manual Axioskop 40/Axioskop 40 FL, Carl Zeiss Optical Microscopy, Göttingen, Germany.
- Carlton, R.A. (2011). Chapter 2 - Polarized Light Microscopy, in: Pharmaceutical Microscopy, 1st ed., Springer-Verlag, New York, pp. 7.
- Delly, J.G. (ed.). (2008). Essentials of Polarized Light Microscopy. 5th ed. Westmont, Illinois, College of Microscopy, 28 p.
- Gaffney, J.S., Marley, N.A. & Jones, D.E. (2012). Fourier Transform Infrared (FTIR) Spectroscopy, in: Kaufmann, E.N. (ed.), Characterization of Materials, 2nd ed., John Wiley & Sons, Inc.
- Hatakeyama, T. & Quinn, F.X. (ed.). (1999). Thermal Analysis - Fundamentals and Applications to Polymer Science. 2nd ed. John Wiley & Sons Ltd., 190 p.
- Keck-Antoine, K., Lievens, E., Bayer, J., Mara, J., Jung, D. & Jung, S. (2010). Chapter 4 - Additives to design and improve the performance of multilayer flexible packaging,

in: Wagner, J.R. (ed.), *Multilayer Flexible Packaging*, William Andrew Publishing, Boston, pp. 37-56.

Lobo, H. & Bonilla, J.V. (ed.). (2003). *Handbook of Plastics Analysis*. New York, Basel, Marcel Dekker, Inc.

Maier, C. & Calafut, T. (1998). *Polypropylene: The Definitive User's Guide and Data-book*, Plastics Design Library, New York, United States, 456 p.

Massey, L.K. (2004). *Film Properties of Plastics and Elastomers: A Guide to Non-Wovens in Packaging Applications*, 2nd ed., Plastics Design Library, New York, United States, 221 p.

Mokwena, K.K. & Tang, J. (2012). Ethylene Vinyl Alcohol: A Review of Barrier Properties for Packaging Shelf Stable Foods, *Critical Reviews in Food Science and Nutrition*, Vol. 52(7), pp. 640-650.

Morris, B.A. (2013). 15 - Polymer Blending for Packaging Applications, in: Ebnesajjad, S. (ed.), *Plastic Films in Food Packaging*, William Andrew Publishing, Oxford, pp. 311-343.

Morris, B.A. (2010). Chapter 12 - Polymer blending for packaging applications, in: Wagner, J.R. (ed.), *Multilayer Flexible Packaging*, William Andrew Publishing, Boston, pp. 137-162.

Netzsch. (2016). Functional principle of a heat-flux DSC, web page. Available (accessed 03/14): <https://www.netzsch-thermal-analysis.com/en/landing-pages/principle-of-a-heat-flux-dsc/>.

Ockenga, W. (2011). Polarization Contrast - An Introduction, Leica Microsystems, web page. Available (accessed 03/11): <http://www.leica-microsystems.com/science-lab/polarization-contrast/>.

Pardos Marketing. (2005). Market overview: Multilayer films, Rapra international conference, Brussels, web page. Available (accessed 04/29): [http://www.pardos-marketing.com/paper\\_b02.htm](http://www.pardos-marketing.com/paper_b02.htm)

Ravve, A. (2012). *Principles of Polymer Chemistry*, 3rd ed., Springer, Niles, IL, USA. 810 p.

Robeson, L.M. (2007). *Polymer Blends: A Comprehensive Review*, Carl Hanser Verlag GmbH & Co. KG., 471p.

Sabu, T., Groeninckx, G. & Harrats, C. (ed.). 2005. *Micro- and Nanostructured Multi-phase Polymer Blend Systems*. Taylor & Francis Group, LLC, 456 p.

Salamone, J.C. (1999). *Polymeric Materials Encyclopedia*, CRC Press, Boca Raton, 1706 p.



- Schnell, R. & Stamm, M. (1998). Direct Correlation between Interfacial Width and Adhesion in Glassy Polymers, *Macromolecules*, Vol. 31(7), pp. 2284–2292.
- Sharma, K.R. (2011). *Polymer Thermodynamics: Blends, Copolymers and Reversible Polymerization*, 1st ed., CRC Press, pp. 124.
- Stuart, B.H. (2004). *Infrared Spectroscopy: Fundamentals and Applications*, John Wiley & Sons, Inc., 244 p.
- Tekkanat, B., Faust, H. & McKinney, B.L. (1993). Polyester-polyolefin blends containing a functionalized elastomer, Patent, 0 533 304 A1, 92250260.4.
- Utracki, L.A. (ed.). (2003). *Polymer Blends Handbook*, Kluwer Academic Publishers, Dordrecht, The Netherlands, 1448 p.
- Vasile, C. & Pascu, M. (2005). *Practical guide to polyethylene*, Smithers Rapra, Shrewsbury, 188 p.
- Wagner Jr., J.R. & Marks, S.B. (2010). Chapter 1 - Introduction, in: Wagner, J.R. (ed.), *Multilayer Flexible Packaging*, William Andrew Publishing, Boston, pp. 3-11.
- Wunderlich, B. (2005). *Thermal Analysis of Polymeric Materials*, Springer, Berlin Heidelberg, 908 p.
- Wypych, G. (ed.). (2012). *Handbook of Polymers*, ChemTec Publishing, Toronto, 680 p.

## APPENDIX A: CROSS-SECTION FIGURES

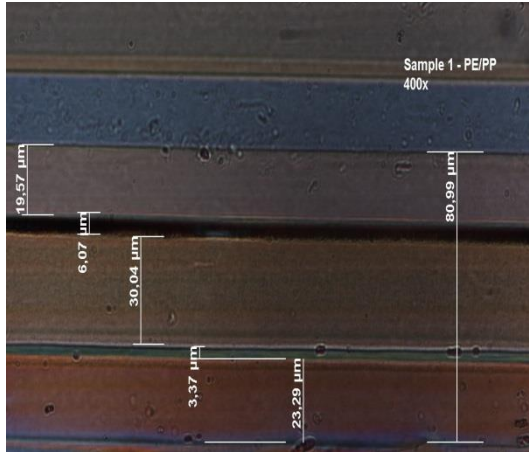


*Figure A-1. Cross-section of sample 1.*

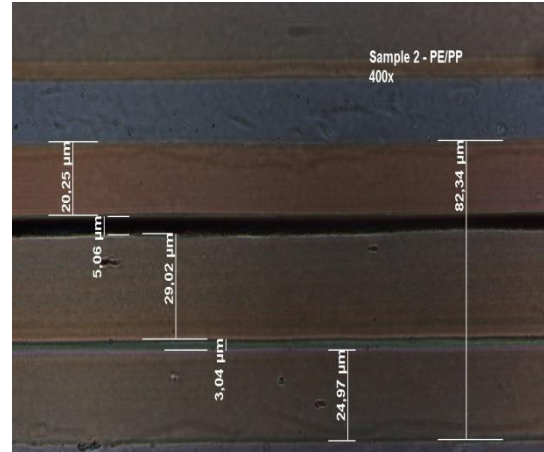


*Figure A-2. Cross-section of sample 2.*

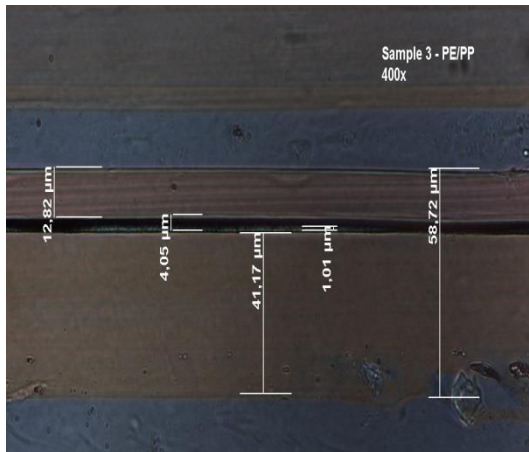


*Figure A-3. Cross-section of sample 3.*

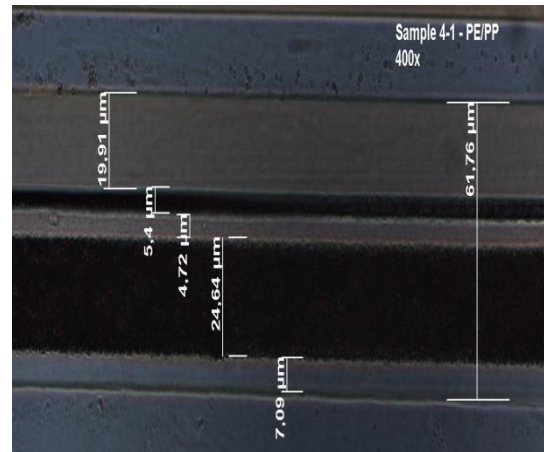


*Figure A-4. Cross-section of sample 4-1.*

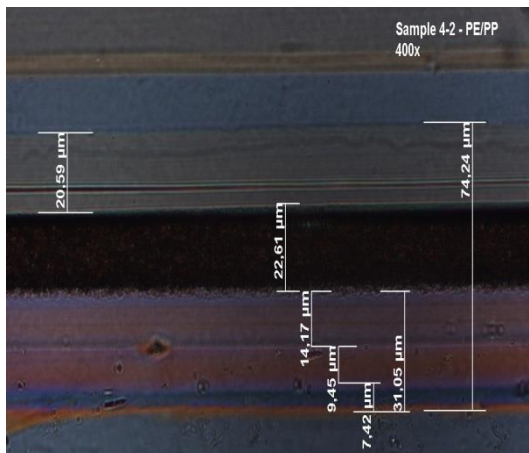


*Figure A-5. Cross-section of sample 4-2.*

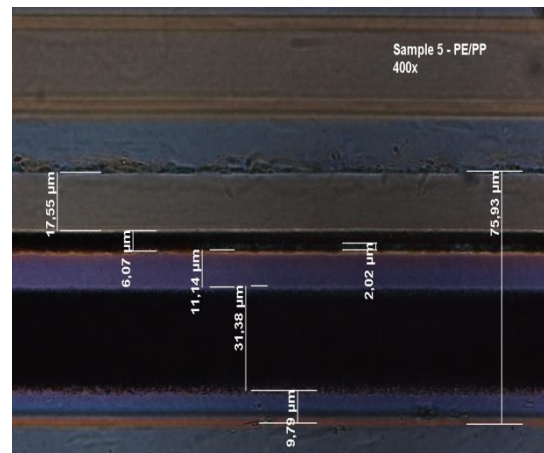


*Figure A-6. Cross-section of sample 5.*

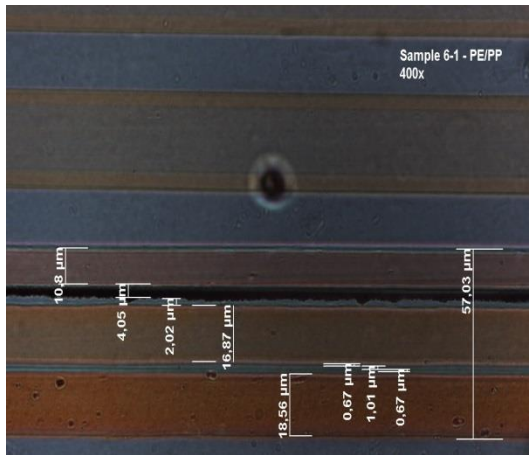


**Figure A-7.** Cross-section of sample 6-1.

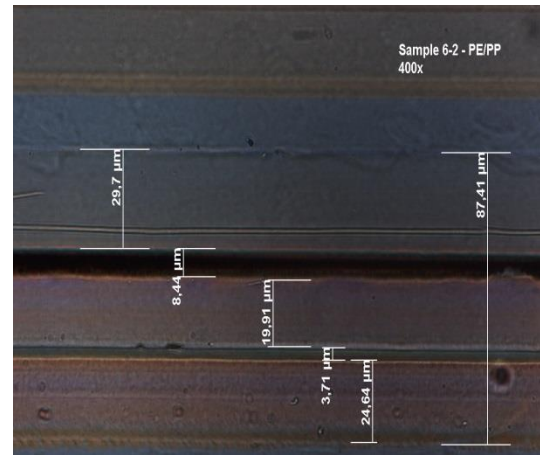


**Figure A-8.** Cross-section of sample 6-2.

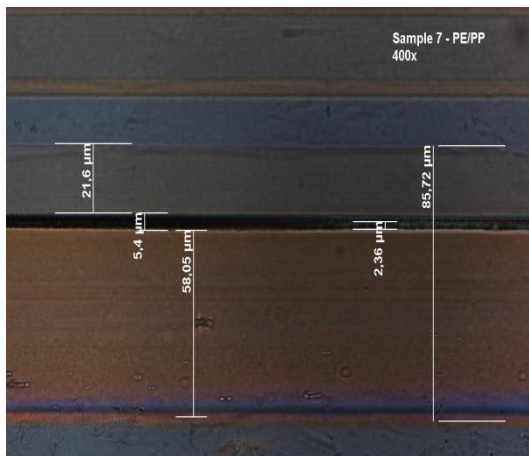


**Figure A-9.** Cross-section of sample 7.

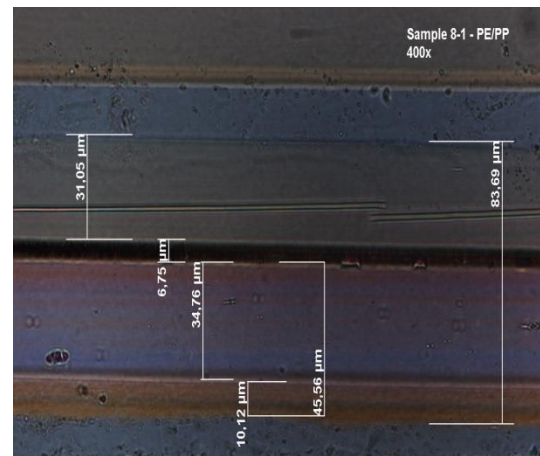


**Figure A-10.** Cross-section of sample 8-1.

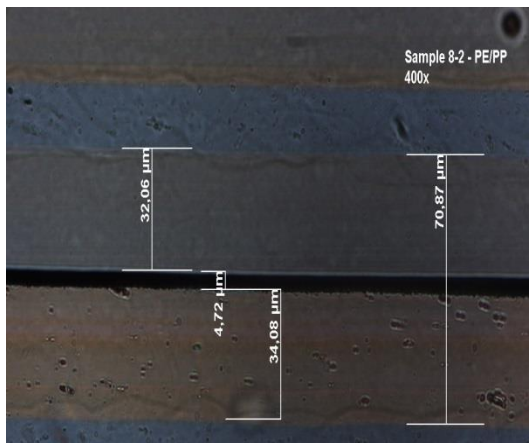


**Figure A-11.** Cross-section of sample 8-2.

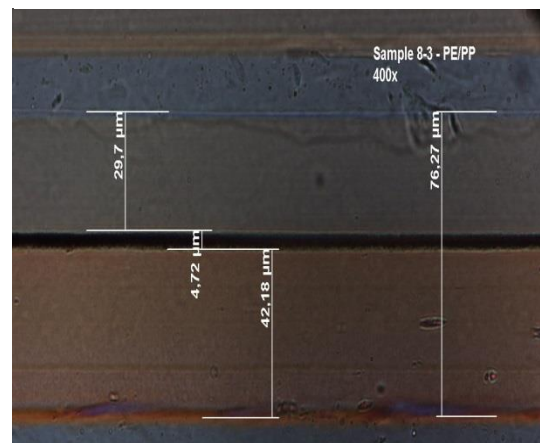


**Figure A-12.** Cross-section of sample 8-3.

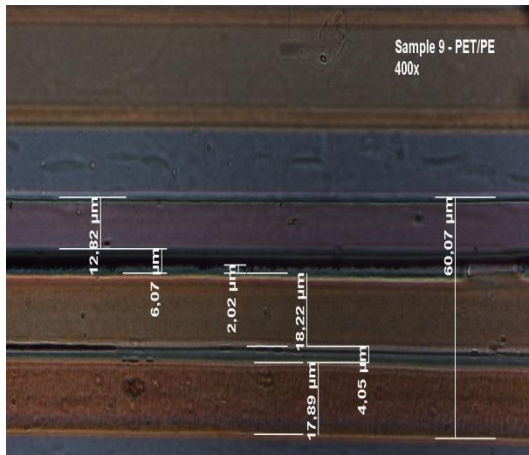


**Figure A-13.** Cross-section of sample 9.

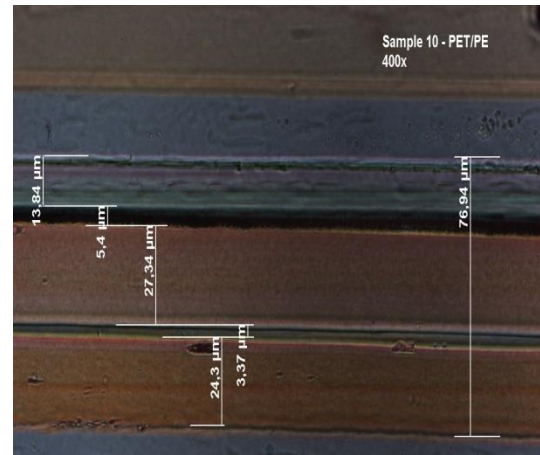


**Figure A-14.** Cross-section of sample 10.

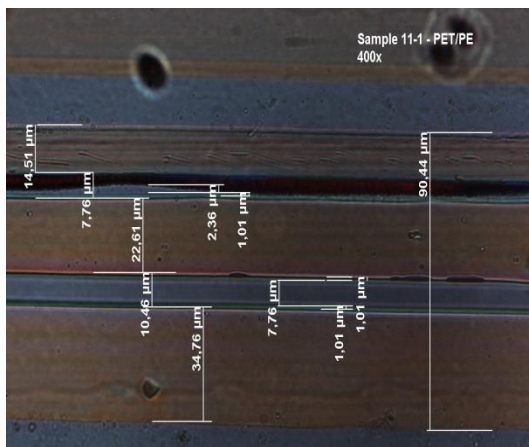


**Figure A-15.** Cross-section of sample 11-1.

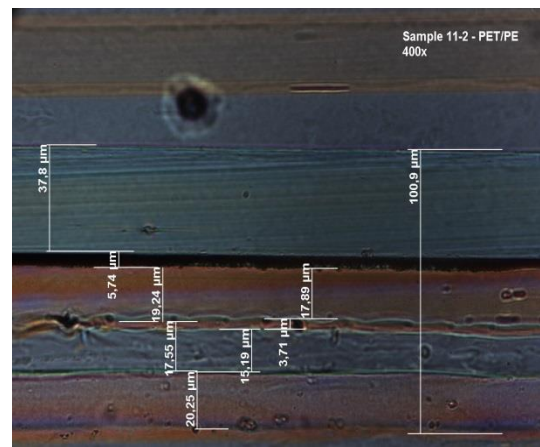


**Figure A-16.** Cross-section of sample 11-2.

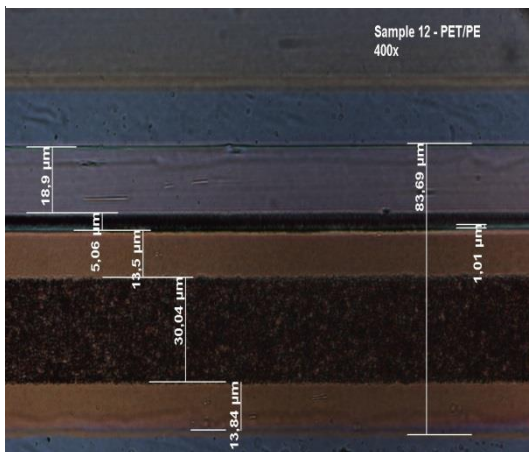


**Figure A-17.** Cross-section of sample 12.

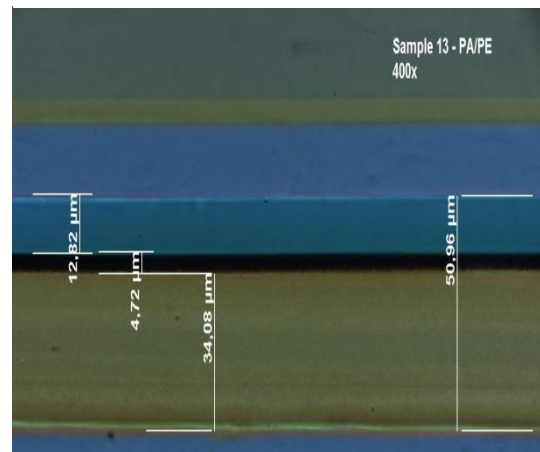


**Figure A-18.** Cross-section of sample 13.

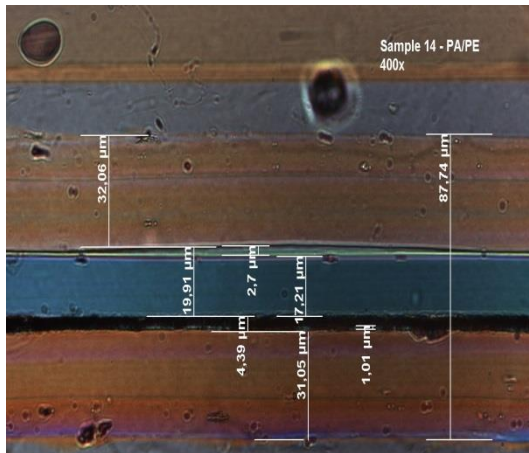


**Figure A-19.** Cross-section of sample 14.

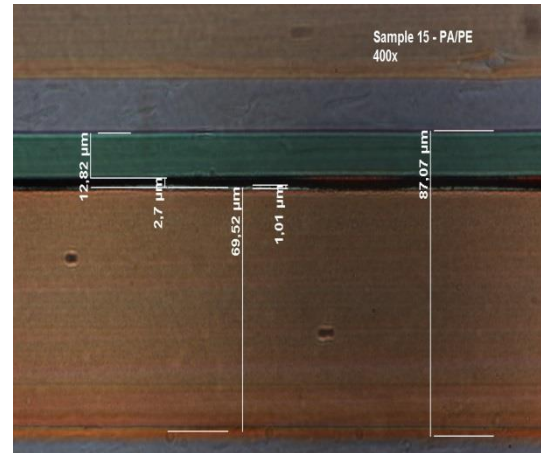


**Figure A-20.** Cross-section of sample 15.

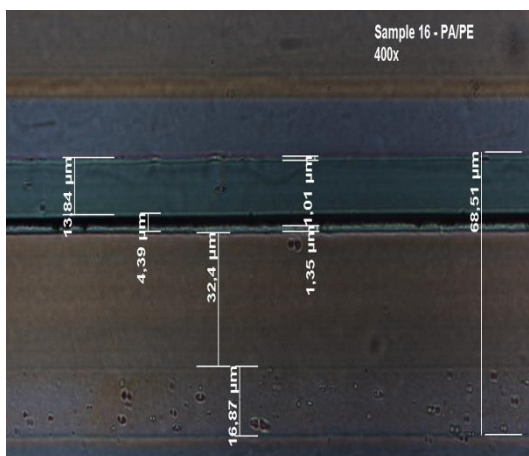


**Figure A-21.** Cross-section of sample 16.

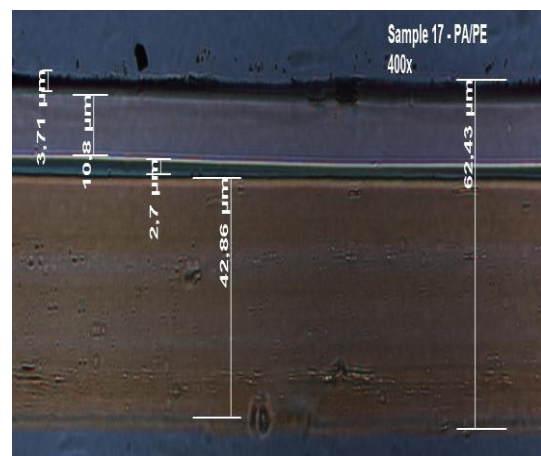


**Figure A-22.** Cross-section of sample 17.

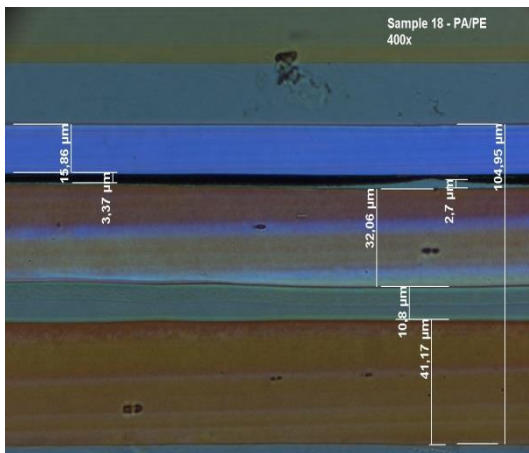


**Figure A-23.** Cross-section of sample 18.

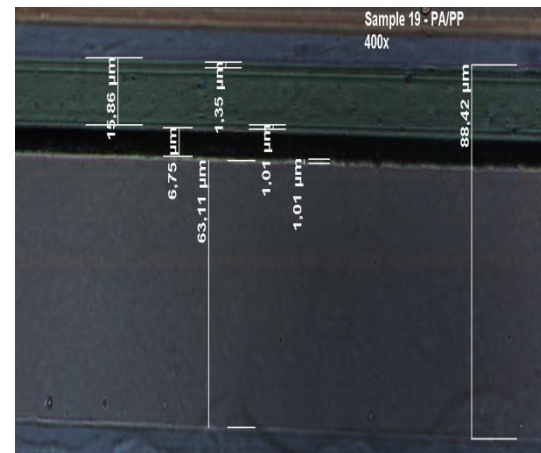


**Figure A-24.** Cross-section of sample 19.

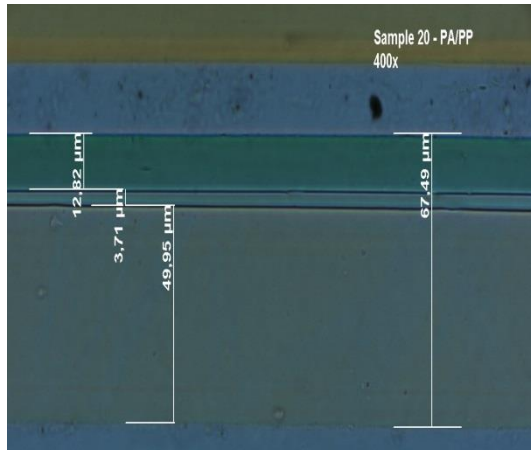


**Figure A-25.** Cross-section of sample 20.

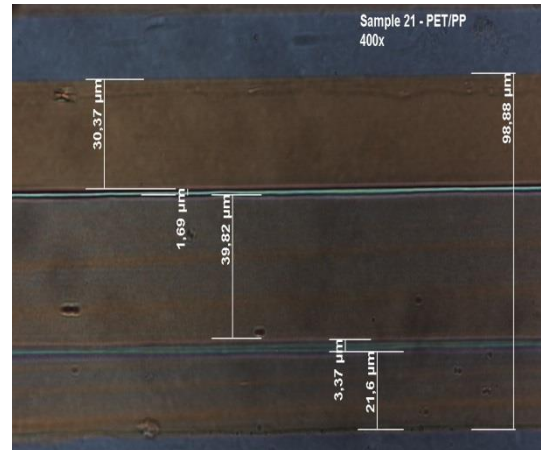


**Figure A-26.** Cross-section of sample 21.

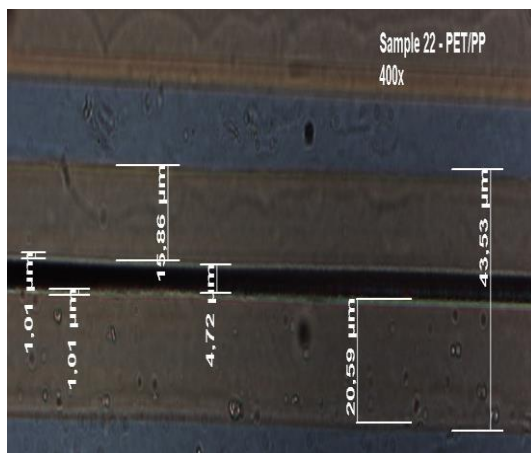


**Figure A-27.** Cross-section of sample 22.

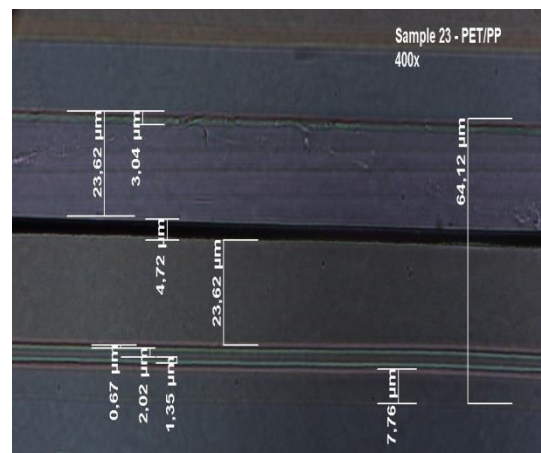


**Figure A-28.** Cross-section of sample 23.

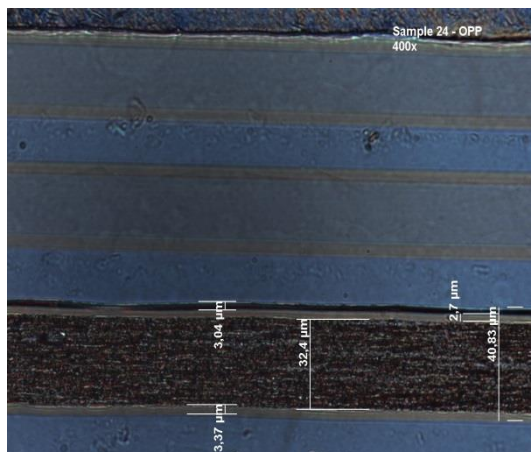


**Figure A-29.** Cross-section of sample 24.

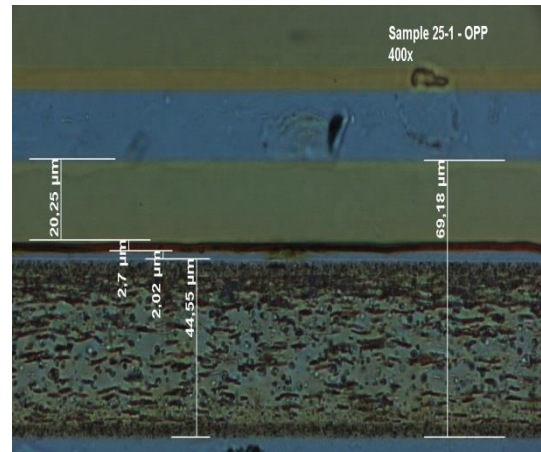


**Figure A-30.** Cross-section of sample 25-1.

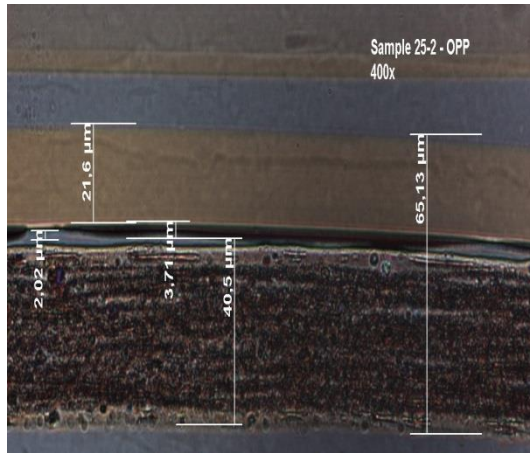


**Figure A-31.** Cross-section of sample 25-2.

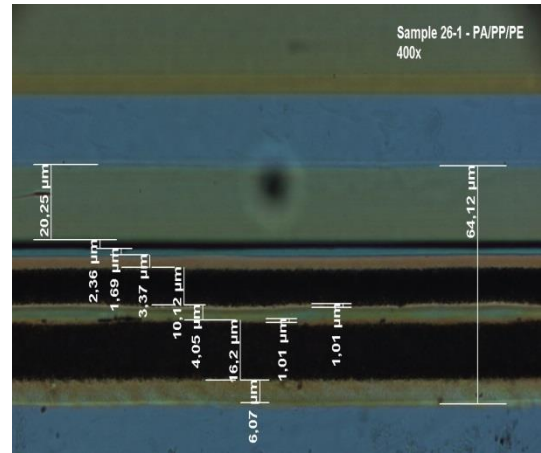


**Figure A-32.** Cross-section of sample 26-1.

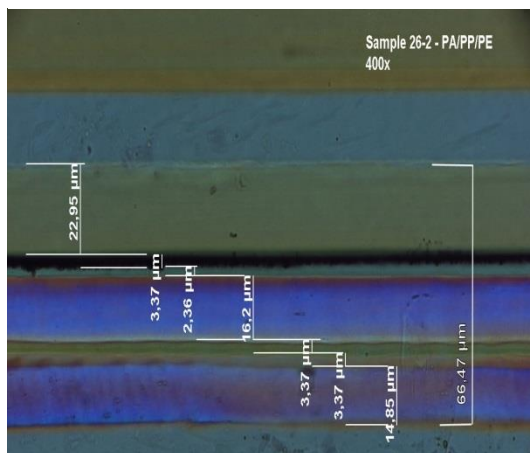


**Figure A-33.** Cross-section of sample 26-2.

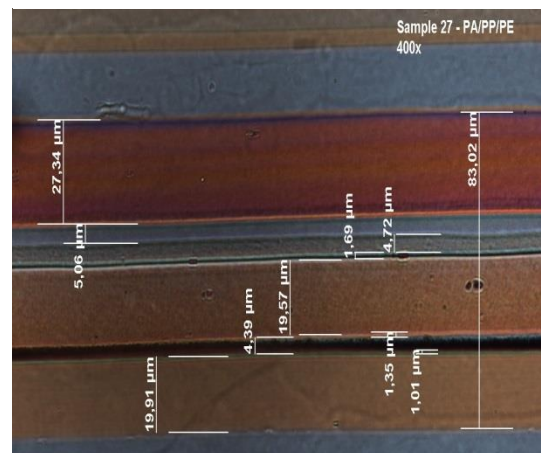


**Figure A-34.** Cross-section of sample 27.

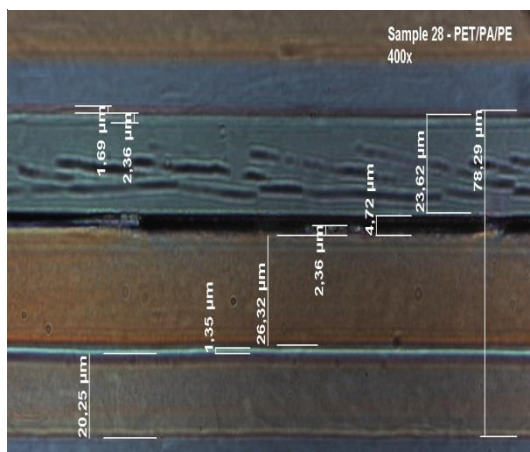


**Figure A-35.** Cross-section of sample 28.

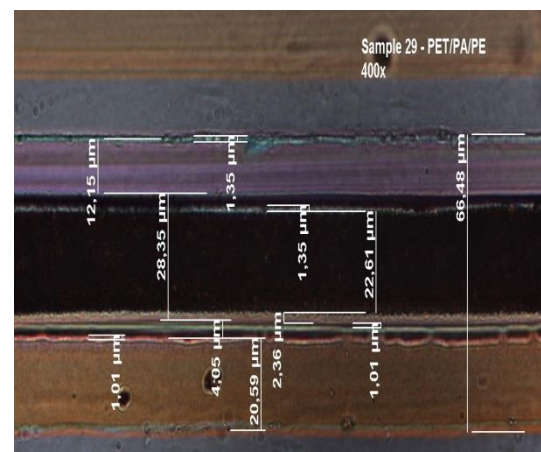


**Figure A-36.** Cross-section of sample 29.

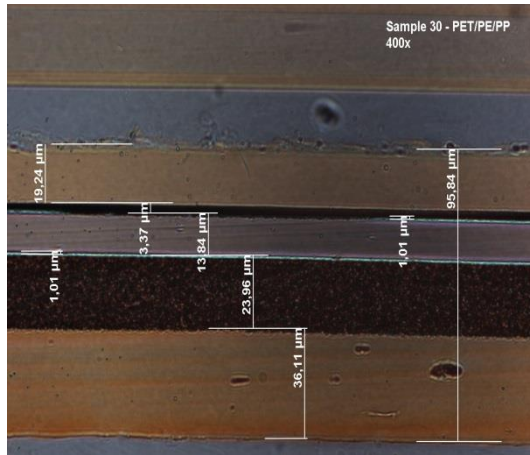


**Figure A-37.** Cross-section of sample 30.

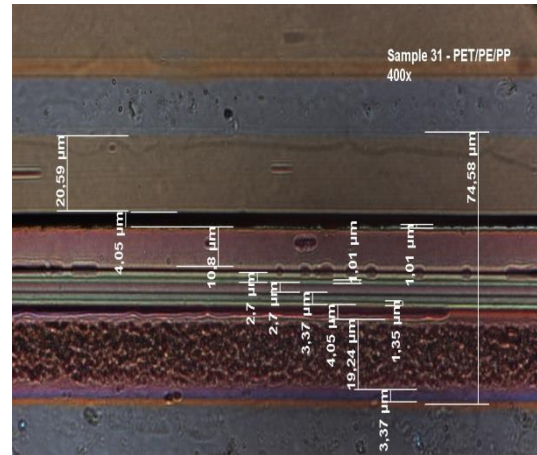


**Figure A-38.** Cross-section of sample 31.

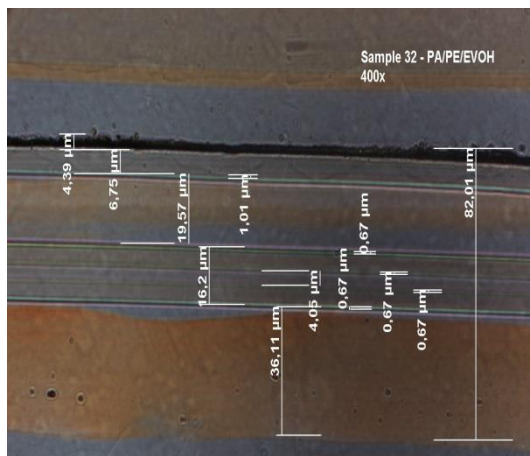


**Figure A-39.** Cross-section of sample 32.

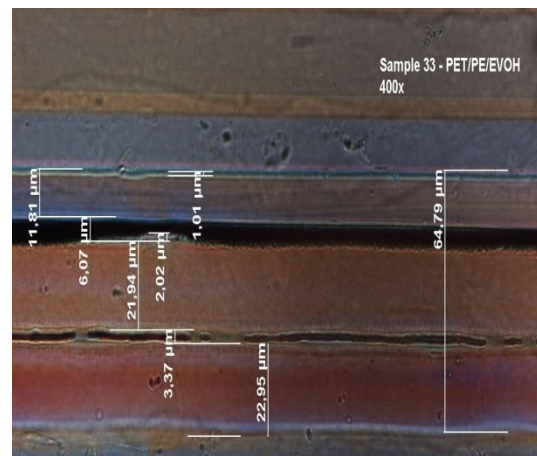


**Figure A-40.** Cross-section of sample 33.

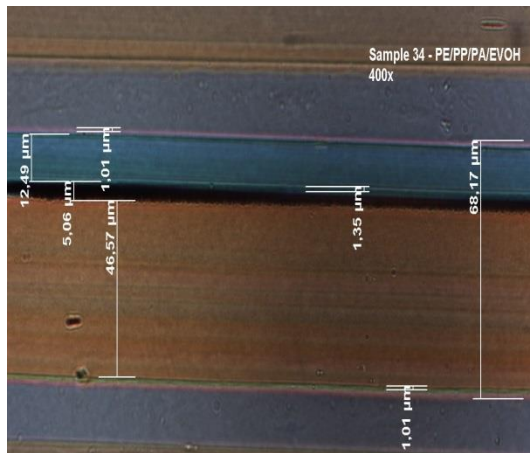


**Figure A-41.** Cross-section of sample 34.

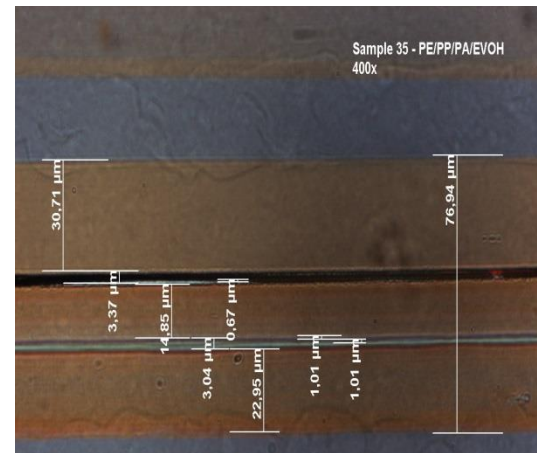


**Figure A-42.** Cross-section of sample 35.



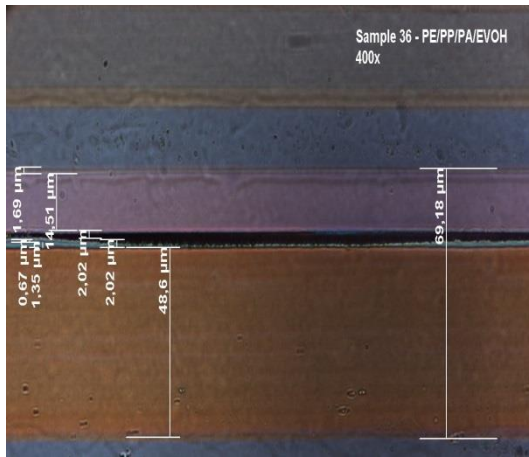


**Figure A-43.** Cross-section of sample 36.

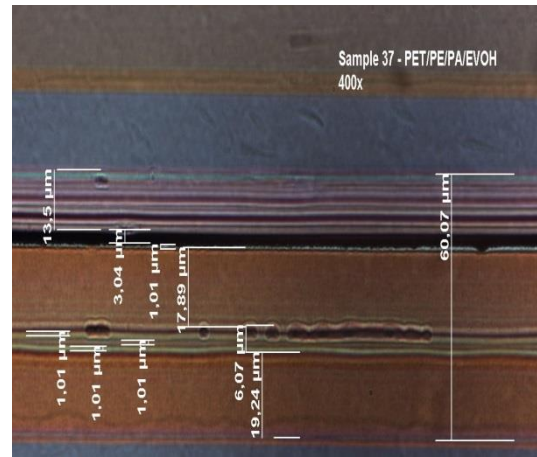


**Figure A-44.** Cross-section of sample 37.

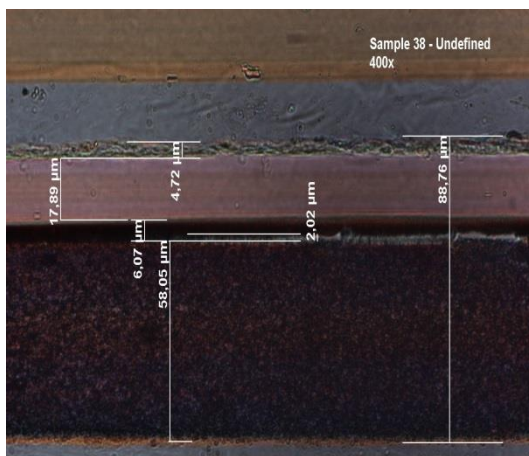


**Figure A-45.** Cross-section of sample 38.

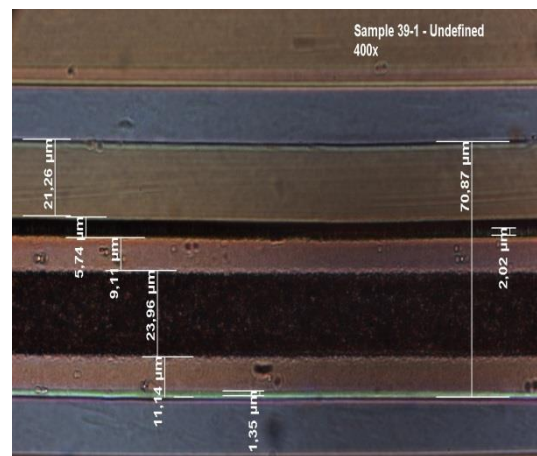


**Figure A-46.** Cross-section of sample 39-1.

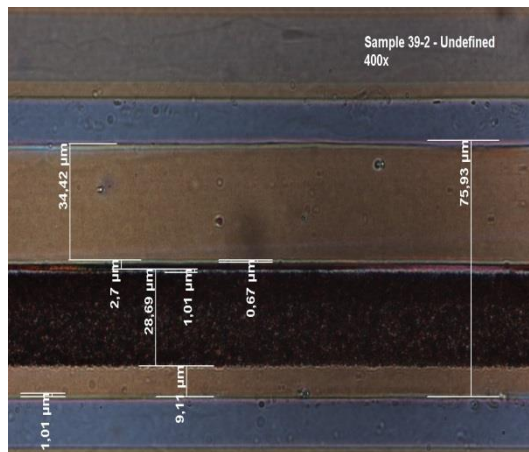


**Figure A-47.** Cross-section of sample 39-2.

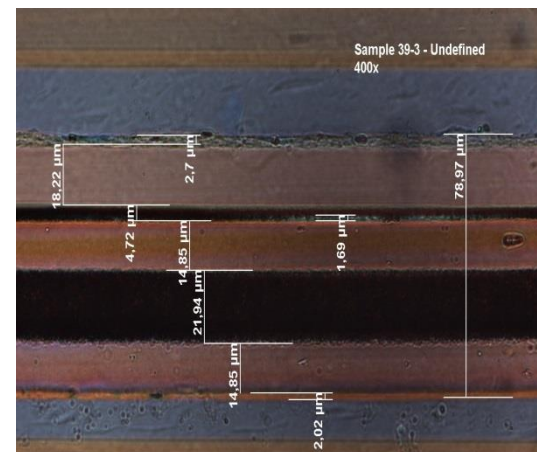


**Figure A-48.** Cross-section of sample 39-3.

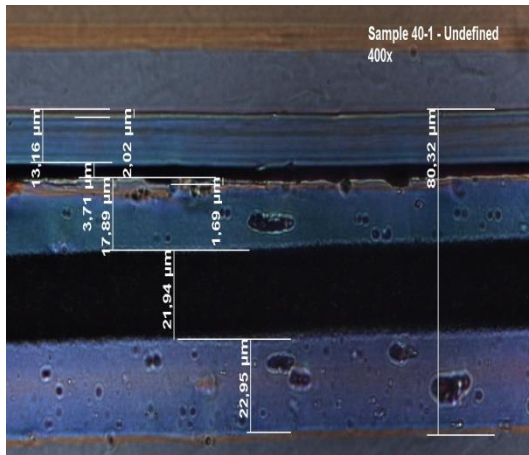


**Figure A-49.** Cross-section of sample 40-1.

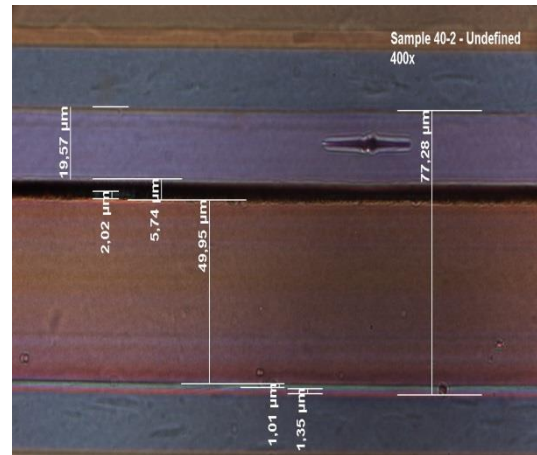


**Figure A-50.** Cross-section of sample 40-2.

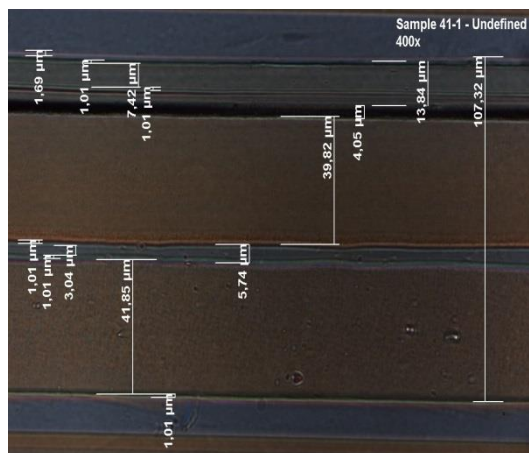


**Figure A-51.** Cross-section of sample 41-1.

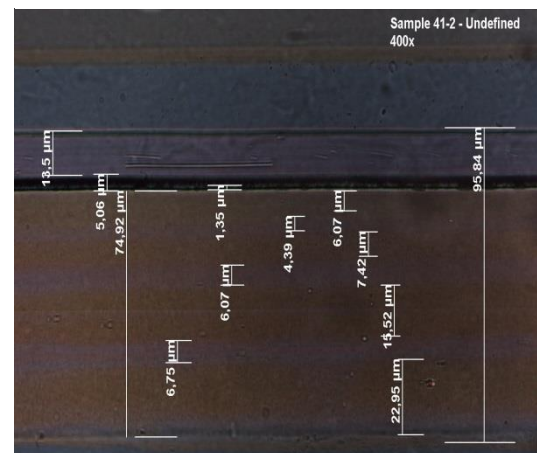


**Figure A-52.** Cross-section of sample 41-2.

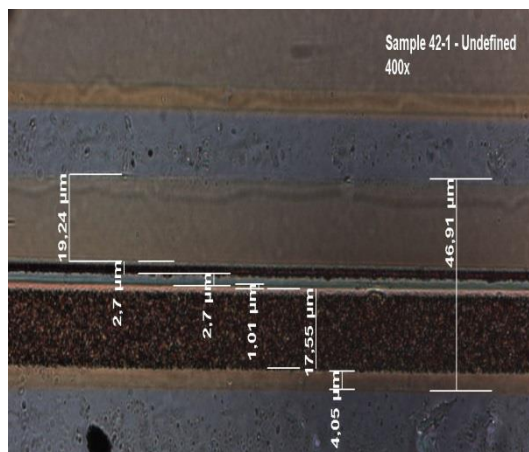


**Figure A-53.** Cross-section of sample 42-1.

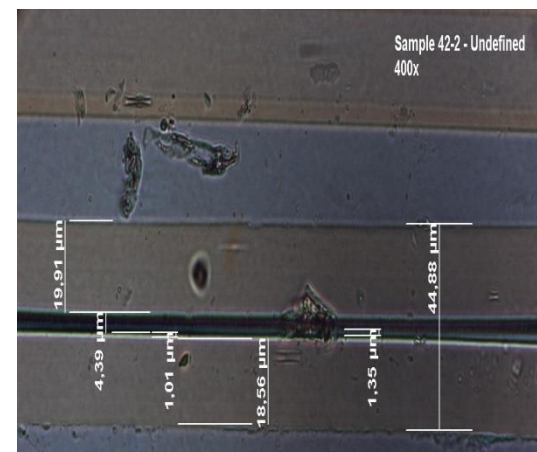


**Figure A-54.** Cross-section of sample 42-2.

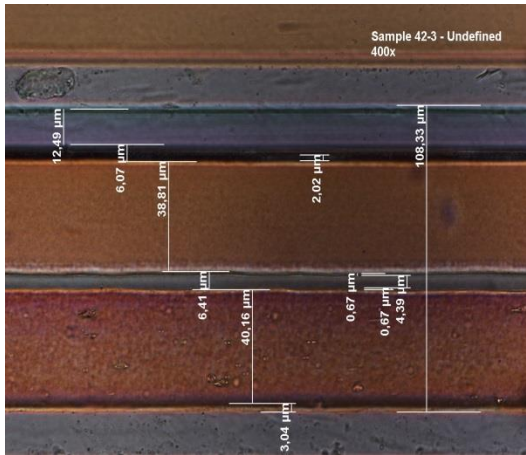


**Figure A-55.** Cross-section of sample 42-3.

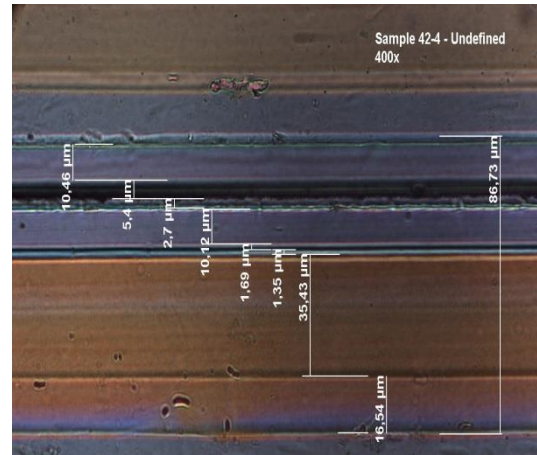


**Figure A-56.** Cross-section of sample 42-4.

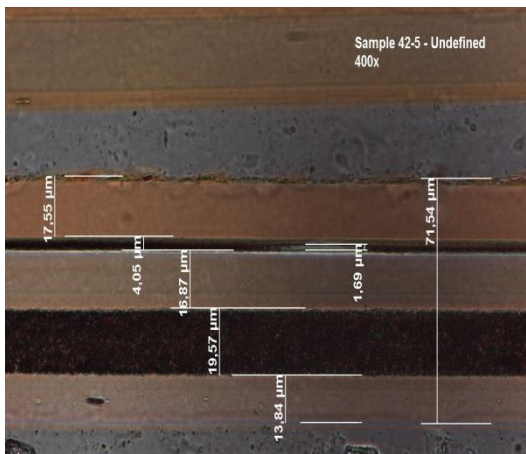


**Figure A-57.** Cross-section of sample 42-5.

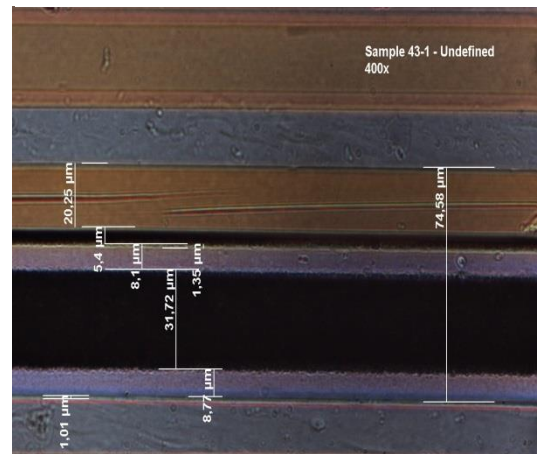


**Figure A-58.** Cross-section of sample 43-1.

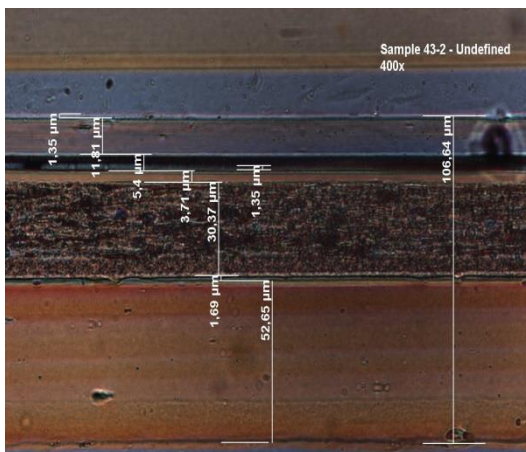


**Figure A-59.** Cross-section of sample 43-2.

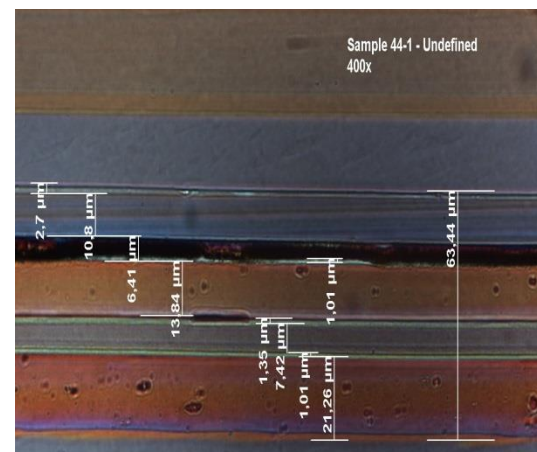


**Figure A-60.** Cross-section of sample 44-1.

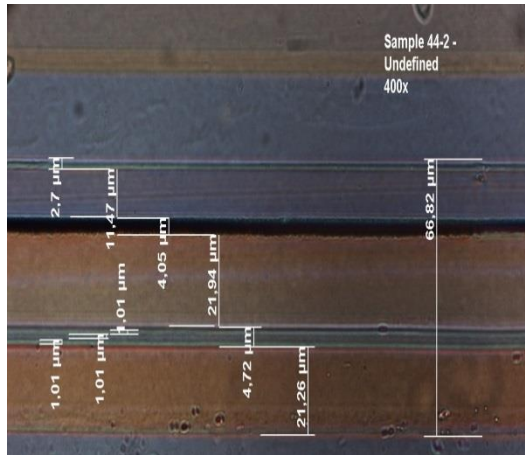


**Figure A-61.** Cross-section of sample 44-2.

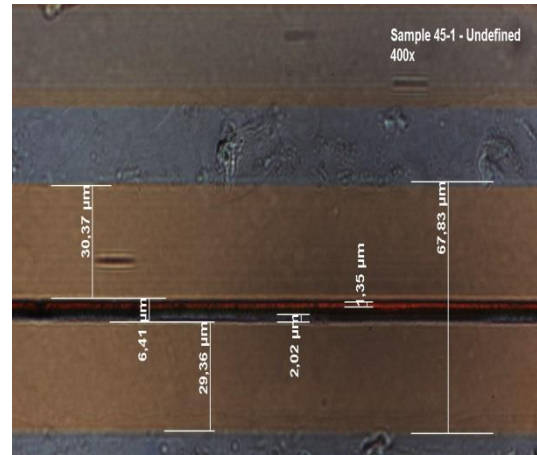


**Figure A-62.** Cross-section of sample 45-1.

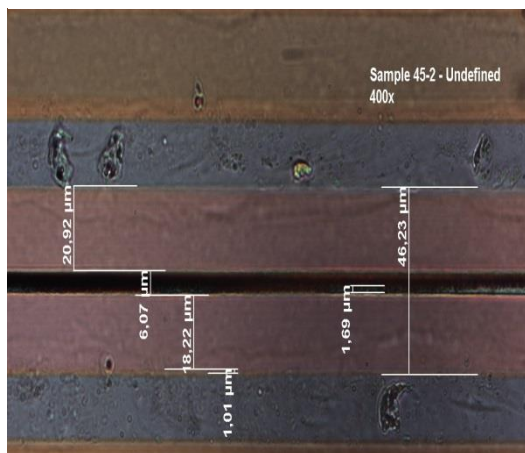


**Figure A-63.** Cross-section of sample 45-2.

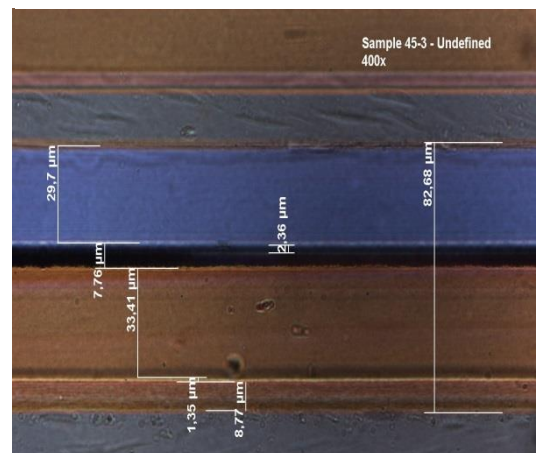


**Figure A-64.** Cross-section of sample 45-3.

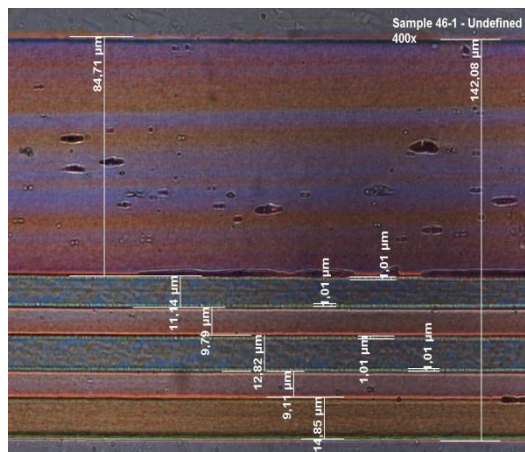


**Figure A-65.** Cross-section of sample 46-1.

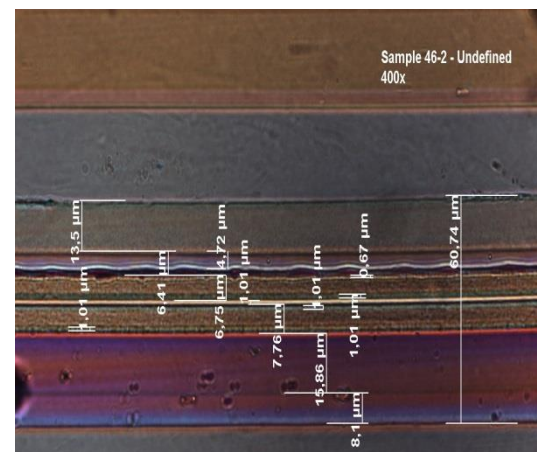


**Figure A-66.** Cross-section of sample 46-2.

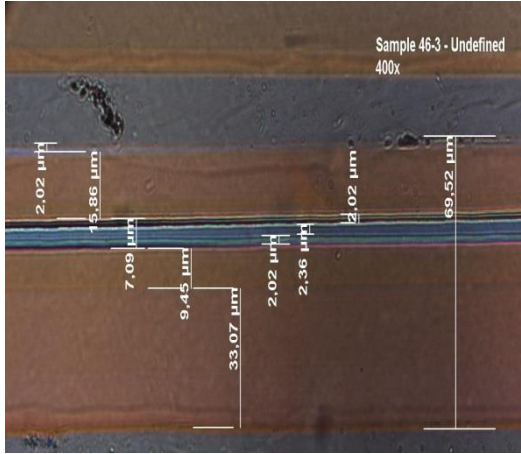


**Figure A-67.** Cross-section of sample 46-3.

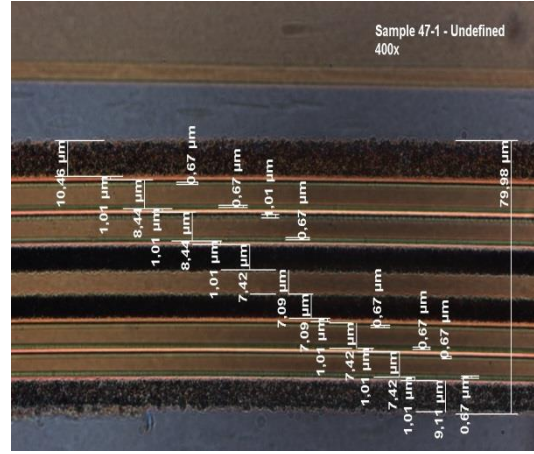


**Figure A-68.** Cross-section of sample 47-1.

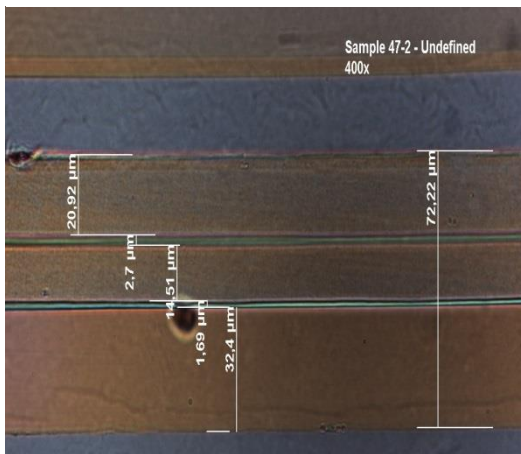


**Figure A-69.** Cross-section of sample 47-2.

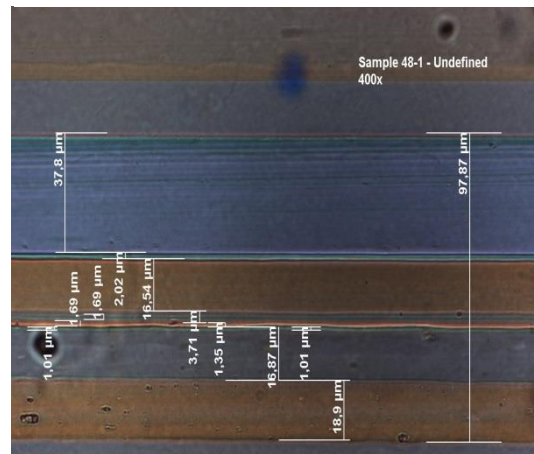


**Figure A-70.** Cross-section of sample 48-1.

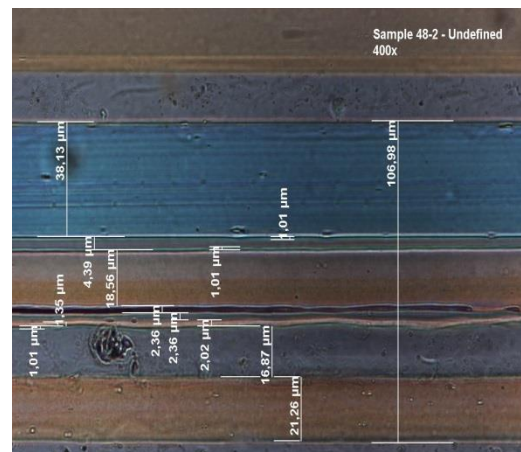


**Figure A-71.** Cross-section of sample 48-2.

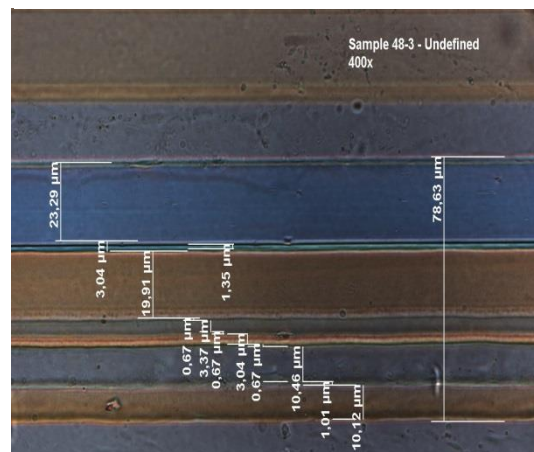


**Figure A-72.** Cross-section of sample 48-3.

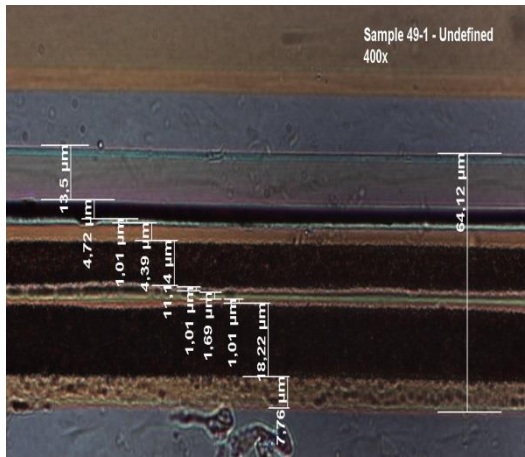


**Figure A-73.** Cross-section of sample 49-1.

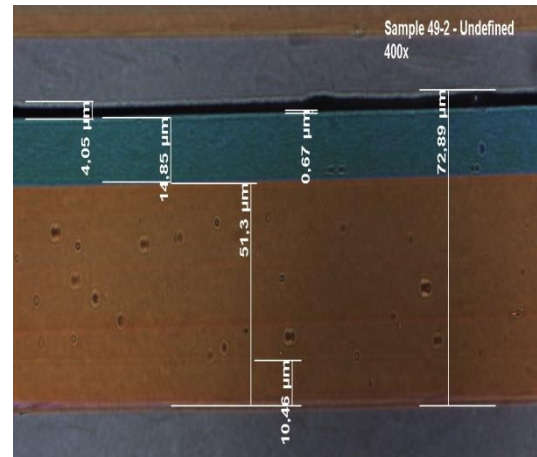


**Figure A-74.** Cross-section of sample 49-2.

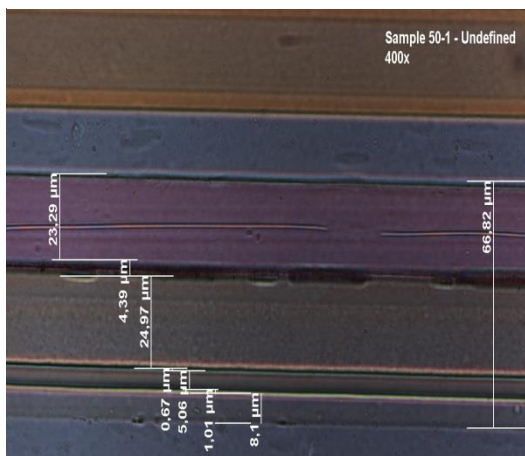


**Figure A-75.** Cross-section of sample 50-1.

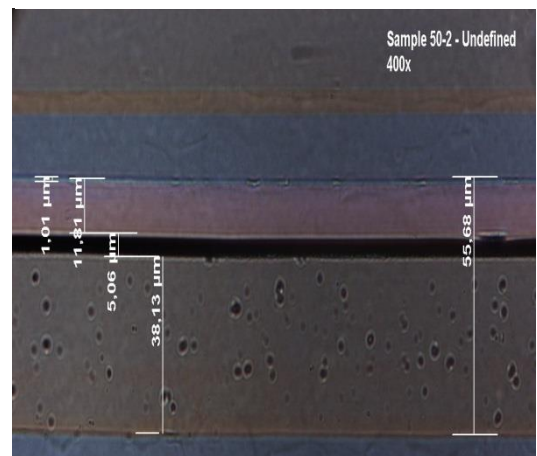


**Figure A-76.** Cross-section of sample 50-2.

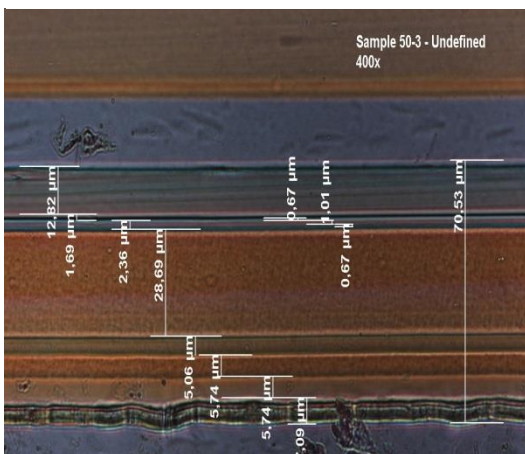


**Figure A-77.** Cross-section of sample 50-3.

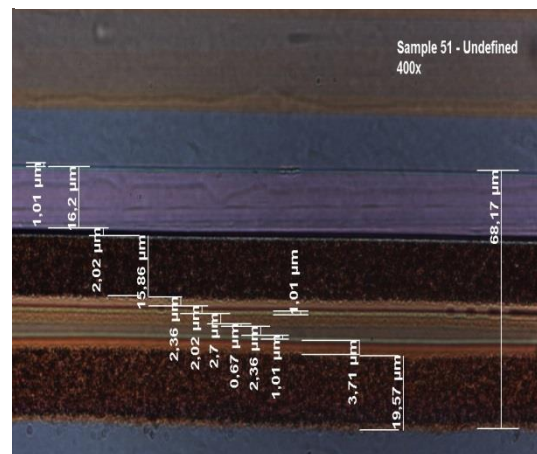


**Figure A-78.** Cross-section of sample 51.



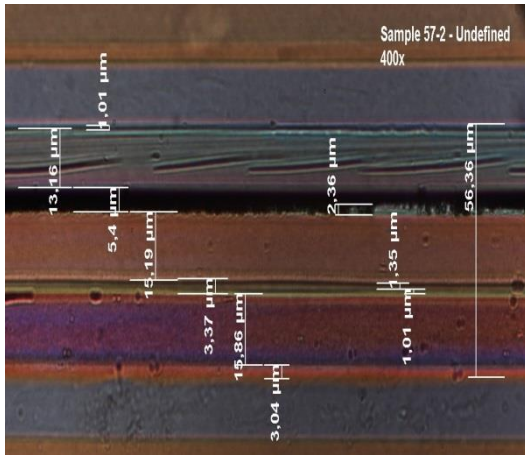


**Figure A-85.** Cross-section of sample 57-3.

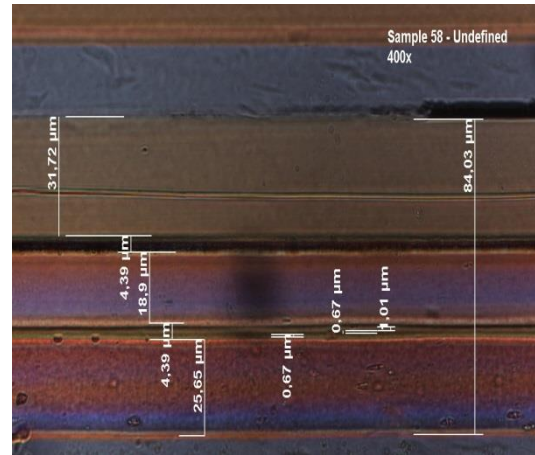


**Figure A-86.** Cross-section of sample 58.

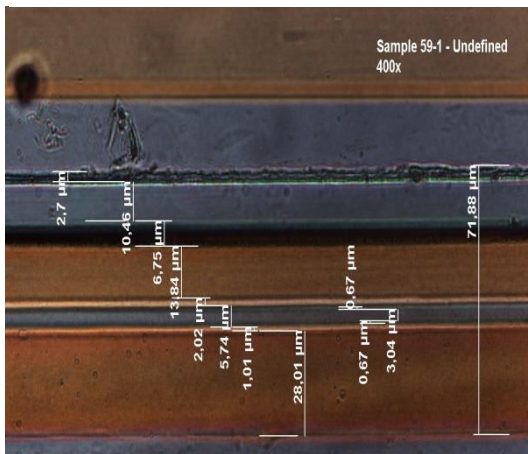


**Figure A-87.** Cross-section of sample 59-1.

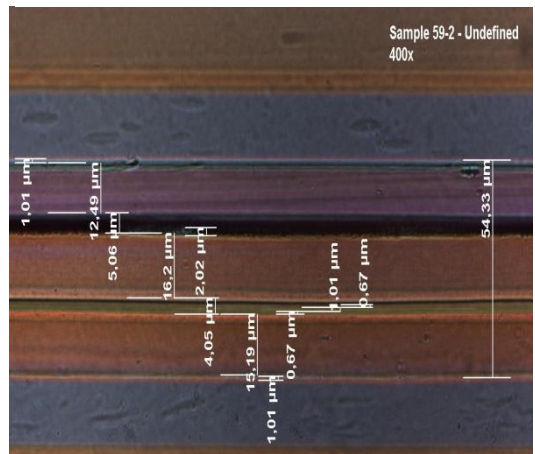


**Figure A-88.** Cross-section of sample 59-2.

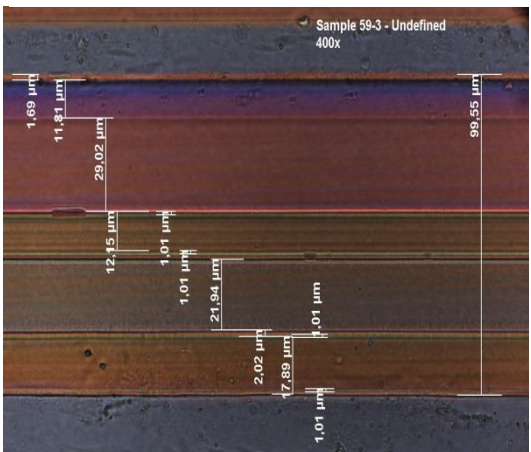


**Figure A-89.** Cross-section of sample 59-3.

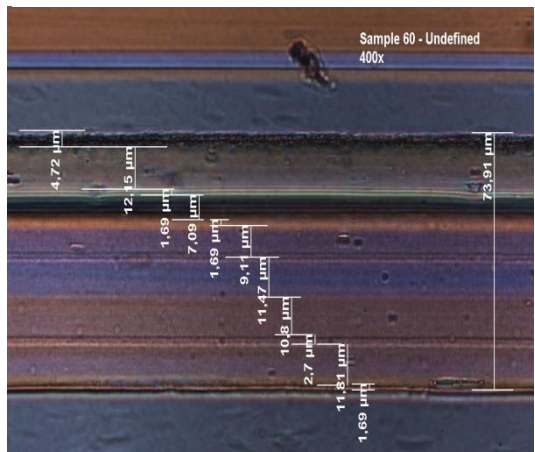


**Figure A-90.** Cross-section of sample 60.



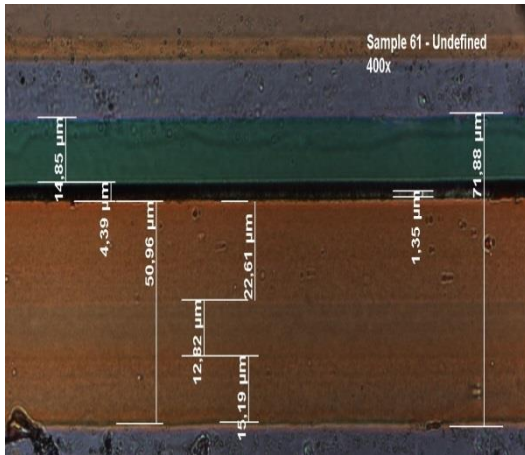


**Figure A-91.** Cross-section of sample 61.

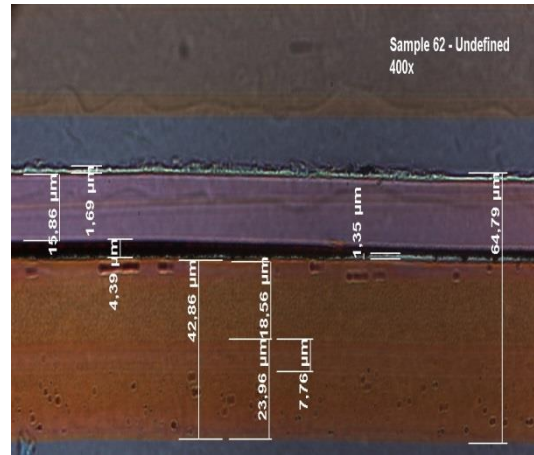


**Figure A-92.** Cross-section of sample 62.

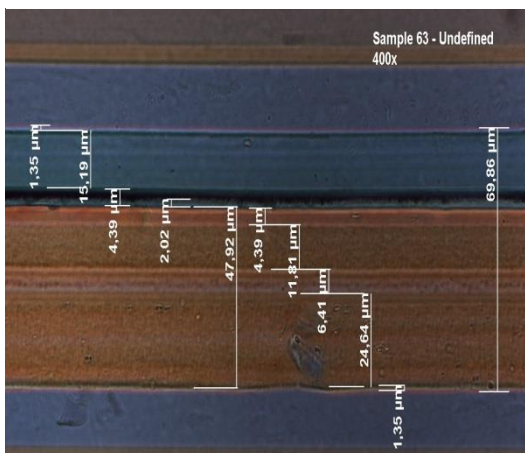


**Figure A-93.** Cross-section of sample 63.

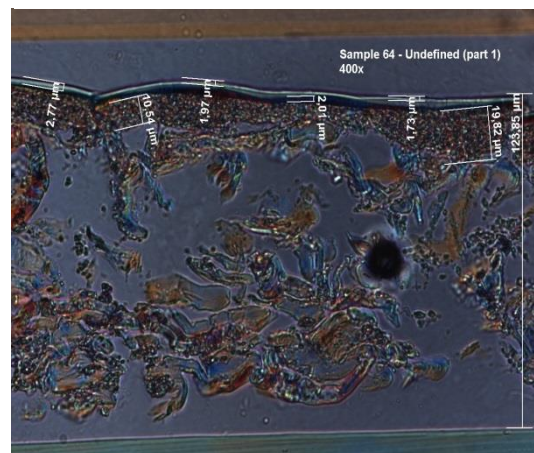


**Figure A-94.** Cross-section of sample 64 (part 1).

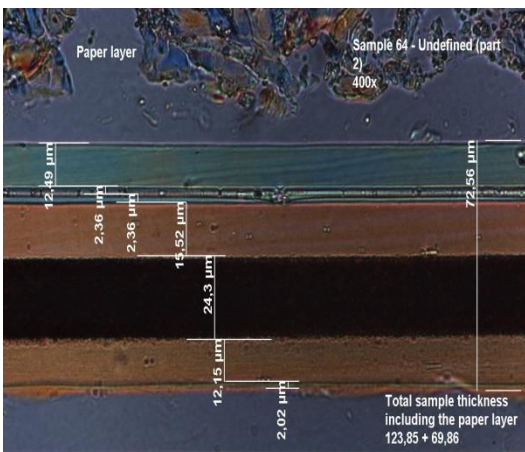


**Figure A-95.** Cross-section of sample 64 (part 2).

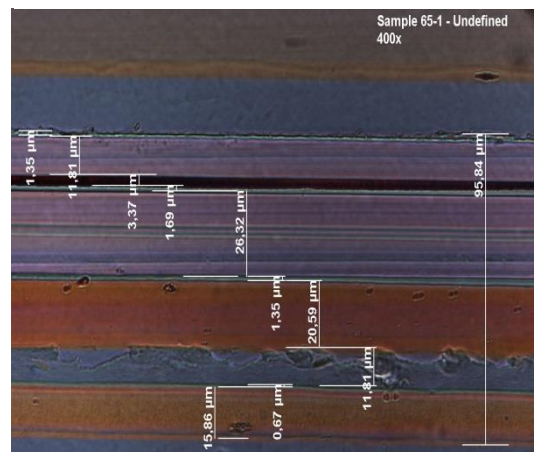


**Figure A-96.** Cross-section of sample 65-1.

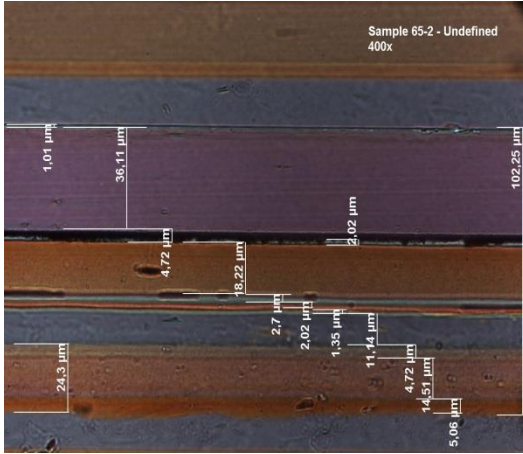


**Figure A-97.** Cross-section of sample 65-2.

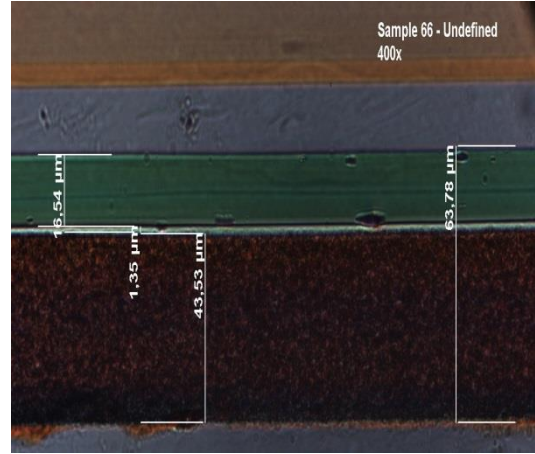


**Figure A-98.** Cross-section of sample 66.

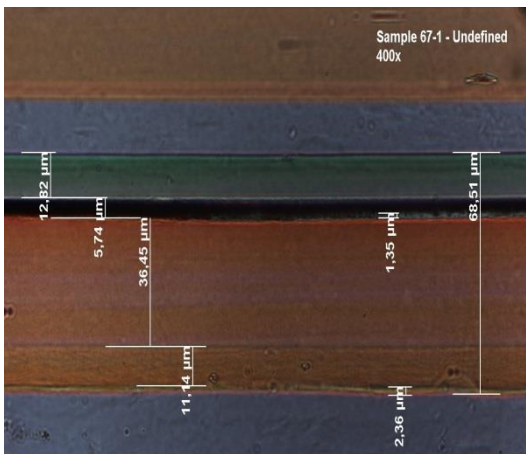


**Figure A-99.** Cross-section of sample 67-1.

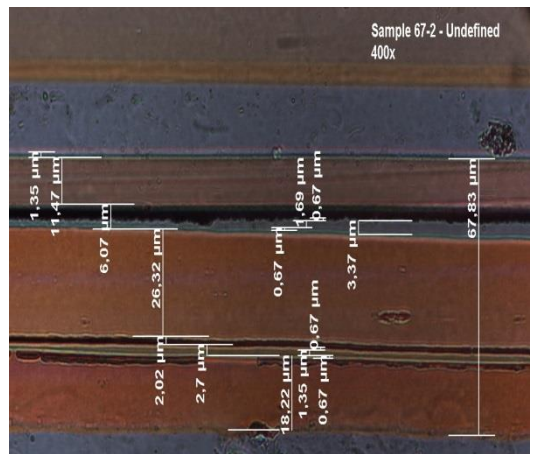


**Figure A-100.** Cross-section of sample 67-2.

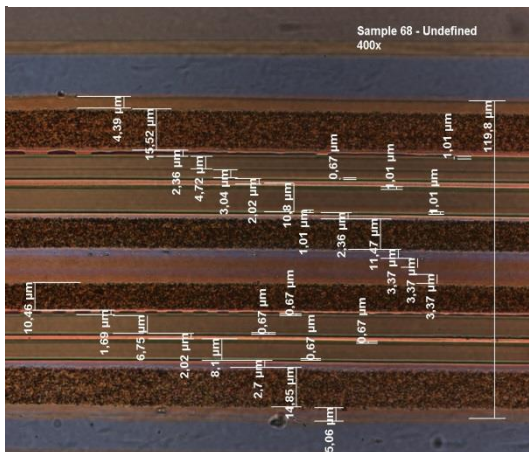


**Figure A-101.** Cross-section of sample 68.

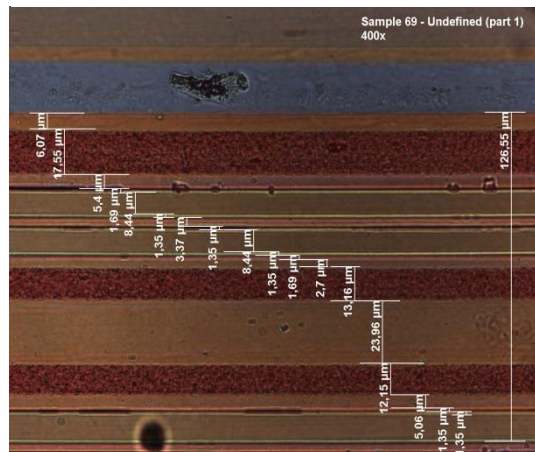


**Figure A-102.** Cross-section of sample 69 (part 1).

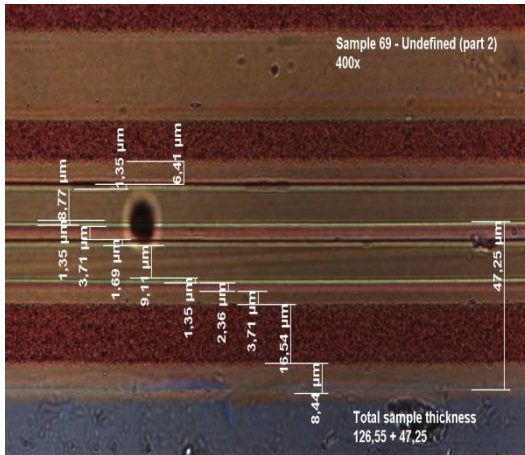


**Figure A-103.** Cross-section of sample 69 (part 2).

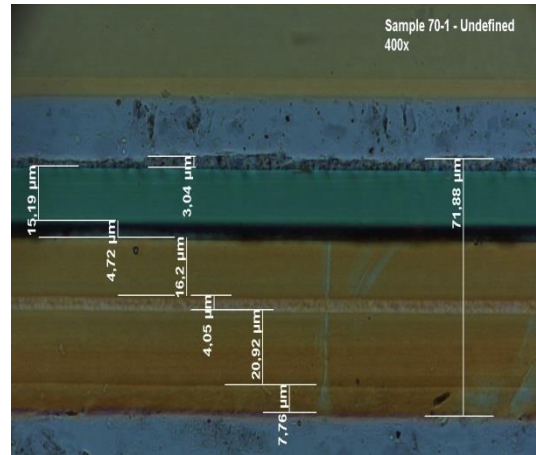


**Figure A-104.** Cross-section of sample 70-1.

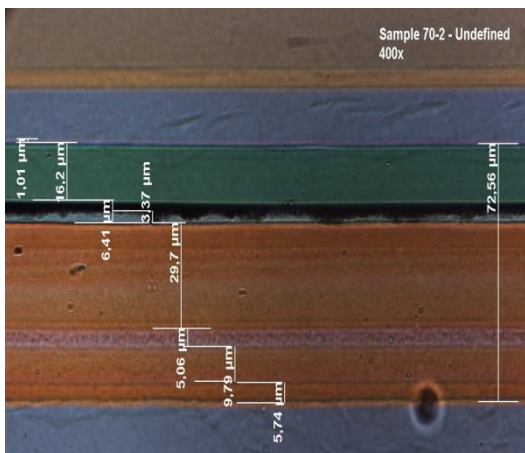


**Figure A-105.** Cross-section of sample 70-2.

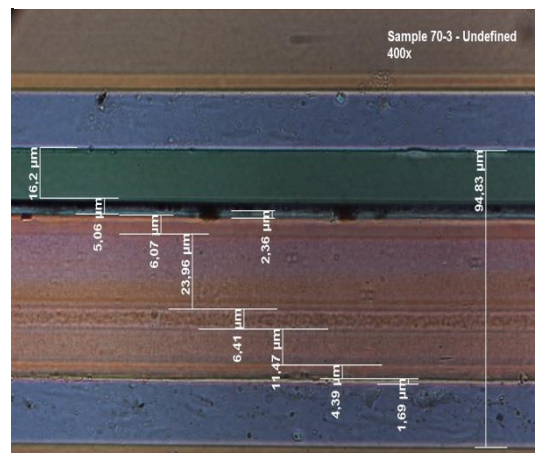


**Figure A-106.** Cross-section of sample 70-3.

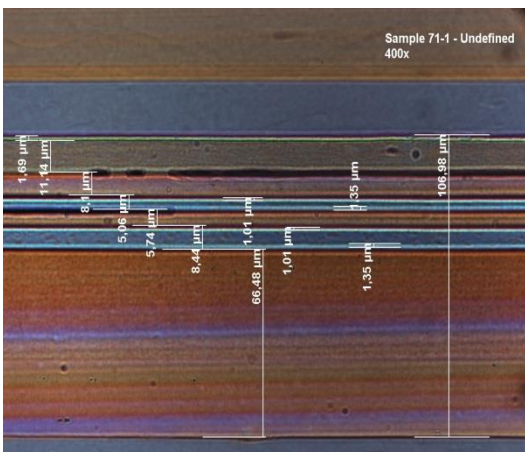


**Figure A-107.** Cross-section of sample 71-1.

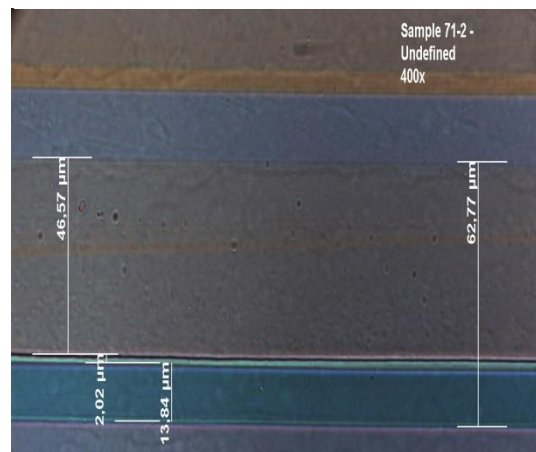


**Figure A-108.** Cross-section of sample 71-2.

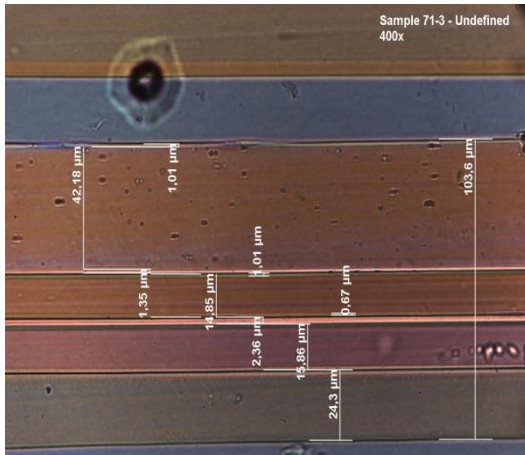


**Figure A-109.** Cross-section of sample 71-3.

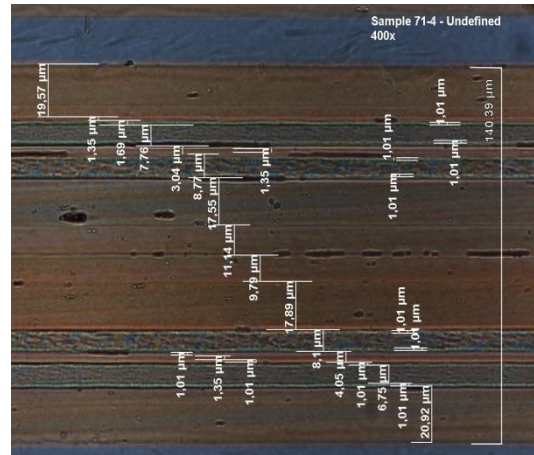


**Figure A-110.** Cross-section of sample 71-4.

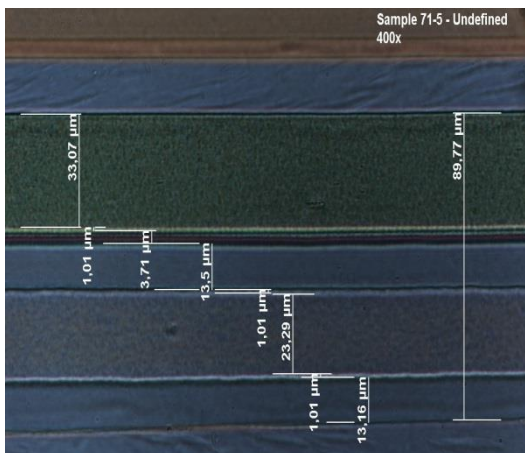


**Figure A-111.** Cross-section of sample 71-5.

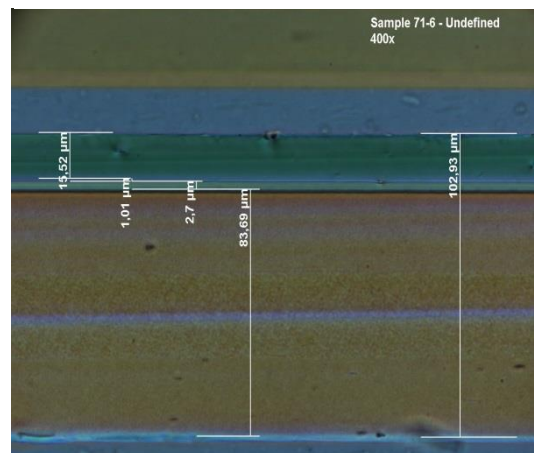


**Figure A-112.** Cross-section of sample 71-6.

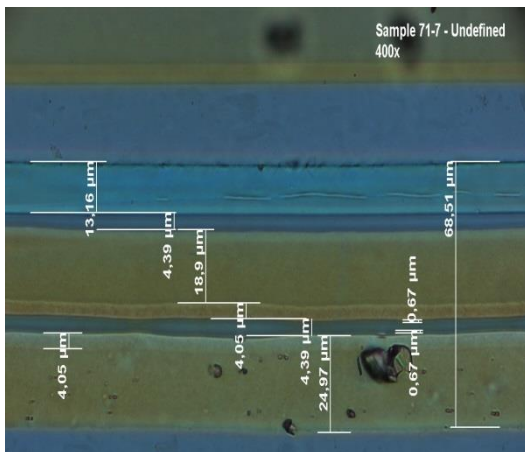


**Figure A-113.** Cross-section of sample 71-7.

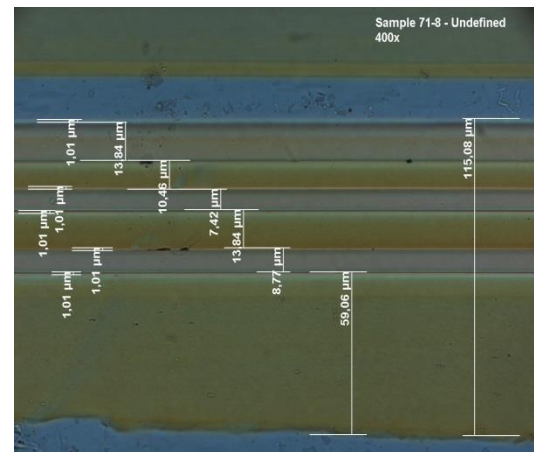


**Figure A-114.** Cross-section of sample 71-8.

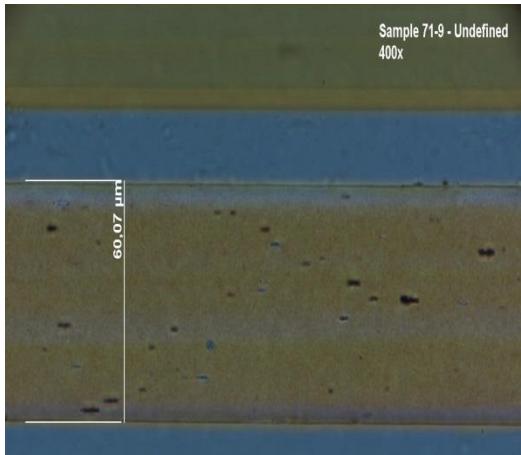


**Figure A-115.** Cross-section of sample 71-9.

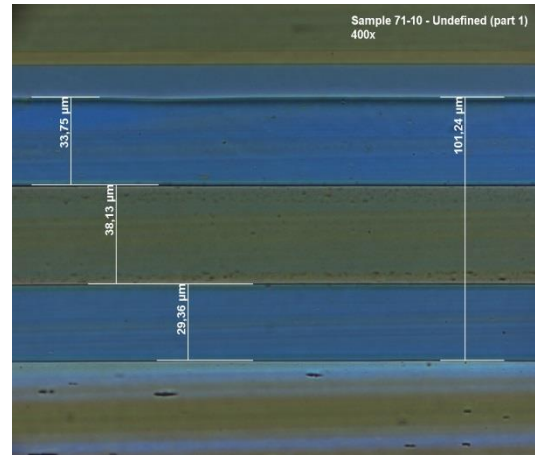


**Figure A-116.** Cross-section of sample 71-10 (part 1).

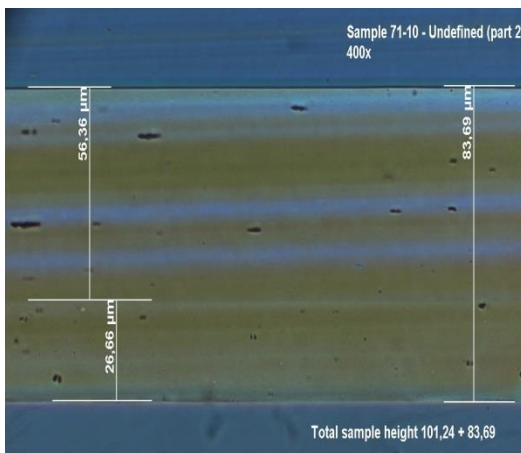


**Figure A-117.** Cross-section of sample 71-10 (part 2).

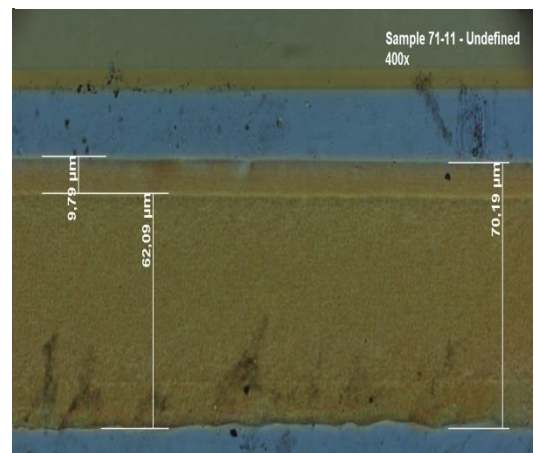


**Figure A-118.** Cross-section of sample 71-11.

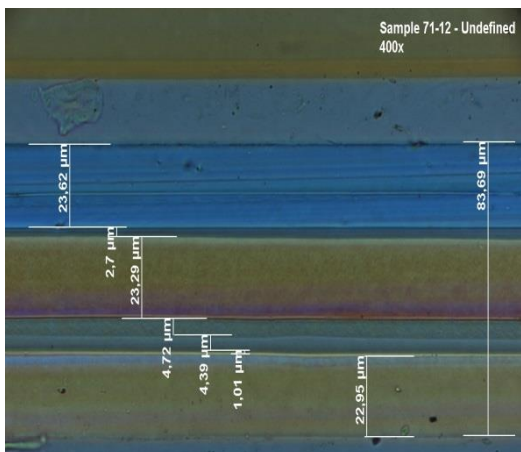


**Figure A-119.** Cross-section of sample 71-12.

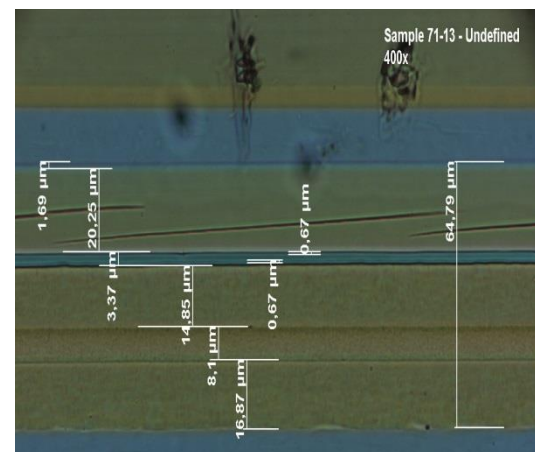


**Figure A-120.** Cross-section of sample 71-13.

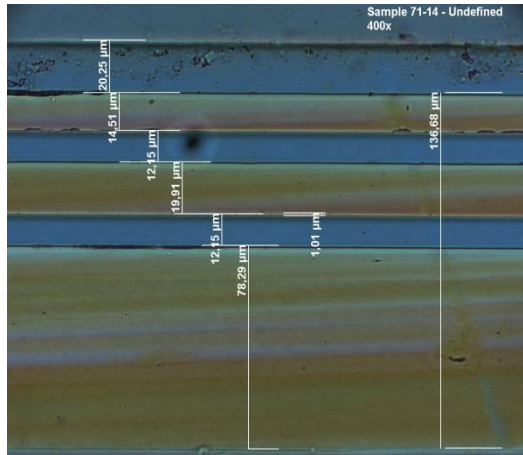


**Figure A-121.** Cross-section of sample 71-14.

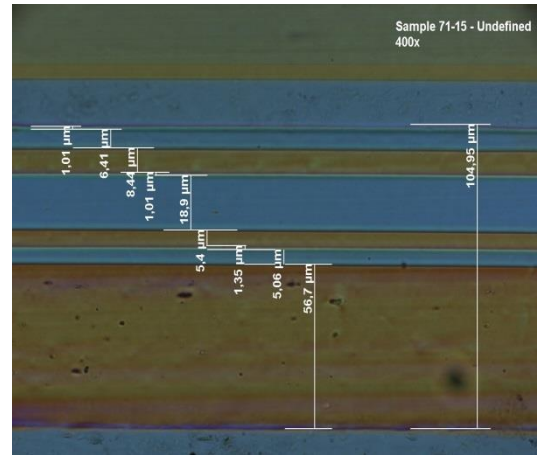


**Figure A-122.** Cross-section of sample 71-15.

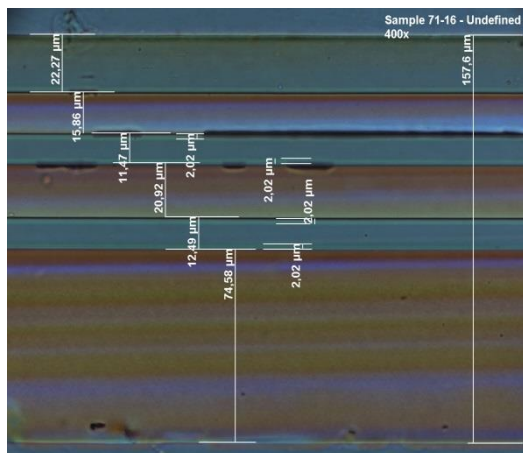


**Figure A-123.** Cross-section of sample 71-16.

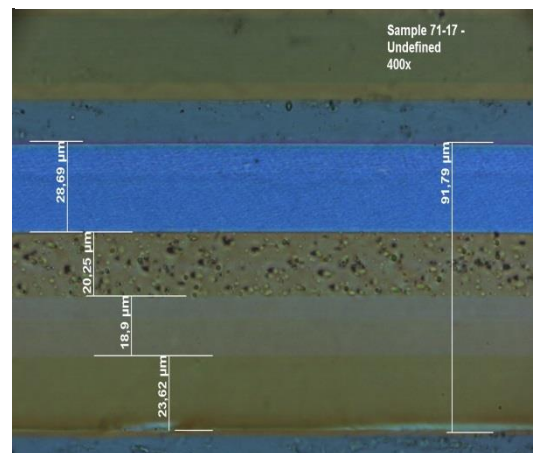


**Figure A-124.** Cross-section of sample 71-17.

## APPENDIX B: DSC FIGURES

14 of the DSC curves are presented in Appendix B. Rest of the analyzed DSC curves are similar to the curves presented in this appendix.

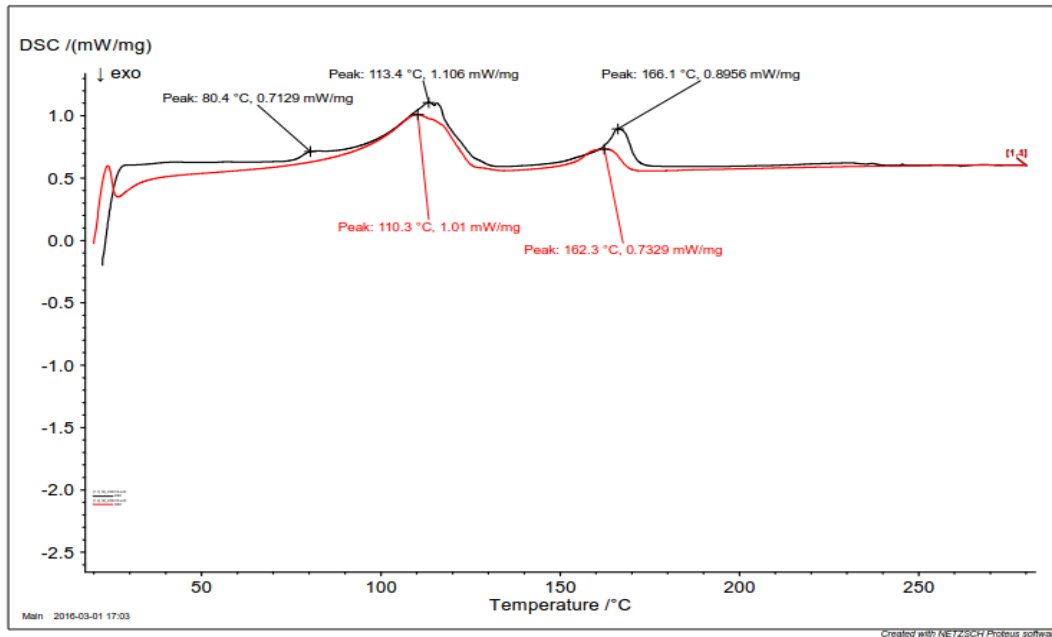


*Figure B-1. DSC curve from sample 38 with peaks from EVA, LDPE and PP.*

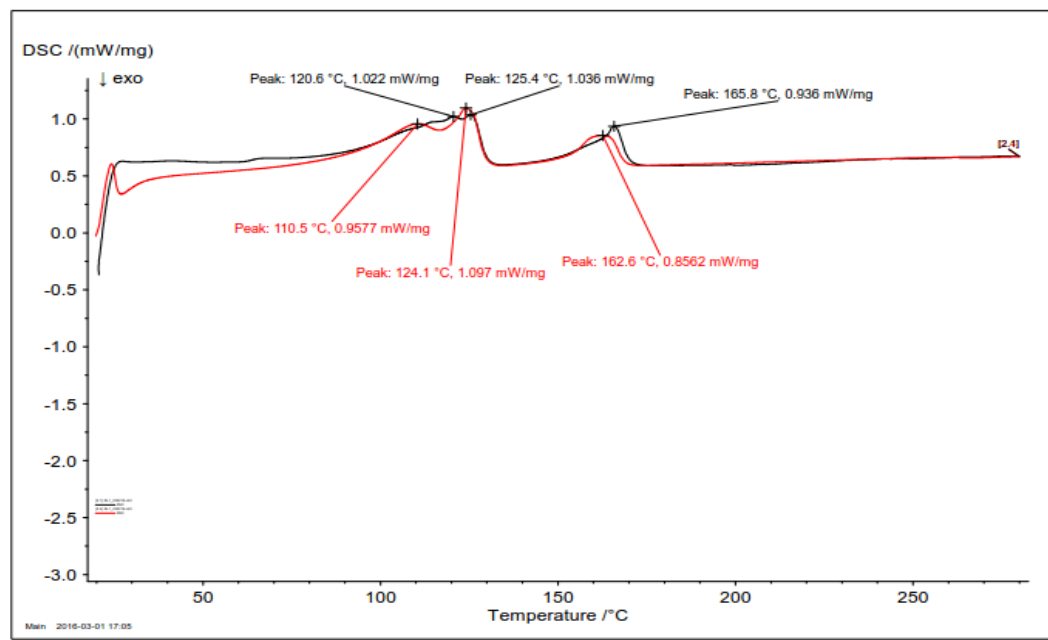


*Figure B-2. DSC curve of sample 39-1 with peaks from LDPE, LLDPE and PP.*

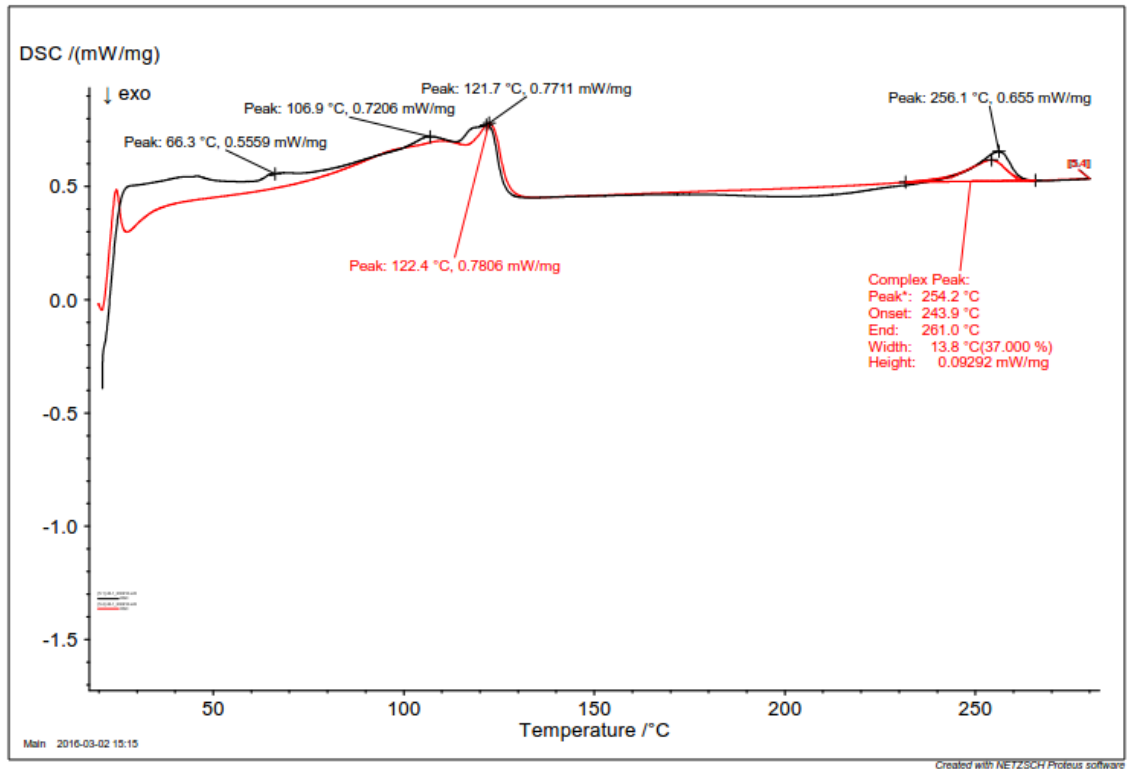


**Figure B-3.** DSC curve of sample 40-1 with peaks from EVA, LDPE, LLDPE and PET.

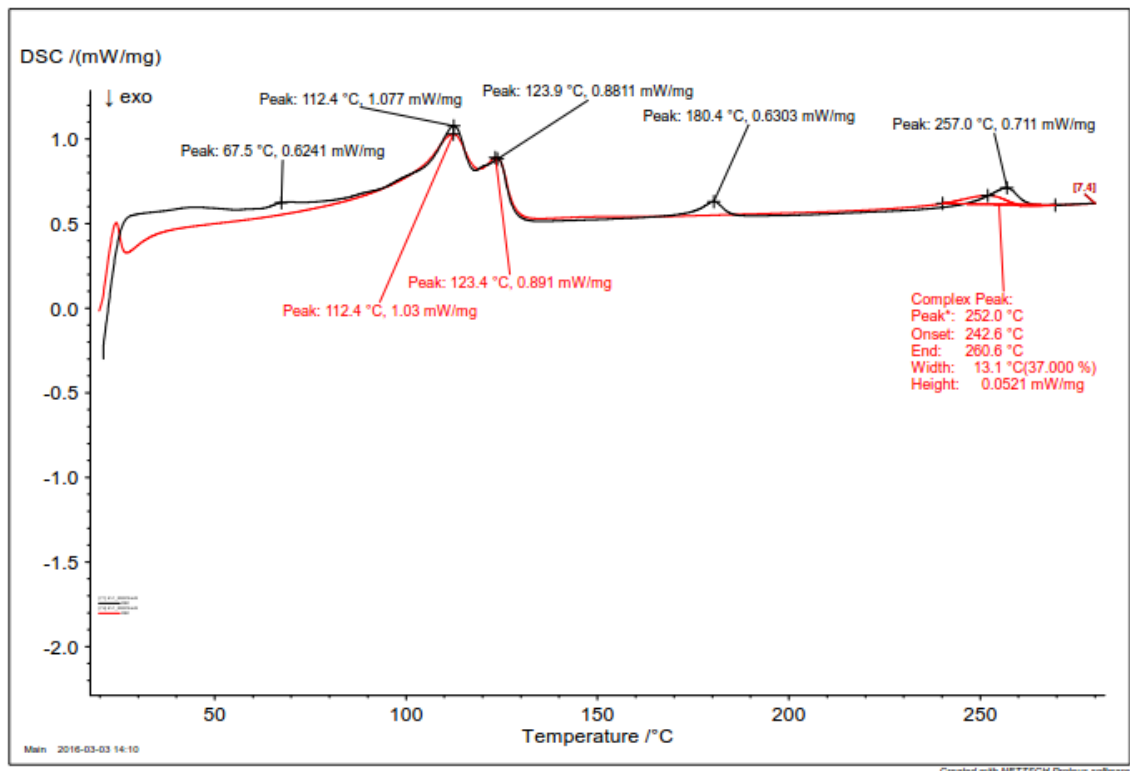


**Figure B-4.** DSC curve of sample 41-1 with peaks from EVA, LDPE, LLDPE, EVOH and PET.



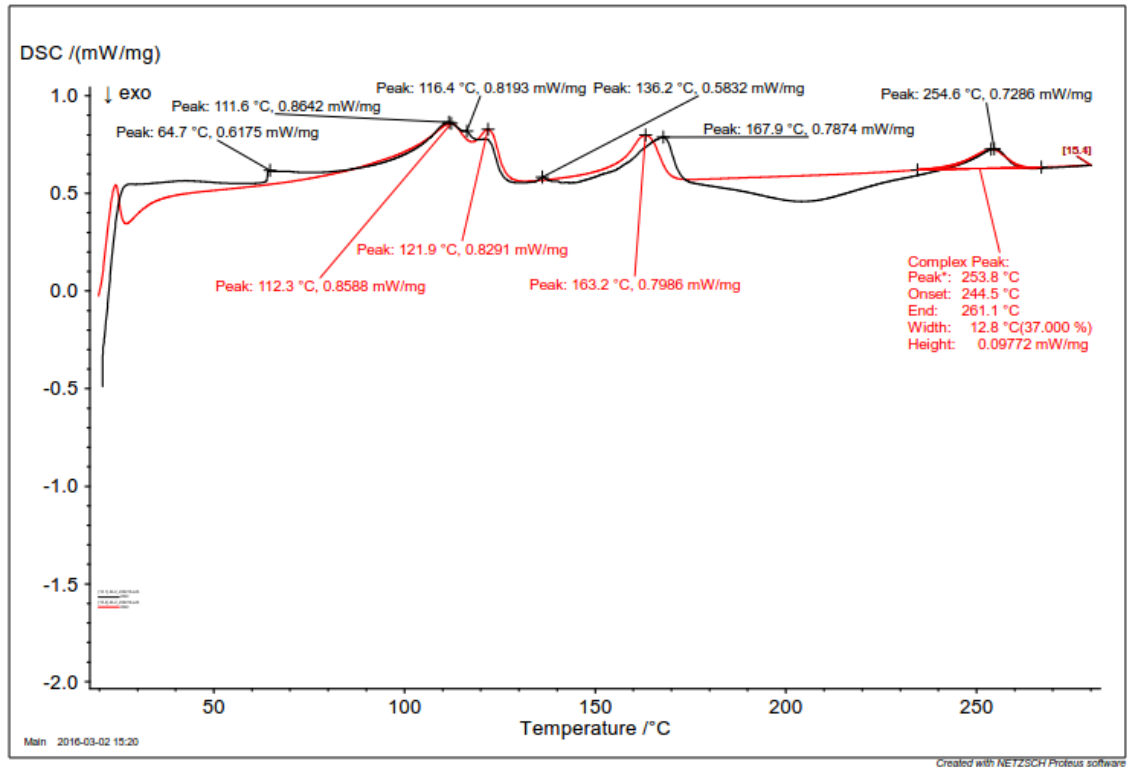


**Figure B-5.** DSC curve of sample 43-2 with peaks from EVA, LDPE, LLDPE, PP and PET.

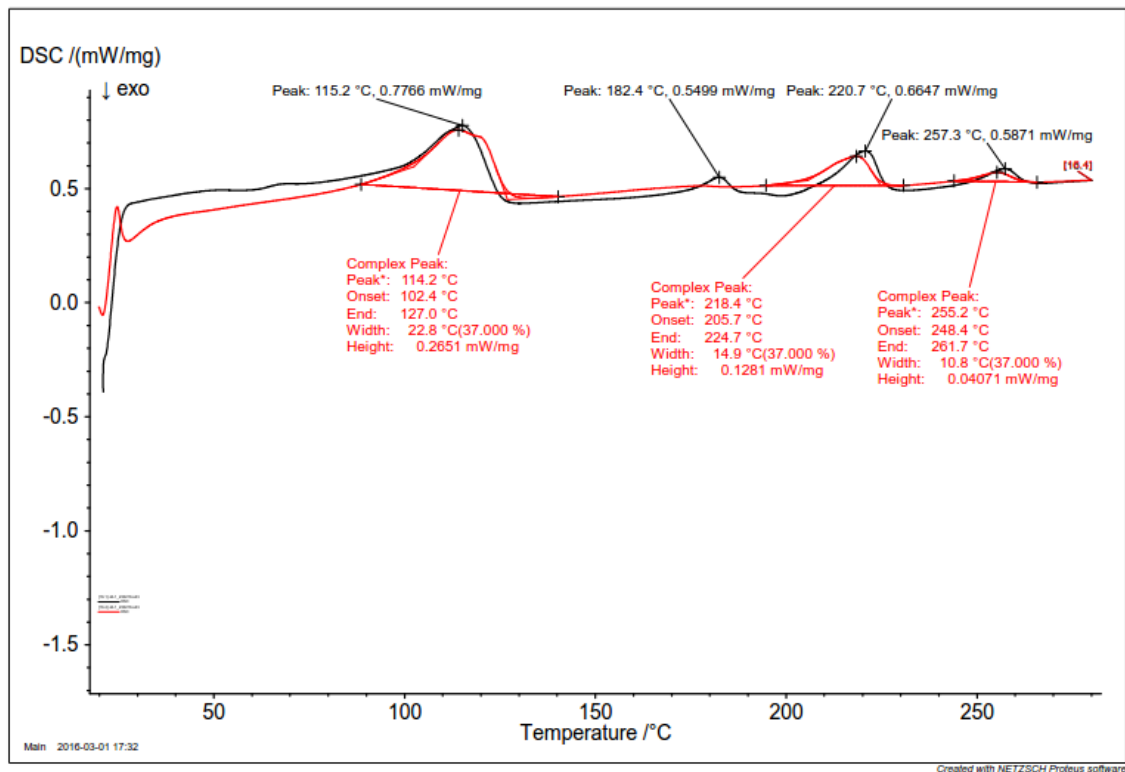


**Figure B-6.** DSC curve of sample 44-1 with peaks from LDPE, EVOH, PA-6 and PET.

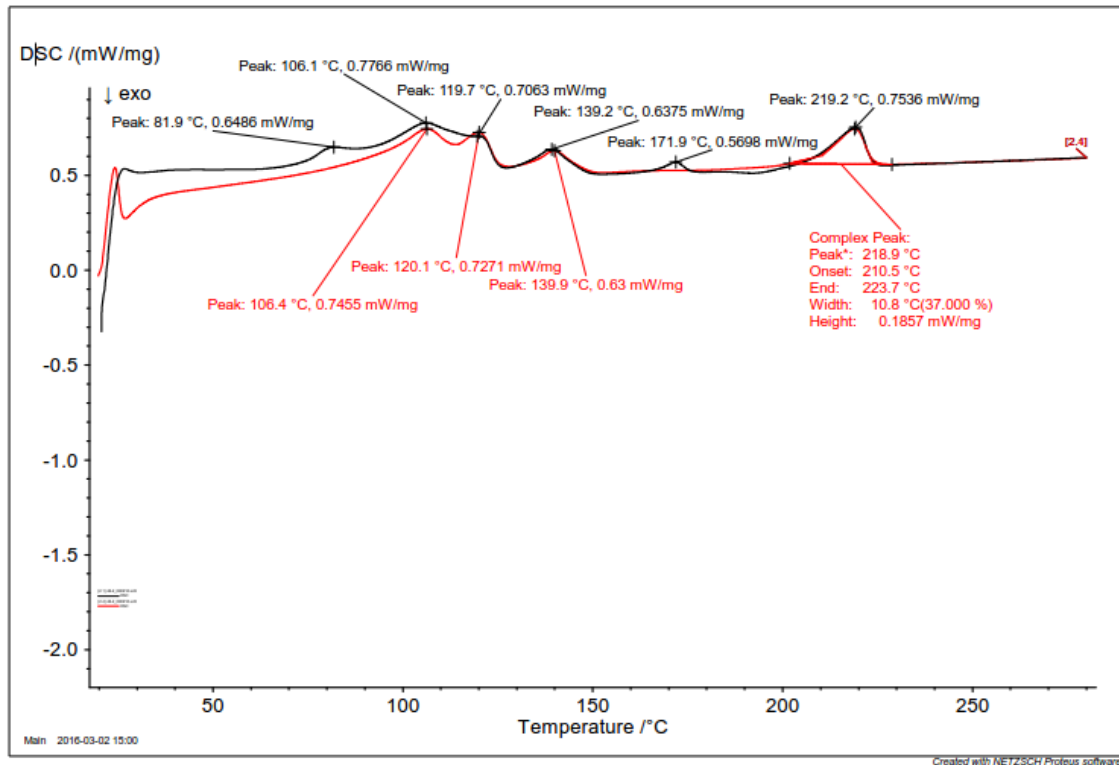


**Figure B-7.** DSC curve of sample 46-2 with peaks from EVA, LDPE, LLDPE, aPP, EVOH and PA-6.

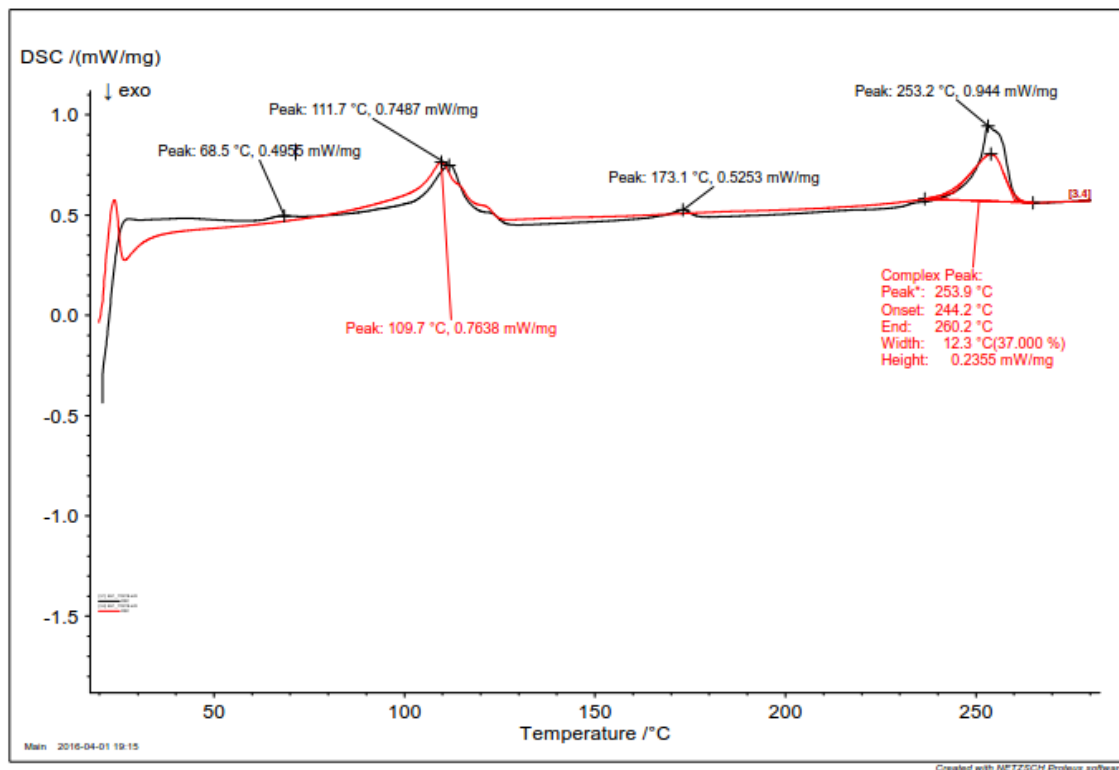


**Figure B-8.** DSC curve of sample 48-1 with peaks from EVA, LDPE, EVOH and PA-6.

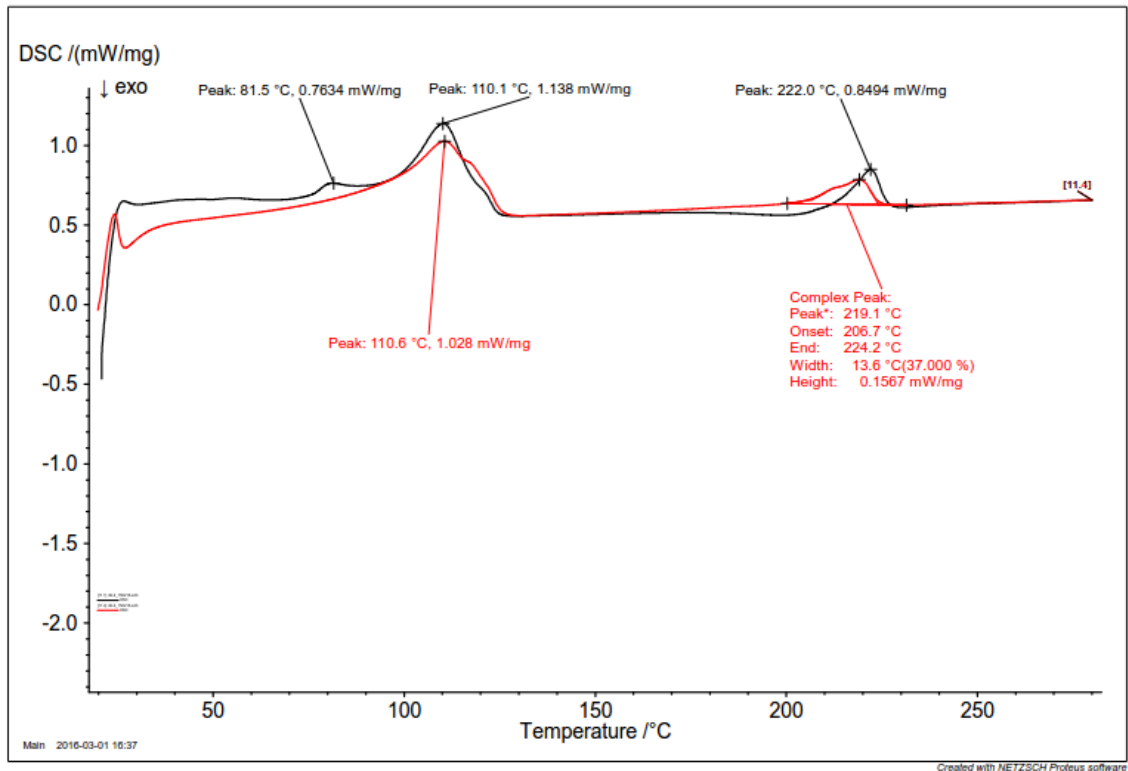


**Figure B-9.** DSC curve of sample 49-2 with peaks from EVA, LDPE and PA-6.

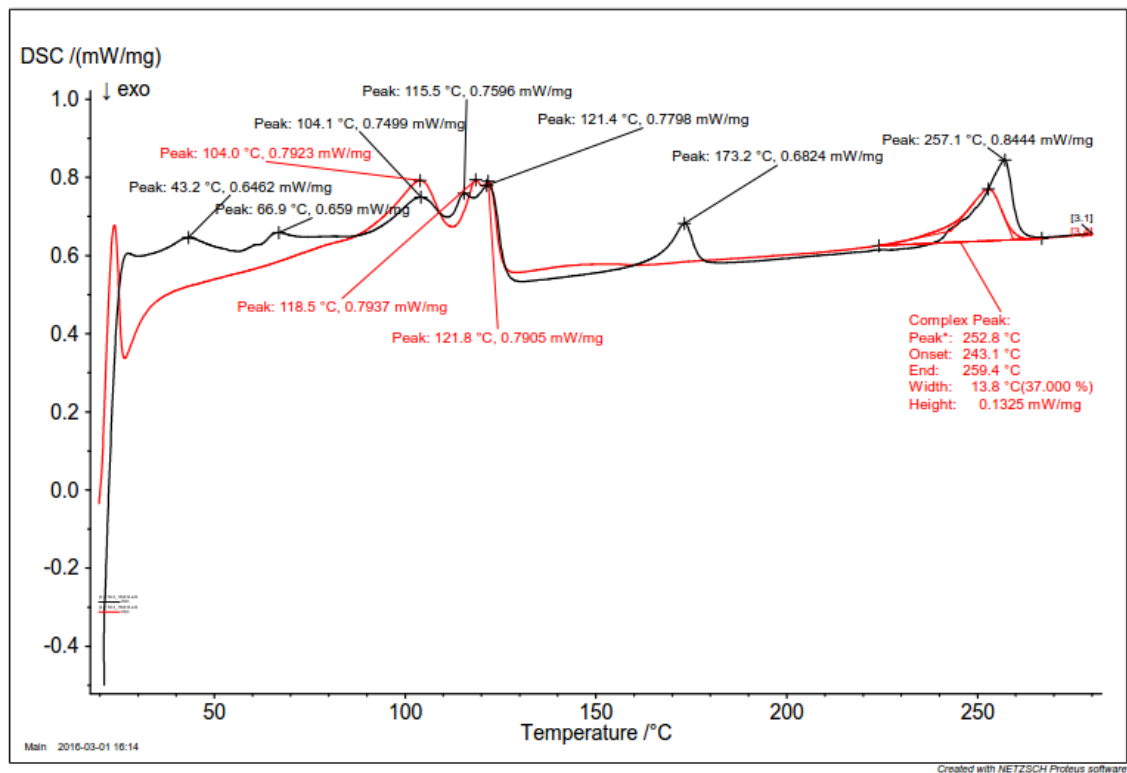


**Figure B-10.** DSC curve of sample 50-3 with peaks from EVA, LDPE, LLDPE, EVOH and PET.

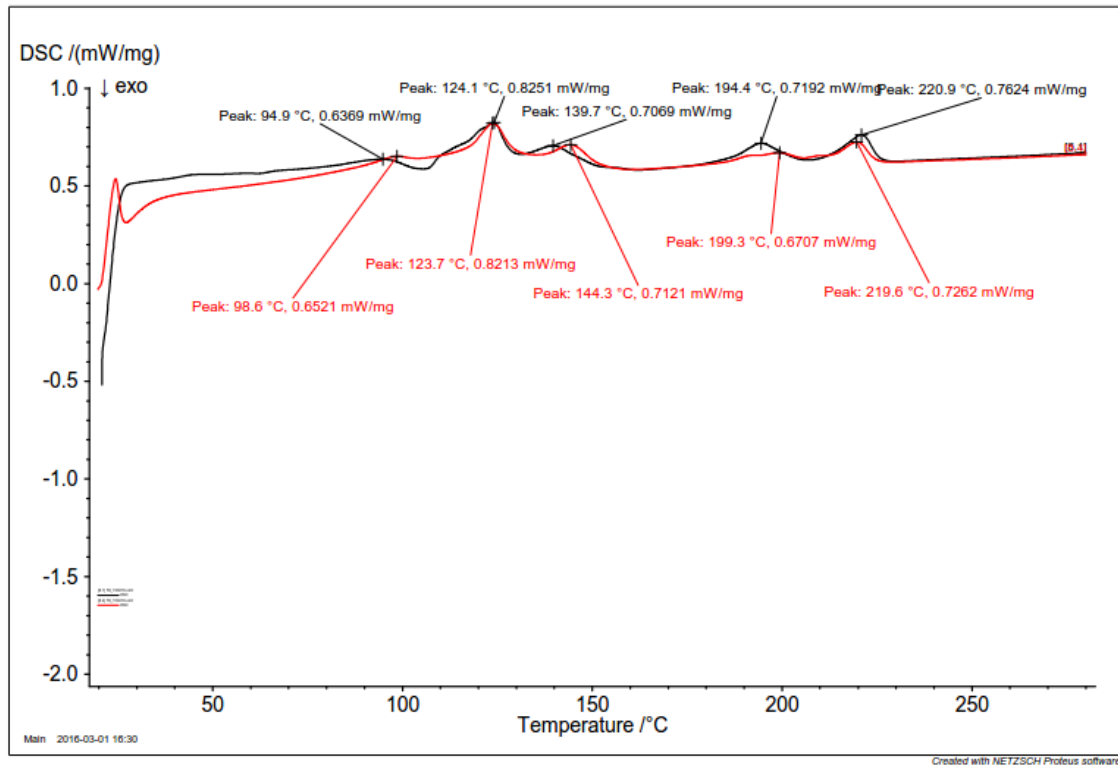


**Figure B-11.** DSC curve of sample 55 with peaks from LDPE, LLDPE, aPP, EVOH and PA-6.

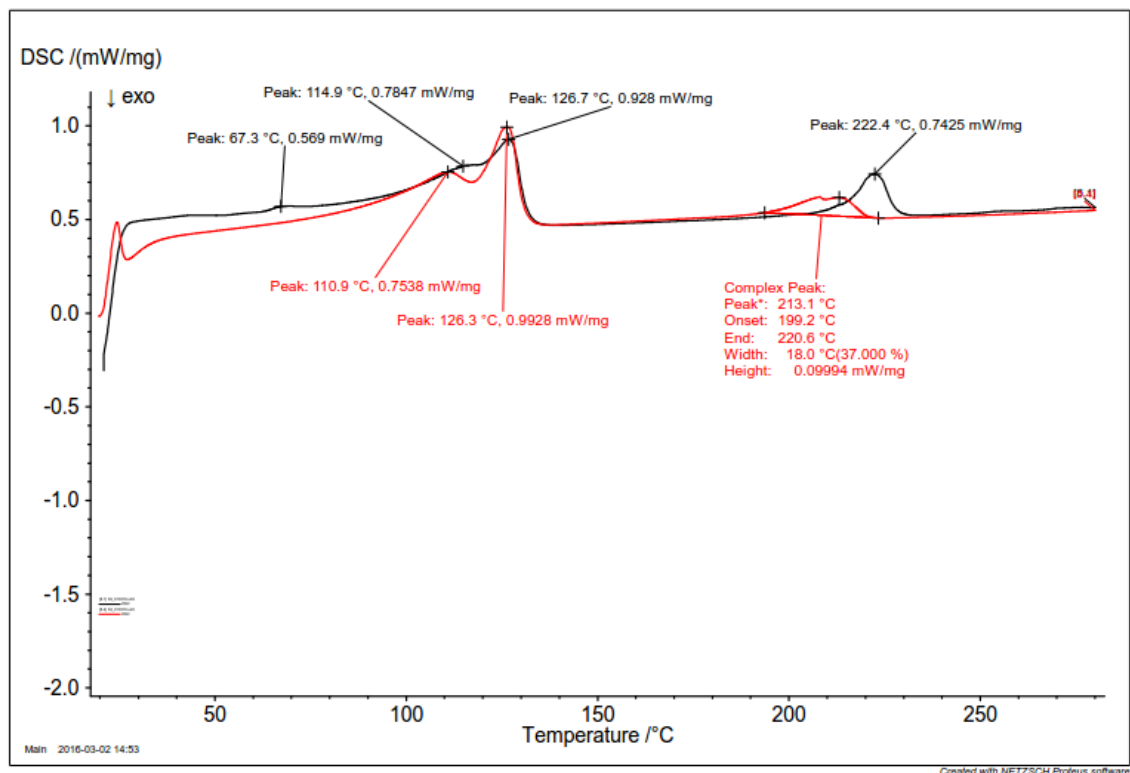


**Figure B-12.** DSC curve of sample 63 with peaks from EVA, LDPE, LLDPE and PA-6.

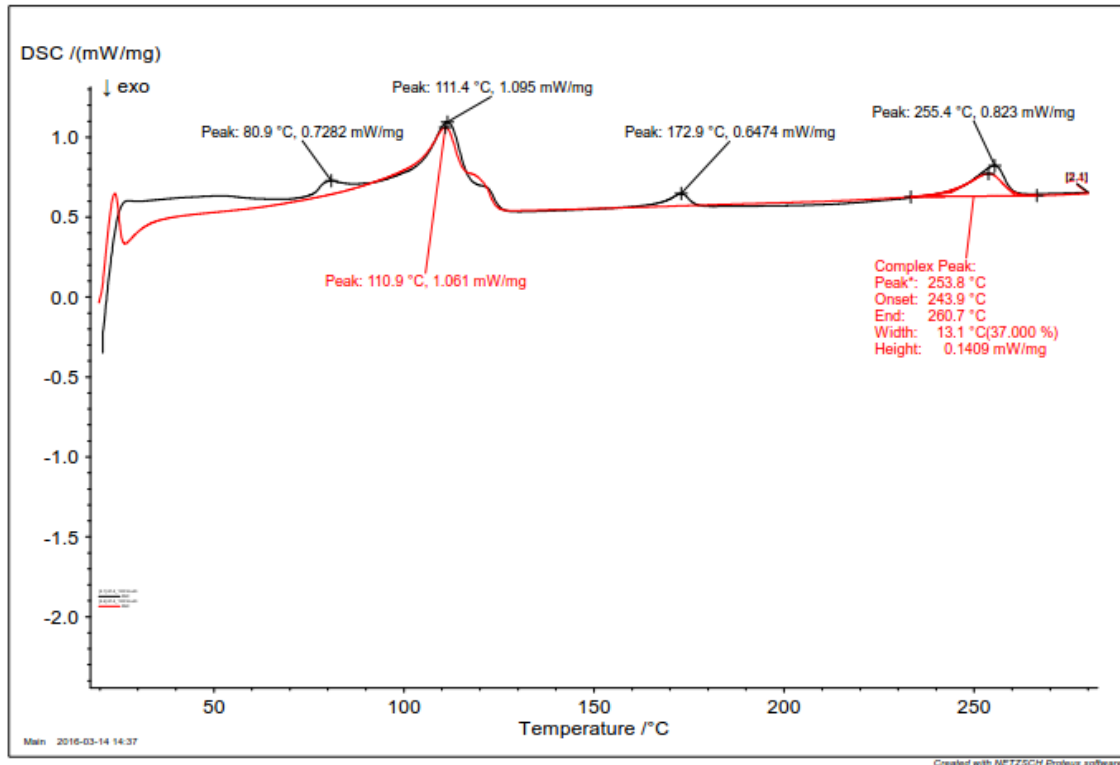


**Figure B-13.** DSC curve of sample 67-2 with peaks from EVA, LDPE, EVOH and PET.

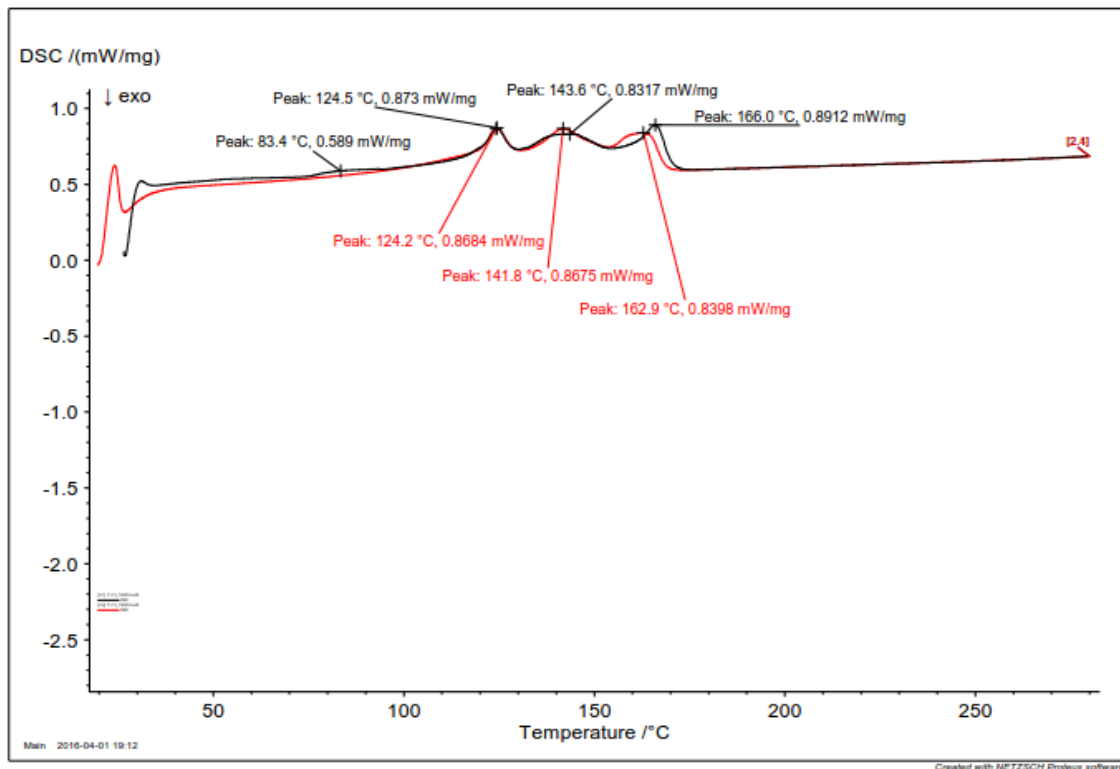


**Figure B-14.** DSC curve of sample 71-13 with peaks from EVA, LLDPE, aPP and PP.

## APPENDIX C: FTIR SPECTRA

The most common FTIR spectra that were analyzed in this thesis are presented in Appendix C.

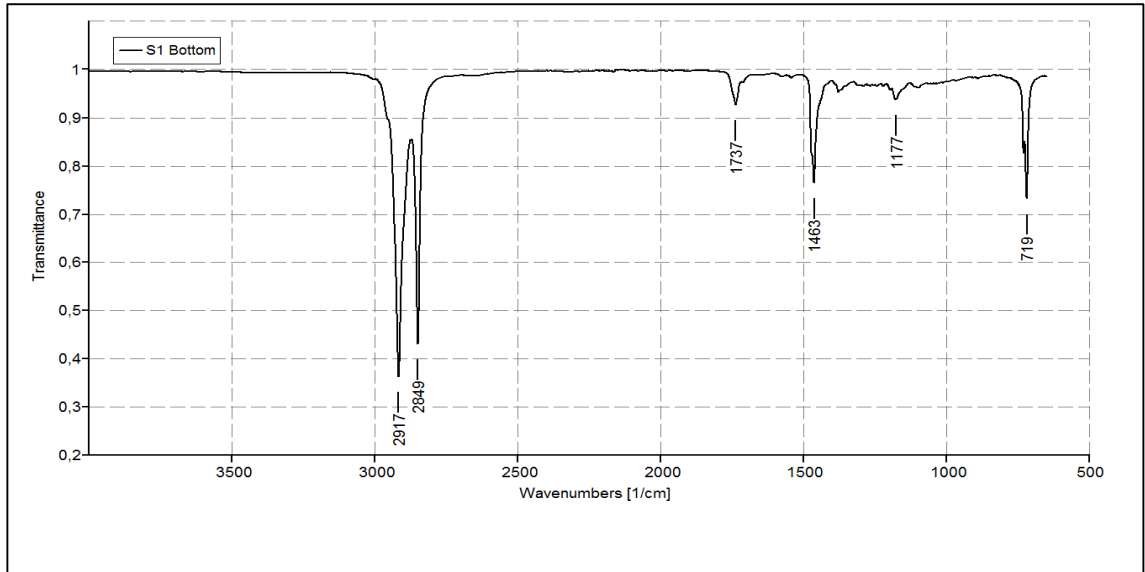


**Figure C-1.** FTIR spectrum of the bottom layer of sample 1 identified as LDPE with additive peaks at 1737 and 1177  $\text{cm}^{-1}$ .

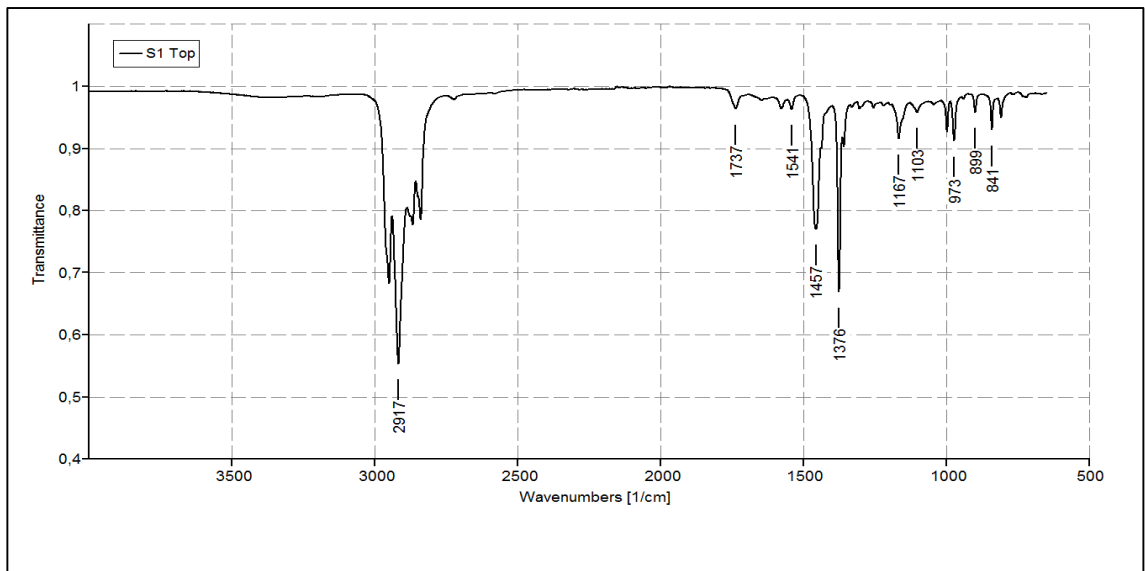


**Figure C-2.** FTIR spectrum of the top layer of sample 1 identified as PP with additive peaks at 1737 and 1541  $\text{cm}^{-1}$ .

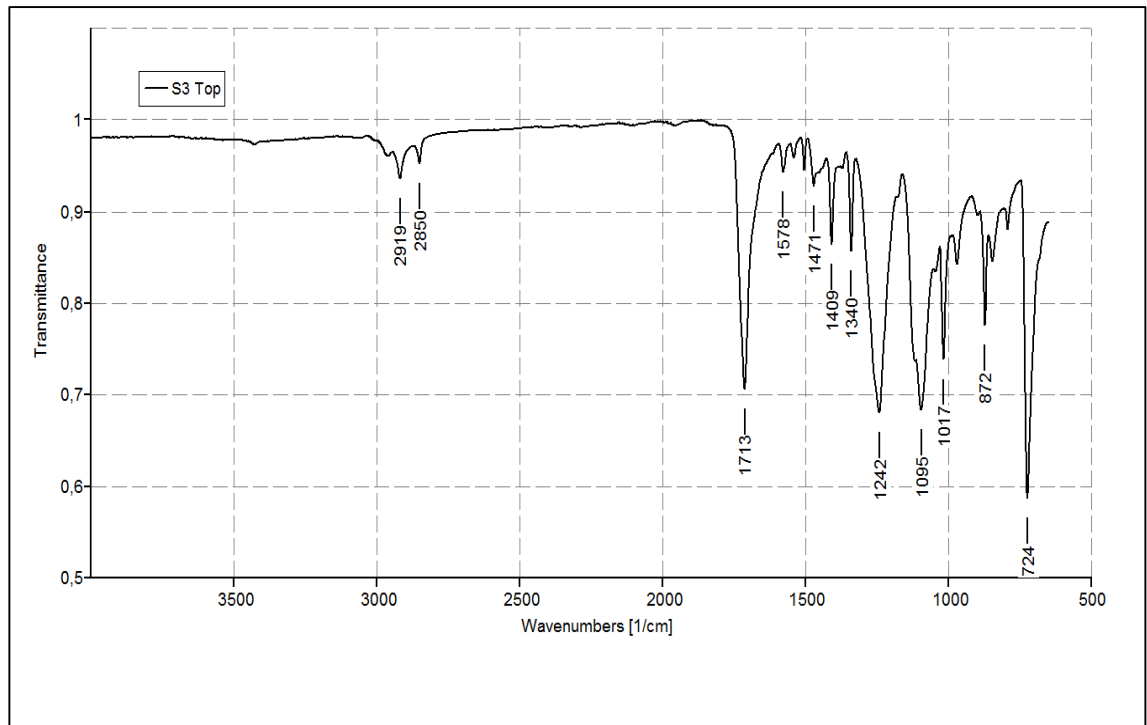


**Figure C-3.** FTIR spectrum of the top layer of sample 3 identified as PET.

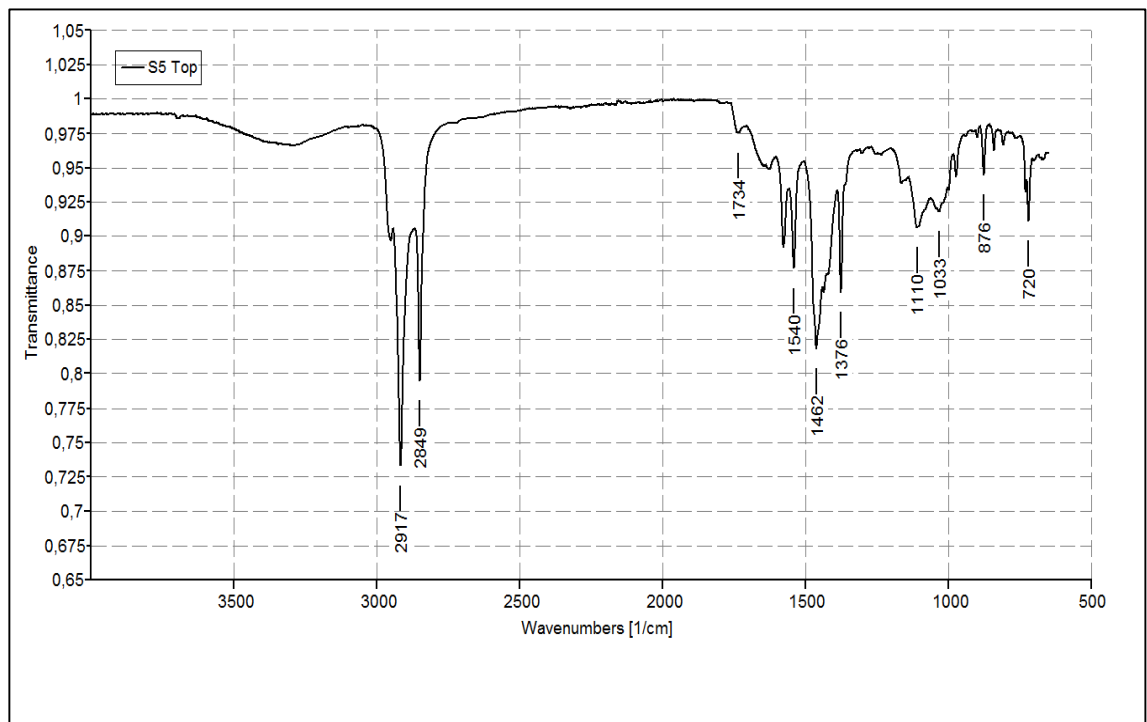


**Figure C-4.** FTIR spectrum of the top layer of sample 5 identified as PP with a high concentration of additives.

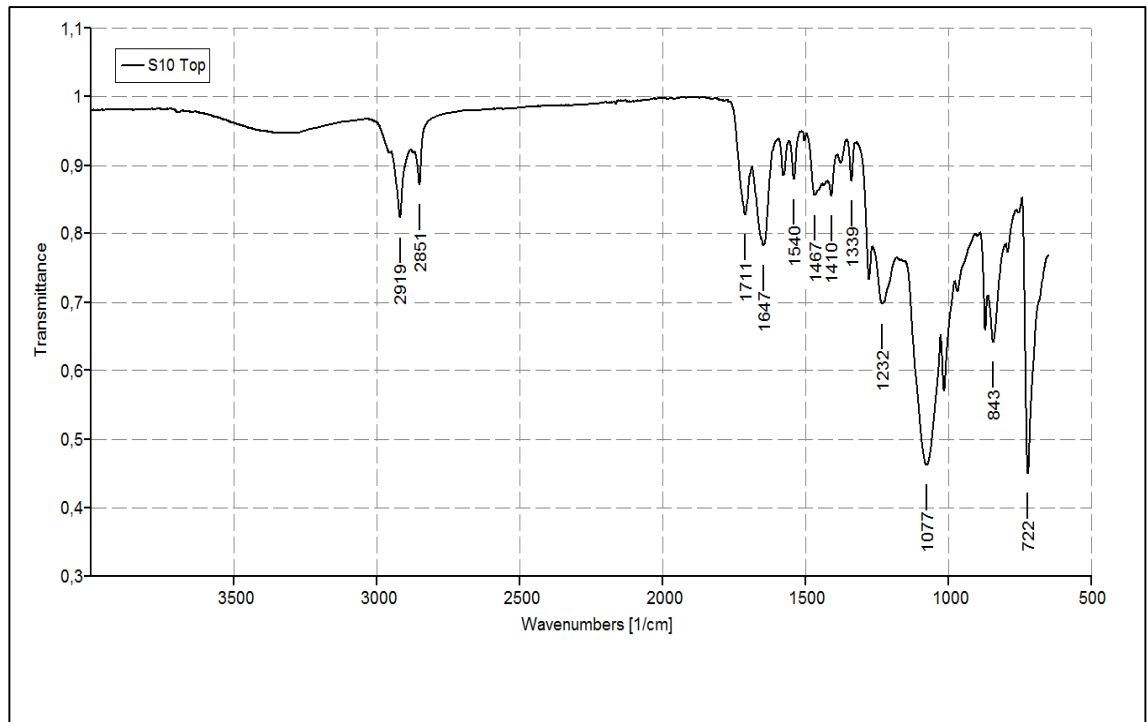


**Figure C-5.** FTIR spectrum of the top layer of sample 10 identified as PET with a high concentration of additives.

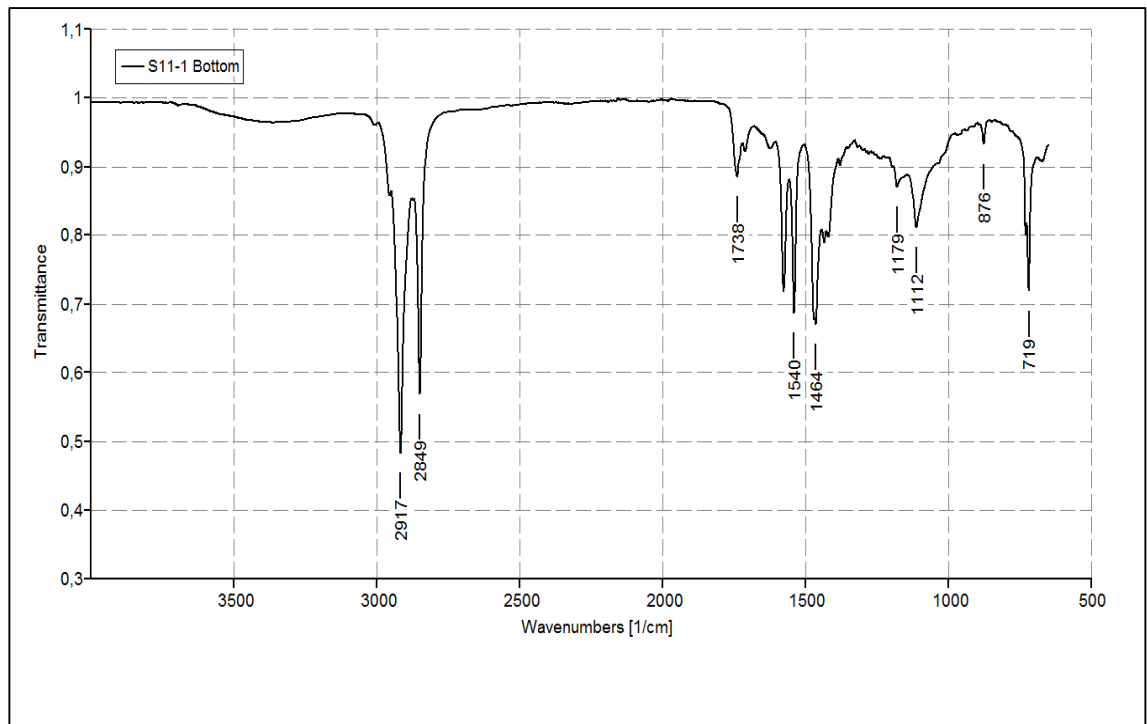


**Figure C-6.** FTIR spectrum of the bottom layer of sample 11-1 identified as LDPE with high concentration of additives.



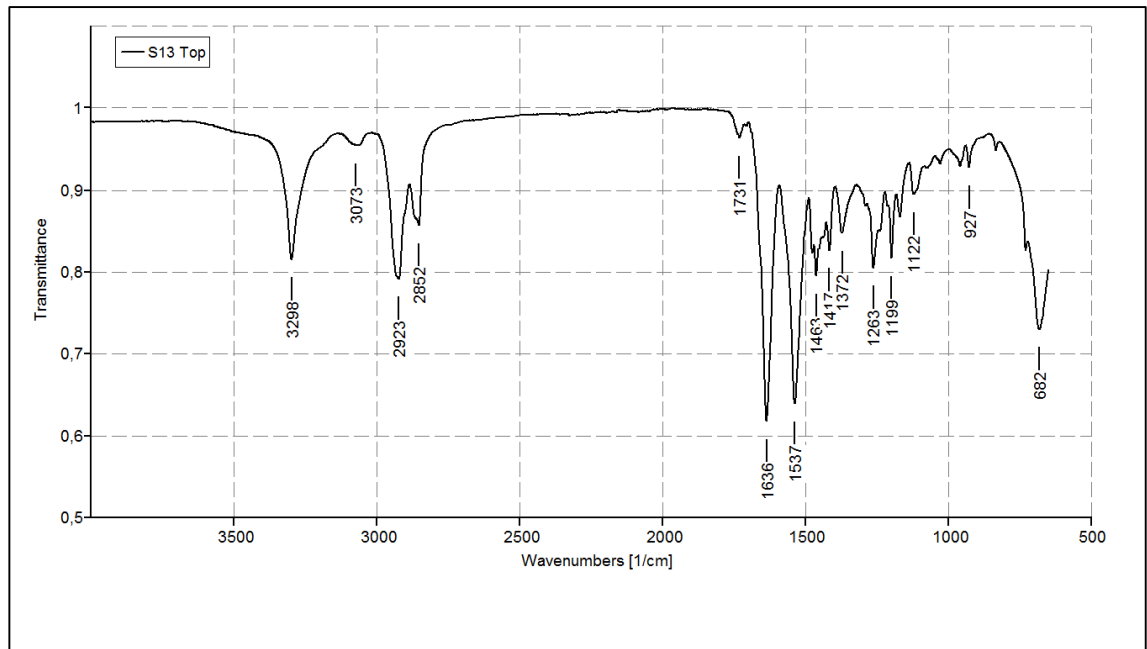


**Figure C-7.** FTIR spectrum of the top layer of sample 13 identified as PA-6 with an additive peak at  $1731\text{ cm}^{-1}$ .

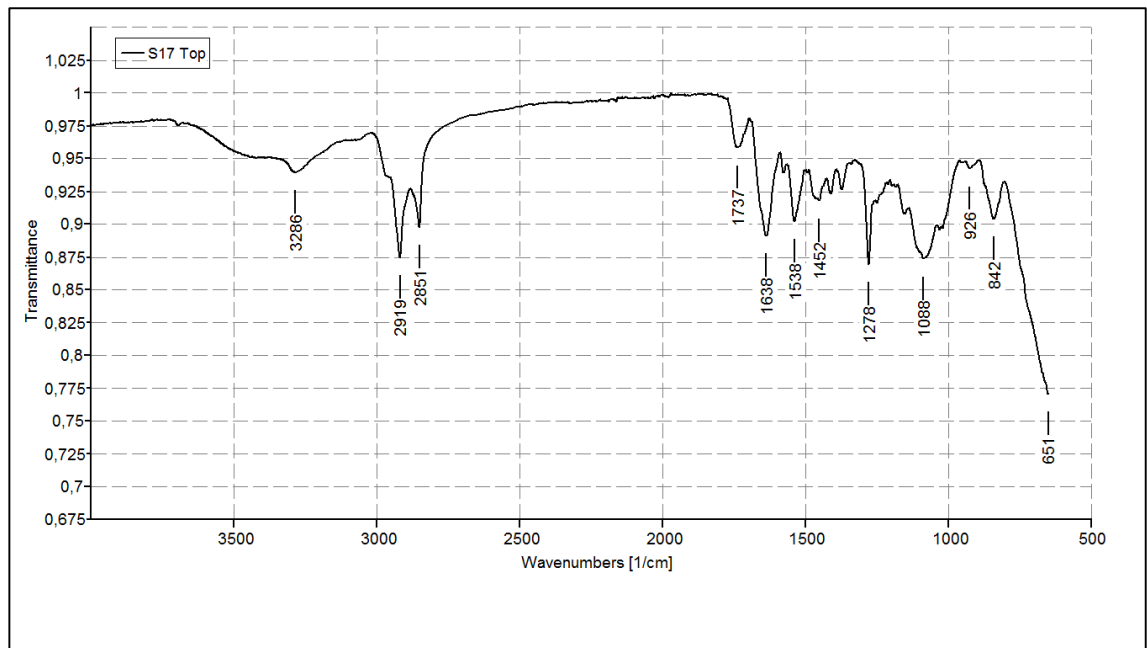


**Figure C-8.** FTIR spectrum of the top layer of sample 17 identified as PA-6 with a high concentration of additives.

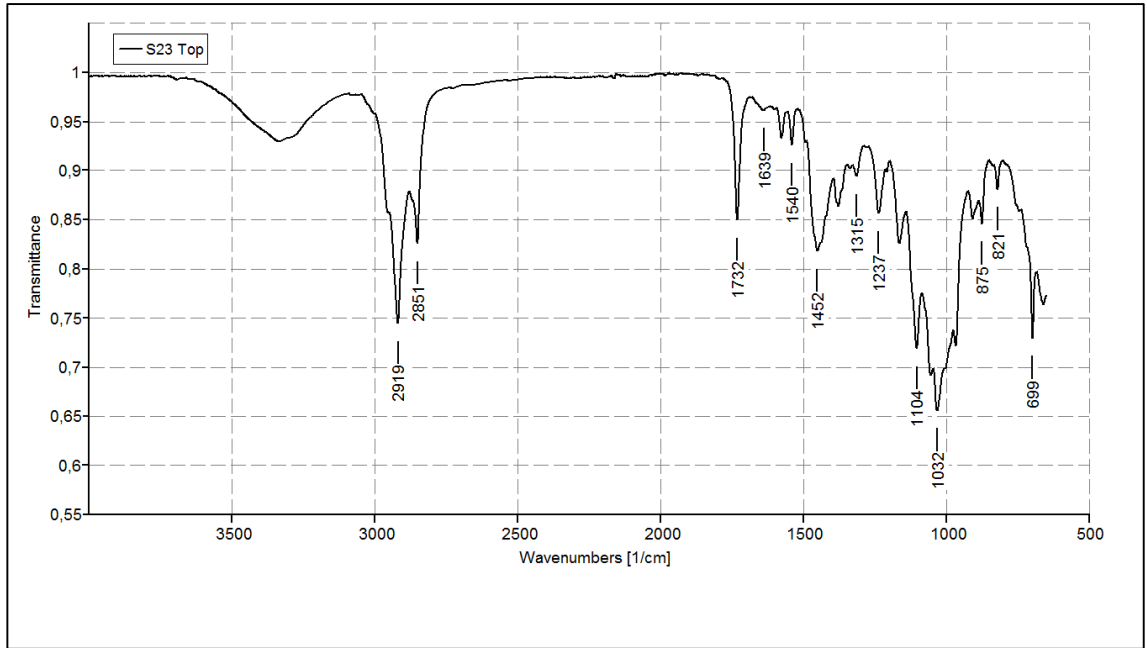


**Figure C-9.** FTIR spectrum of the top layer of sample 23 identified as PET with a high concentration of additives.

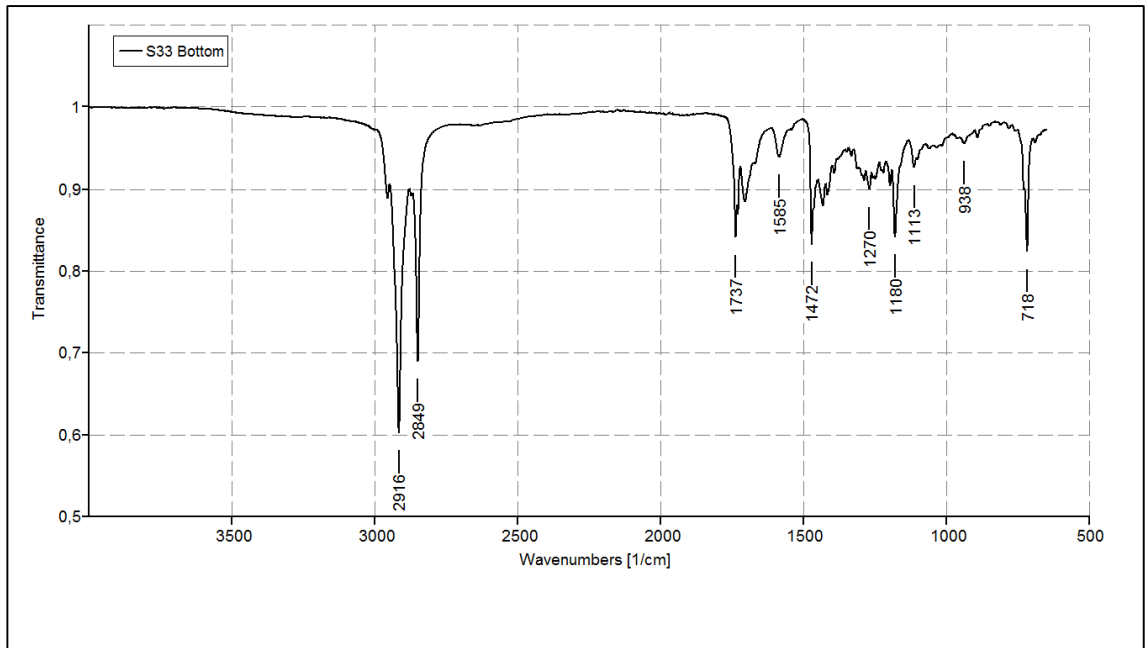


**Figure C-10.** FTIR spectrum of the bottom layer of sample 33 identified as a copolymer of LDPE and PP.

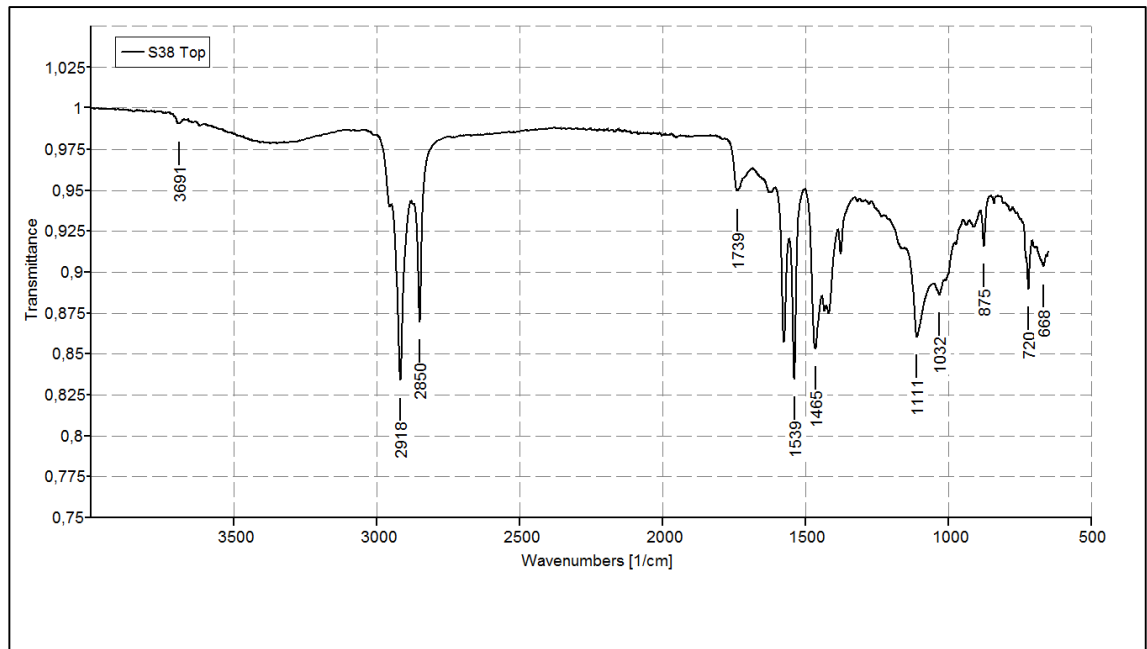


**Figure C-11.** FTIR spectrum of the top layer of sample 38 identified as a copolymer of LDPE and PP with a high concentration of additives.

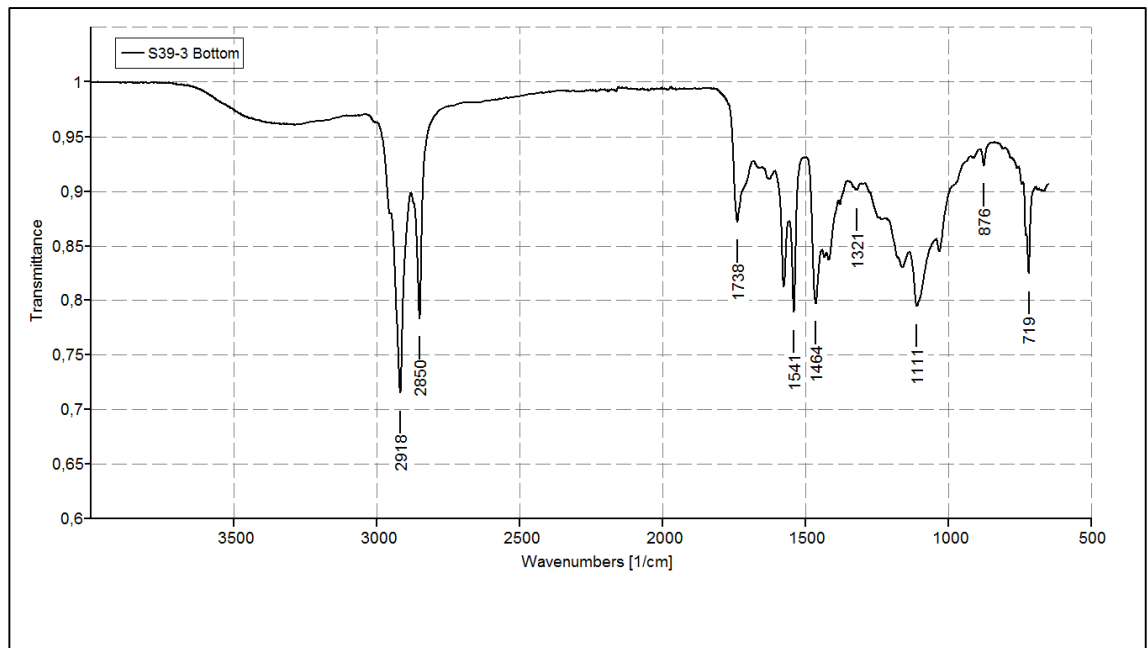


**Figure C-12.** FTIR spectrum of the bottom layer of sample 39-3 identified as LDPE with high concentration of additives.

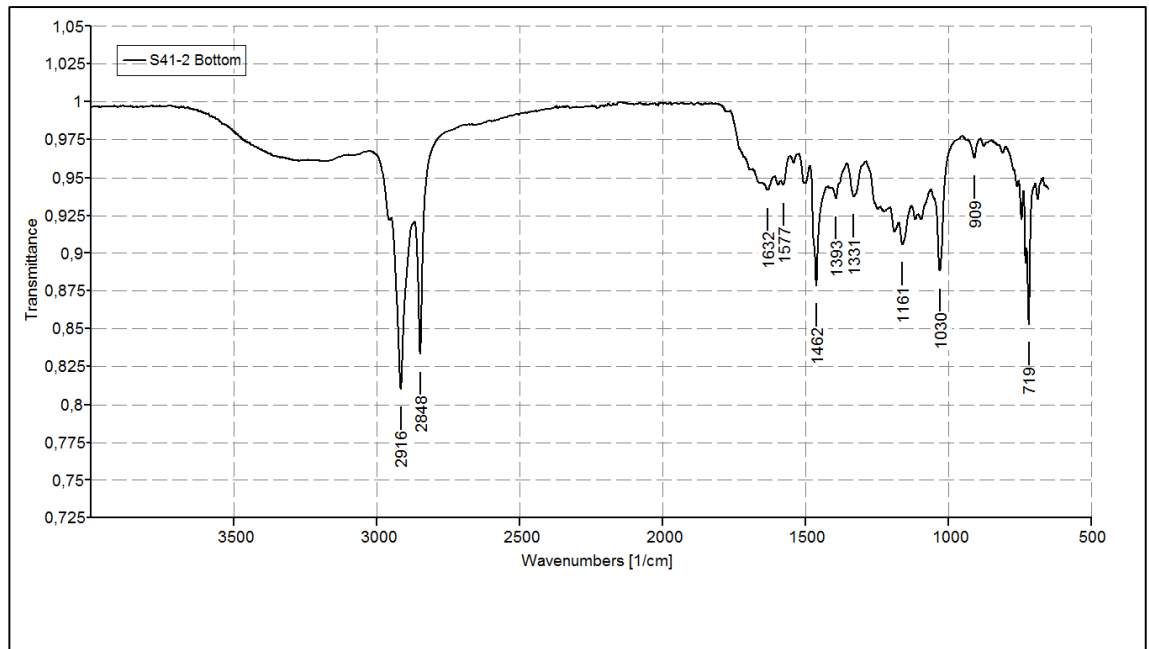


**Figure C-13.** FTIR spectrum of the bottom layer of sample 41-2 identified as LDPE with a high concentration of additives.

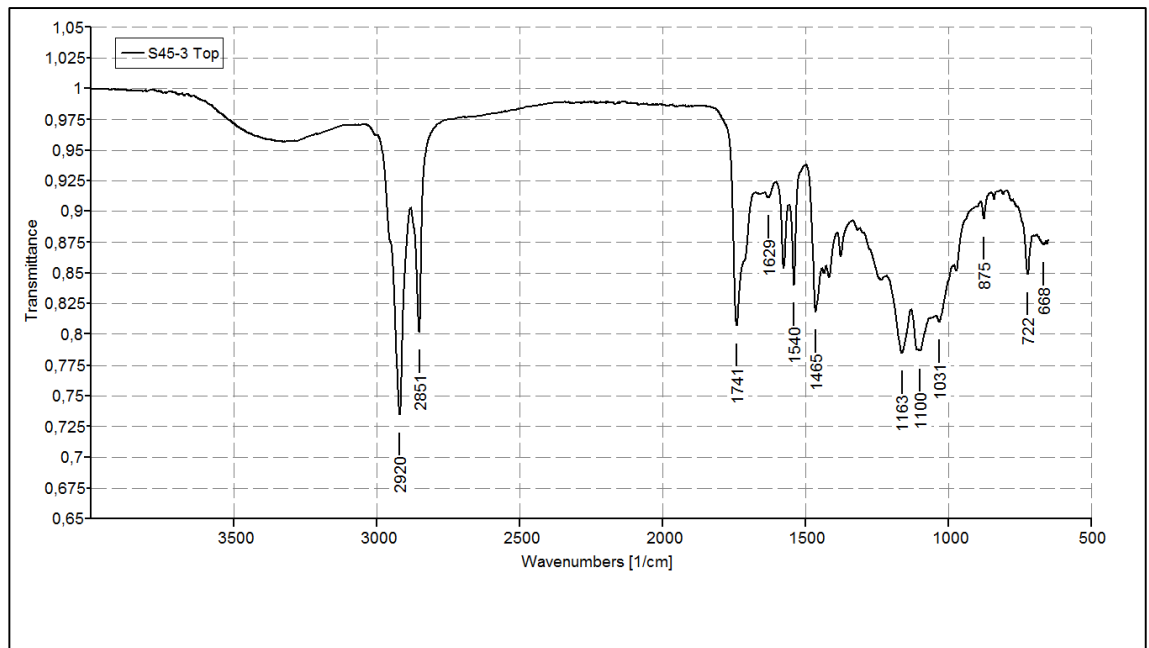


**Figure C-14.** FTIR spectrum of the top layer of sample 45-3 identified as a copolymer of LDPE and PP.

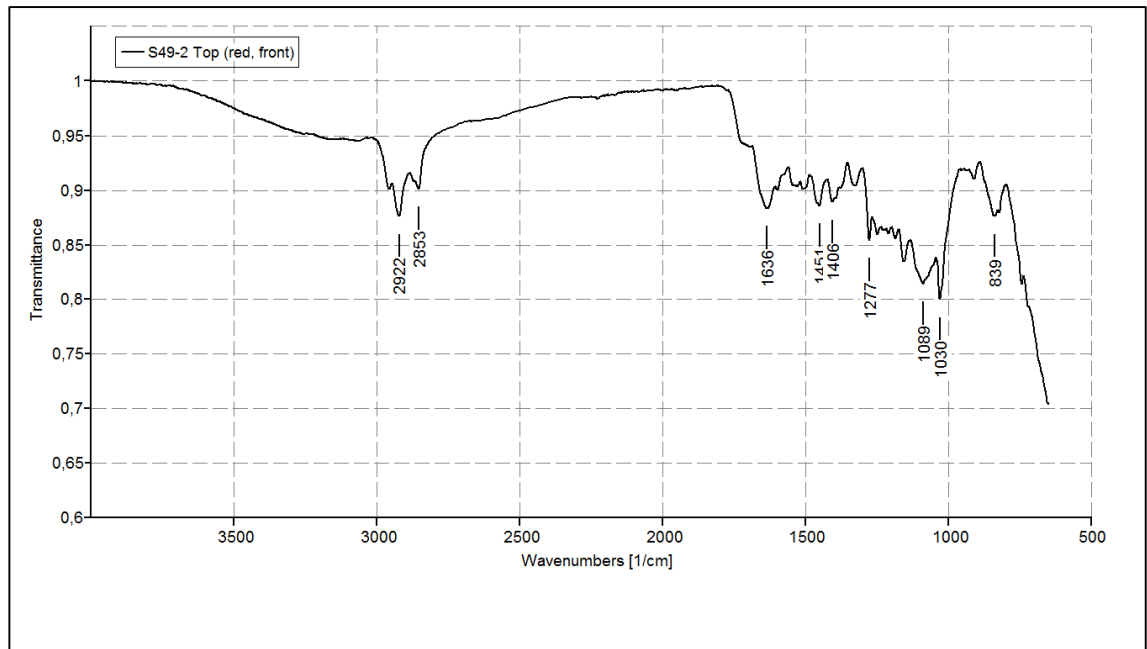


**Figure C-15.** FTIR spectrum of the top layer of sample 49-2 identified as PA-6 with a high concentration of additives.

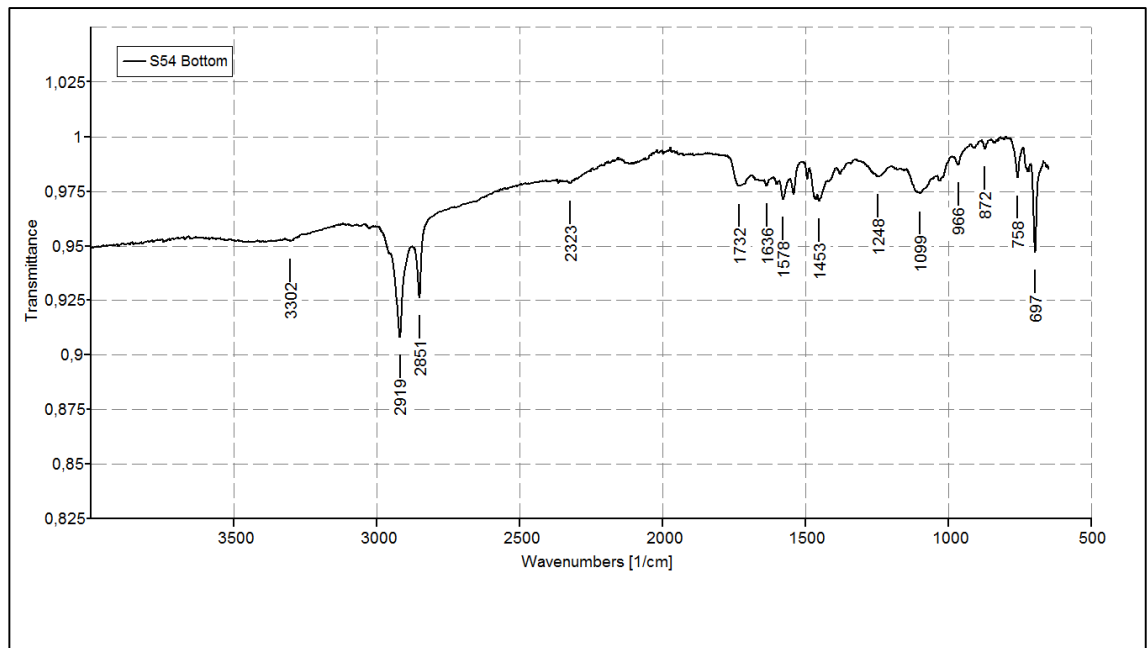


**Figure C-16.** FTIR spectrum of the bottom layer of sample 54 identified as PET with a small amount of PA-6.